Performance Analysis of Parabolic Trough Solar Steam Generators: Acase of Wenji Pulp and Paper Factory

M.Sc. Thesis

By

Abdi Abrahim Umer

Thermal and Aerospace Engineering Program

School of Mechanical, Chemical and Materials Engineering

Adama Science and Technology University

Adama, Ethiopia

February, 2019

Performance Analysis of Parabolic Trough Solar Steam Generators: Acase of Wenji Pulp and Paper Factory

A Thesis Submitted to Thermal and Aerospace Engineering Program of School of Mechanical, Chemical and Materials Engineering, Adama Science and Technology University in partial fulfillment of the requirement of the degree of Master of Science in Thermal Engineering.

By

Abdi Abrahim Umer

Advisor: Dr. Gezahegn Habtamu

Adama, Ethiopia

February,2019

APPROVAL OF BOARD OF EXAMINERS

We, the undersigned, members of the board of Examiners of the final open defense by Abdi Abrahim have read and evaluated his thesis entitle ‘‘Performance Analysis of Parabolic TrougSolar Steam Generators: Acase of Wenji Pulp and Paper Factory’’ and examined the candidate. This is,therefore,to certify that thesis has been accepted in partial fulfilment of the requirement of the Degree of Masters of Science in Thermal Engineering.

Chairperson	Signature	Date
Internal Examiner	Signature	Date
External Examiner	Signature	Date

Declaration

I hereby declare that this M.Sc. Thesis entitled "Performance Analysis of Parabolic Trough Solar Steam Generators: Acase of Wenji Pulp and Paper Factory" in partial fulfillment of the requirement of the degree of Master of Science in Thermal Engineering is an authentic record of my own work carried out from September 2017 to February 2019 under supervision of Dr. Gezahegn Habtamu, Assistant Professor of Thermal Engineering program, Adama Science and Technology University.

The matter embedded in this thesis has not been submitted for the award of a degree or diploma in any other university. All relevant resource information used in this paper has been duly acknowledged.

……………………………. ……………………………..

Student Signature:

This is to certify that the above statement made by the candidate is correct to the best of our knowledge and belief. This has been submitted for examination with our approval.

………………………………… ………………………………..

Main Advisor Signature:

Acknowledgements

All praise to almighty Allah whose knowledge and compassion extends to all His creations. This work would not have been possible without His endless grace and kindness upon me. May countless blessings be upon the Holy Prophet, Mohammad, whose teachings inspired in me the desire to not only acquire knowledge but also to impart it onto others.

I would especially like to express my deepest appreciation to my supervisor Dr. Gezahegn Habtamu for his support and enlightening guidance. He has given me general concepts about my work.

I am also grateful to Wenji Pulp and Paper Factory staff for their indispensable advice and supporting for me during the research work.

Finally, I would like to thank my beloved family, all my friends and classmates who are either directly or indirectly involved during the process of this thesis work.

Abstract

Wenji Pulp and Paper Factory is one of the most energy consuming factory in which thermal energy is utilize. In this factory thermal energy is used for drying the paper .The main source of thermal energy for drying paper is electricity. The factory uses steam which has a temperature of 215 °C for drying the paper. This steam is produced using resistor electric boiler.

In Wenji Pulp and Paper factory, there are two resistor electric boilers that have different capacity of steam production. The first one has a capacity to generate 4,302 kg/hr of steam and the second one has able to produce 8,600 kg/hr steam at full load.

This electric boiler is consuming more electric energy and can be partially or wholly replaced by a solar parabolic trough steam generator.

This thesis aims in performance analysis of parabolic trough steam generation for Wenji pulp and paper factory which is located in Wenji town.

The simulation result from thermal performance analysis study shows that the parabolic trough steam generator can meet the steam demand of the factory during the day. The parabolic trough aperture area required to fulfil this steam demand by the factory is obtained to be equal to 8,843 m^2.

During cloudy day the conventional electric steam generation system can be used to meet the daily energy demand for generating steam only for few days in a year.

In this paper the required data is collected from Wenji Pulp and Paper Factory and weather data was taken from Adama meteorology agency. Thermal modelling of the parabolic trough solar steam generator system is developed. The proposed system functionality is tested using MATLAB software. In present study three different mass flow rates (0.3kg/s, 0.4kg/s and 0.5kg/s) are taken to test temperature of HTF outlet from solar collector. It's observed that the temperature of HTF is inversely proportional to mass flow rate. So it's possible to increasing or decreasing the temperature of HTF by decreasing or increasing mass flow rate respectively.

When mass flow rate of 0.3kg/s is flow through the collectors; the outlet temperature HTF is ranged between 250^oC *to* 340^oC*.When mass flow rate of 0.4 kg/s is flow through the collectors; the HTF outlet temperature is ranged between* 220^oC *to* 300^oC*.When mass flow rate of 0.5 kg/s is flow through the collectors; the HTF outlet temperature is ranged between* 200^oC *to* 275^oC*. It's observed that with increasing mass flow rate HTF temperature is decreased.*

The corresponding efficiency of the system was found to be equal to 69%. The optical efficiency of collector was higher i.e 75 %.The maximum value of thermal efficiency can reach up 68 %.

Table of Contents

List of Tables

List of Figures

Acronyms

AC	Alternating current
CF	Capacity factor
CFWHs	Closed feed water heaters
CL	Cleanness
CR	Clean reflectivity
CST	Concentrating solar thermal technologies
DNI	Direct Normal Irradiation
DSG	Direct steam generation
EEPCo	Electric Tariff of the Ethiopian Electric Power Corporation
EL	End loss
FOB	Free On Board
Gsm	Gram square meter
HCE	Heat collecting elements
HTF	Heat transfer fluid
HX	Heat exchanger
i	Nominal depreciation rate
IFC	International Finance Corporation
LCOE	Levilized cost of energy [$/kWh]
LF	Linear Fresnel
n	Age in years
NTU	Number of transfer units
P	Original price
PCM	phase-chance materials
PD	Parabolic dish
PTC	Parabolic-trough collector
PV	Photovoltaic

RS	Row shading
S	Salvage value
SCA	Solar collecting assembly
SEGS	Solar electric generation systems
ST	Solar tower

Nomenclature

a	Accommodation coefficient
A	Coefficient
A_{eff}	Solar field aperture area [m^2]
b	Interaction coefficient
b	Interaction coefficient of annulus gas
B	Coefficient
C	Coefficient
C_c	Capacitance rate of the cold side fluid (steam) [kW/K]
C_H	Capacitance rate of the hot side fluid (HTF) [kW/K]
C, m, n	Constants
C_{max}	The bigger capacitance rate between the steam and the HTF [kW/K]
C_{min}	The smaller capacitance rate between the steam and the HTF [kW/K]
$C_{p,HTF}$	Average specific heat of HTF between inlet and outlet [kJ/kg-K]
C_r	The ratio of C_{min} to C_{max}
D	Coefficient
D_2	Absorber inside diameter [m]
D_3	Absorber outside diameter [m]
D_4	Inner glass envelope diameter [m]
D_5	Glass envelope outer diameter [m]
D_h	Hydraulic diameter of absorber pipe [m]

D_{HCE}	Diameter of the steel absorber tube [m]
E	Equation of time (minutes)
EFF	Effectiveness
EXP_UA	Power law exponent to UA
f	Focal length [m]
g	Gravitational constant [9.81 m/s^2]
H_o	Daily extraterrestrial radiation on a horizontal surface (J/day.m^2)
I_{ext}	Extraterrestrial radiation [W/m^2]
I_o	Solar radiation for a horizontal surface at any time between sunrise and sunset
I_{on}	Extraterrestrial radiation measured on the plane normal to the radiation
I_{sc}	Solar constant [W/m^2]
K	Incident angle modifier
k_{std}	Thermal conductance of annulus gas at standard temperature and pressure [W/m.K]
L_{LOC}	The longitude of the location in question [^{o}]
L_{SCA}	Length of one solar collector assembly loop [m]
$L_{spacing}$	Distance between the collector rows [m]
L_{ST}	The standard meridian for the local time zone [^{o}]
$m_{steam,HTF}$	Mass flow rate of steam, HTF [kg/s]
M_{SF}	Mass of the HTF in the solar field [kg/s]
N	Number of days in the year
N_{sca}	Number solar collector loops
Nu_{D5}	Average Nusselt number based on the glass envelope outer diameter
P_a	Annulus gas pressure [mmHg]
RPM	Revolution per minute [rad/min]
T_{amb}	Ambient temperature [^{o}C]
T_{avg}	Average temperature of the HTF in the solar field [^{o}C]
UA	Overall heat transfer coefficient [W/K]
W	Collector aperture width [m]

WS	Wind speed [m/s]

Greek letter

α_{56}	Thermal diffusivity for air at T_{56} [m^2/s]
ε_3	Absorber selective coating emissivity
ε_4	Glass envelope emissivity
α	Solar altitude angle [^{o}]
α_1	Thermal diffusivity of HTF [m^2/s]
β	Volumetric thermal expansion coefficient [1/K]
γ	Ratio of specific heats for the annulus gas
γ	Solar azimuth angle [^{o}]
δ	Declination angle [^{o}]
ΔT	Average fluid temperature [^{o}C]
ΔT_{in}, ΔT_{out}	Difference between inlet and outlet temperature of the HTF from the solar field
ε	Effectiveness
ε_5	Emissivity of the glass envelope outer surface
ε_c	Emissivity of the transparent glass envelope
ε_r	Emissivity of the absorber tube
η_o	Optical efficiency [%]
η_{SF}	Efficiency of the solar field [%]
η_{th}	Instantaneous thermal efficiency [%]
θ	Incidence angle [^{o}]
θ_z	Solar zenith angle [^{o}]
λ	Mean-free-path between collisions of a molecule [cm]
ν_1	Kinematic viscosity of the HTF [m^2/s]
ν_{56}	Kinematic viscosity of air at T_{56} [$m^2/2$]
ρ	Density [kg/m^3]

σ	Stefan-Boltzman constant [$W/m^2 – K^4$]
ω	The hour angle [^{o}]
ω_s	Sunset hour angle, in degrees
ϕ	Altitude angle

Subscripts

in	inlet
max	maximum
min	minimum
e	exit
i	inner
o	outer

CHAPTER ONE

INTRODUCTION

Solar energy is the most abundant energy resource on earth and the solar radiation reaching the earth's surface equals about 1 kilowatt per square metre (kW/m^2) under clear conditions when the sun is near the zenith. It is comprised of two components: direct or beam radiation, which comes directly from the sun's disk and diffuse radiation, which reaches the earth after being scattered in all directions by the atmosphere.

Many applications require energy at higher temperatures than those reached from incident solar radiation on to the earth's surface. With the aim of achieving high temperatures, solar energy is concentrated in collectors that capture and focus the solar radiation onto a smaller receiving surface.

Solar thermal collectors and solar PV panels comprise the two main types of solar energy converts. PV panels convert solar radiation into electricity, whereas solar thermal collectors convert the sun's rays directly into usable heat. Once the collector converts the sun's rays into heat, that heat can be used for a variety of purposes in industry (Gosselar and Johnson, 2011).

Concentrating solar thermal (CST) technologies can be applied in industrial processes to desalinise water, improve water electrolysis for hydrogen production, generate heat for combined heat and power applications, and support enhanced oil recovery operations. The use of these technologies in a wide range of applications encourages the improvement of their efficiency, which depends on the direct-beam irradiation.

The four main commercial CST technologies are distinguished by the way they focus the sun's rays and the technology used to receive the solar energy: parabolic-trough collector (PTC), solar tower (ST), linear Fresnel (LF) and parabolic dish (PD). They can be classified according to the focus type (line focus or point focus).

Parabolic trough concentrator is one of the most common solar concentrator to generate steam for CST technology.

Parabolic trough concentrator (PTC) comprises of a cylindrical concentrator of parabolic cross-sectional shape and a circular cylindrical receiver located along the focal line of the parabola. It reflects direct solar radiation onto a receiver tube located in the focal line of the parabola. Since the collector aperture area is bigger than the outer surface of the receiver tube, the direct solar radiation is thus concentrated.

The parabolic trough concentrator (PTC) converts solar beam radiation into thermal energy in its linear focus receiver. The focal line onto which the beam radiation is reflected is comprised of all focal points at each cross-sectional location of the concentrator. The receiver tube is selectively coated to increase its absorptivity. It is generally encased within a glass tube to reduce any convective heat losses. The trough assembly tracks the sun in a single axis so as to always keep the trough aperture towards the sun. The trough is generally mounted with its focal axis parallel towards either east- west direction or north-south direction (Kalogirou, 2009).

The solar field area must be large enough to satisfy the steam demand. Heat exchangers are used to transfer heat energy from the heat transfer fluid (HTF) to steam coming from the feed water heaters.

Process heat is required at different temperature levels. The major part of the required process heat (e.g. in the chemical, food, textile and paper industry) is needed in the medium temperature range between 80 to 250°C.

Wenji pulp and paper factory produce paper using foundries machine which is a standard machine for paper production. The company's paper machine is composed of Forming machine, Press machine, Drying section and calendar /reel section. The paper machine makes printing and writing papers and paperboards in the 45 to 350 grams per square meter (gsm) weight ranges.

Wenji pulp and paper factory uses steam which has a temperature of 215 °C for drying the paper. This steam is produced using resistor electric boiler. In the factory, there are two resistor electric boilers that have different capacity of steam production. The first one has a capacity to generate 4,302 kg/hr of steam and the second one has able to produce 8,600 kg/hr steam at full load. Consumption of the steam depends on different type of paper in the process and smooth functionality of paper machine.

Boiler running consumes large amount of electric power to generate sufficient steam for the factory and thus need high electric running cost. If the boiler can be substituted with Concentrated Solar Steam generation system (parabolic trough) reduction of electric cost would be appreciably.

1.1. Statement of problem

Wenji pulp and paper factory uses steam for drying paper which is generated by the two resistor electric boiler at a temperature of 215 °C. The consumption of the steam depends on types of paper in the process and smooth functionality of paper machines. The factory is consuming high electricity for the steam generation which is the main cause of the factory not to be profitable.

Due to high electric consumption for steam generation and machine operation the factory expends high cost to buy this electric power every month. Only for steam generation the factory pays an average of 7,518,825.14 Birr per year. This is strictly affecting the profit of the factory.

To reduce the cost of electricity required to run the boilers, solar energy as an alternative energy can be used to generate the steam requirements of the factory. In this paper, a parabolic trough solar steam generating system is considered as an alternative to generate steam for drying paper (i.e. partially replace resistor electric boiler) that would make the factory more beneficially or profitable through decreasing its electricity purchasing costs.

1.2 Objectives

The objective of this thesis is to investigate performance of parabolic trough solar steam generators for replacing the existing resistor electric boiler which generates steam for drying paper in Wenji Pulp and Paper Factory.

The specific objectives of this study are:

- ✓ To develop solar thermal performance simulation model for parabolic trough concentrator that satisfy steam demand of Wenji pulp and paper factory.
- ✓ To simulate performances of parabolic trough solar steam generators using MATLAB software in terms of the optical efficiency, thermal efficiency, mass flow rate of HTF.
- ✓ Effective area of the parabolic trough solar steam generator that covers the steam energy demand of the factory using a typical day solar radiation intensity data.
- ✓ To compare the conventional steam generation with the solar steam generation system for Wenji Pulp and Paper Factory.

1.3 Methodology

This paper is concerned with the simulation and performance evaluation of parabolic trough solar system to generate steam for Wenji Pulp and Paper Factory. First literature review of relevant materials on parabolic trough collectors is conducted. The literatures available are from journals and books. Secondary data are referred from previous and related research studies, existing statistical data, etc.

Generally the following activities were accomplished to achieve the thesis objectives:

i. Collecting required data from Wenji Pulp and Paper Factory and weather data was taken from *Adama* meteorology agency.
ii. Thermal modelling of the parabolic trough solar steam generator system using the data collected.
iii. Simulate the proposed system functionality using MATLAB.
iv. Write the thesis results and give discussion about the results found.
v. Finally prepare the final paper and presentation.

1.4 Scope, limitation and significances

1.4.1 Scope of this thesis

This thesis covers only the theoretical performance or simulation of a parabolic trough solar steam generator that would partially replace steam boiler in Wenji Pulp and paper factory.

1.4.2 Limitation of the study

This paper is developed on adama wether condition to simulate parabolic trough solar collector to generate steam for drying paper in wenji pulp and paper factory. So the result of this study is applicable in a place which has the same whether condition with adama and process those need steam at a temperature of 215 ^{o}C.

In this work thermal storage is not consider and the system is works only during the day.

1.4.3 Significance of the thesis

Wenji pulp and paper factory uses electric boiler is to generate the steam. This thesis will tend this factory to use solar technology rather than electric boiler to generate steam. If the factory uses the results obtained in this thesis, it will be benefited by reducing the cost of electricity it is paying for steam production.

CHAPTER TWO

LITERATURE REVIEW

2.1. Solar collector

The solar collector is main component of solar thermal system. Currently different types of collectors are available commercially based on the construction type. Solar collectors can be either concentrating or non-concentrating (Gosselar and Johnson, 2011).

- Non concentrating collectors:-have a collector that is the same as the absorber area .Flat-plate collectors are the most common and are used when temperatures below about 80^{o}C are sufficient, such as for space heating.

- Concentrating collectors:-where the area intercepting the solar radiation is greater than the absorber area. The concentrator helps to collect large amount of solar incoming radiation within a limited collector area and supplies to the absorber pipe.

Concentrating solar collectors are used for high temperature application. Concentrating collectors reflects the solar radiation falling on the collector and this enable to collect high amount of solar energy with small absorber area as the convection and radiation losses are minimized, therefore it attains high temperature.

2.2 History of parabolic trough power plant technology

John Ericsson constructed in 1880 the first known parabolic trough collector. He used it to power a hot air engine. In 1907, the Germans Wilhelm Meier and Adolf Remshardt obtained the first patent of parabolic trough technology. The purpose was the generation of steam. In 1913, the English F. Shuman and the American C.V. Boys constructed a 45 kW pumping plant for irrigation in Meadi, Egypt, which used the energy supplied by trough collectors. The pumps were driven by steam motors, which received the steam from the parabolic troughs. The constructors used parabolic trough collectors with a length of 62 m and an aperture width of 4 m. The total aperture area was 1,200 m^2.The system was able to pump 27,000 litres of water per minute (Günther et al., 2011).

Despite the success of the plant, it was shut down in 1915 due to the onset of World War I and also due to lower fuel prices, which made more rentable the application of combustion technologies.

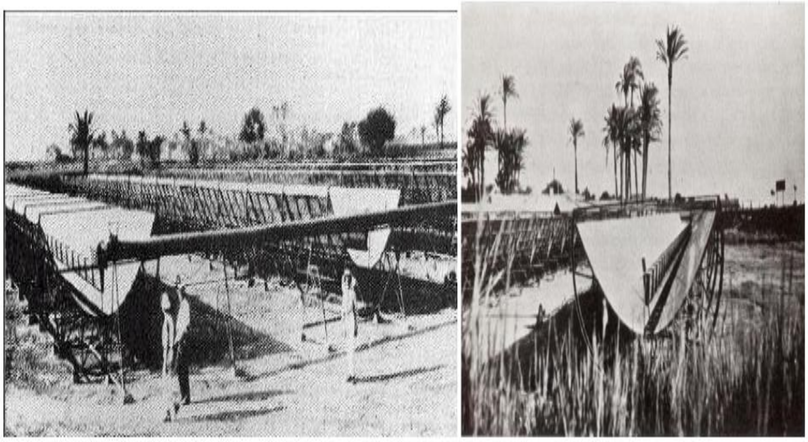

Figure 2- 1:Parabolic trough collector application in Egypt built in 1913 (Ragheb 2011; Günther et al.,2011)

The interest in the parabolic trough technology did not rise again until 1977, when the US Department of Energy as well as the German Federal Ministry of Research and Technology began to fund the development of several process heat machines and water pump systems with parabolic trough collectors. Higher fossil fuel prices encouraged the governments to take new measures. Results of these measures were, for instance, the following (Günther et al., 2011).

- Between 1977 and 1982, the company Acurex installed parabolic trough demonstration systems with a total aperture area of almost 10,000 m^2 in the USA for process heat applications.
- The first modern line-focusing solar power plant was a 150 kW facility that was built in 1979 in Coolidge/Arizona (Duffie and Beckman,2013).

- Nine member states of the International Energy Agency participated in the project of building demonstration facilities with a rated power of 500 kW at the Plataforma Solar de Almeria, which was put into operation in 1981.

- The first private financed process heat machine with 5580 m^2 parabolic trough collectors was successfully put into operation in 1983 in Arizona for thermal heating of electrolyte tanks in a copper processing company. These trough systems developed for industrial process heat application were capable of generating temperatures higher than 260°C.

In 1983, Southern California Edison (SCE) signed an agreement with Luz International Limited to purchase power from the first two commercial solar thermal power plants that should be constructed in the Mojave Dessert in California. These power plants, called Solar Electric Generating System (SEGS) I and II, started operation in the years 1985 and 1986. Later, Luz signed a number of standard offer contracts with SCE that led to the development of the SEGS III to SEGS IX plants. Initially, the plant size was limited to 30 MW. It was later raised to 80 MW. In total, nine plants with a total capacity of 354 MW were built.

Figure 2- 2:SEGS III–SEGS VII solar plants in California (Günther et al.,2011).

Until today these plants still continue in operation. The constructional and operational experience with these plants pushed the parabolic trough technology a considerable step forward and provided the basics for further technologic developments and project planning. A further expansion of the installed capacity of parabolic trough power plants did not take place until 2007, when Nevada Solar One with a capacity of 64MWe was opened in Nevada. The first commercial parabolic trough power plant in Europe, Andasol I, is generating electricity since December 2008 at a high plane near the Sierra Nevada Mountains in the Spanish.

The Andasol power plants were the first CSP plants with large thermal storage systems. Heat can be stored for 7.5 full load hours. In summer, the power plants can be operated nearly 24 hours a day (Günther et al.,2011).

2.3 Related works on parabolic trough collector

Work of other researchers on parabolic trough collector is presented below.

- Mesfin (2009) work on Modeling, Simulation and Performance Evaluation of Parabolic Trough Solar Collector Power Generation System in Addis Ababa University.

He proposed power plant that operates using Rankine power cycle principle. The power plant has two high pressure and three low pressure turbines. Accordingly there are two high and one low pressure closed feed water heaters (CFWHs). Between the high pressure and low pressure feed water heaters a deaerator exists. The complete diagram of the power plant with state points is shown in Figure 2-3.

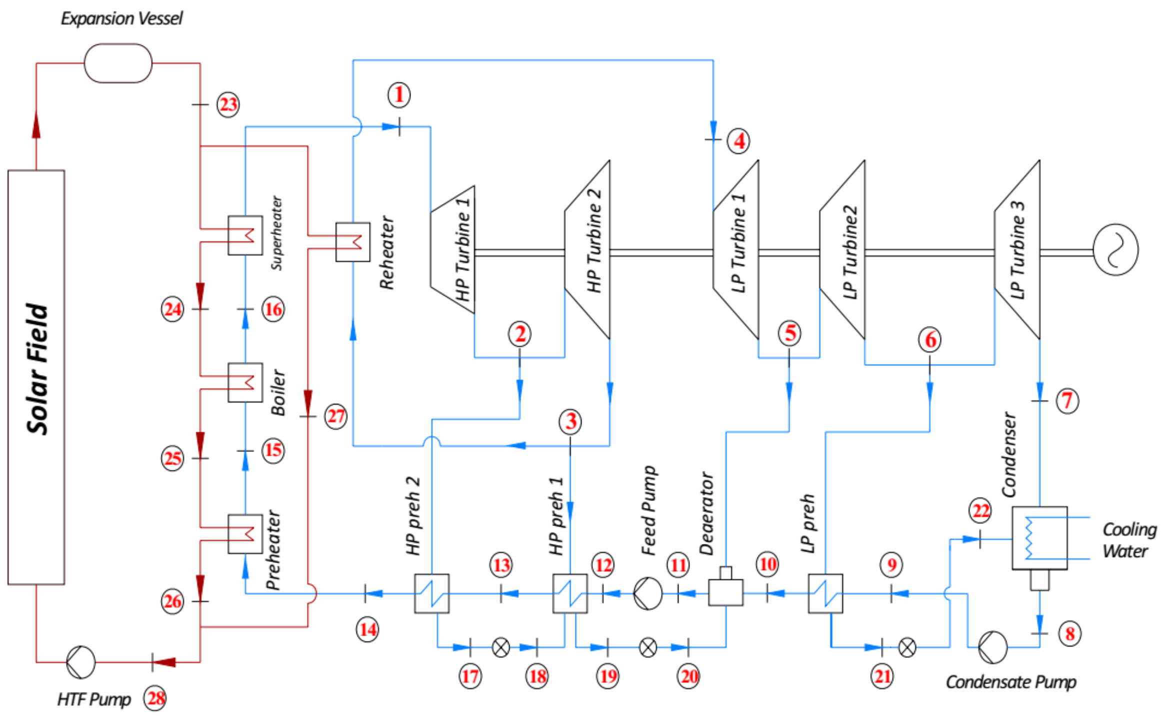

Figure 2- 3: Steam power plant (Mesfin, 2009).

Steam flows from the last turbine stage in to the condenser. The condensate is then pumped to low pressure CFWH. Next the feed water flows through the deaerator. Feed water pump is used to force the feed water to the two high pressure CFWHs and then finally to the heat exchanger train. The heat exchanger train consists of a super heater, steam generator and feed water preheater, in series, as well as a re heater in parallel with the other three heat exchangers.

The power cycle begins by collecting the HTF returning from the solar field in an expansion vessel. The expansion vessel serves to compensate for variation in the volume of the heat transfer fluid throughout the day, since the specific volume of the HTF is dependent on temperature. The heat transfer fluid is pumped from the expansion vessel and delivered to the heat exchanger train as the energy source for the power cycle.

In this work an effective area of solar field was found to be A_{eff} = 81760 m^2 and efficiency of solar field was η_{SF} =58.231%.

In this paper a power plant is designed using appropriate considerations and assumptions. The designed power plant is modeled in two simulation programs: MATLAB and TRNSYS. The MATLAB program is used only to model full load operation of the power plant. The output of the model developed by this program is used as a reference state operation in the TRNSYS model. The TRNSYS model of the power plant is used to model both the solar field and the power field. This model is developed by using component from STEC library, the TRNSYS built in library and a developed component, Type 850. The main purpose of the model developed by the TRNSYS is to investigate the operation of the power plant at weather conditions different from the reference values. Both models are used only for solar only

operation.
The performance of the model developed in the TRNSYS is evaluated for year 2001. Representative days for the selected year are used for the simulation. The results of the simulation have shown that the mass flow rate of the HTF from the solar field and gross power produced are heavily dependent on DNI. This can be seen from graphs above the mass flow rate graph and gross power graph retained the shape of the DNI graph. Cost and financial analysis is made for this power plant using Solar Advisor Model (SAM). The analysis is made by modeling the power plant with a specified capacity under Addis Ababa weather condition.

The results of this model give for rated net turbine capacity of 10 MWe the total installed cost is $60,409,962.It can also be seen that the solar field is the major source of direct costs ($24,501,000) (Mesfin,2009).

- Ghodbane and Boumeddane(2016) paper present the efficiencies study of a linear solar concentrator of a parabolic trough type.

This study was conducted on the device in Guemar area, this region is located in the state of El-Oued, which it is found in the south-east of Algeria. Six typical days were selected to conduct the study. The solar collector has been studied optically and thermally. The optical study was using SolTrace. Matlab was used as device of programing to solve the non-linear system of mathematical equations. The method of finite differences in the implicit case was used as way of solution.

The main objective of this work was to determine the water vapour temperature which can be reached through this collector in Guemar region, Algeria. This technology is mature and highly efficient; it is available today in Algeria (the hybrid power plant of Hassi R'Mel and the solar village of Adrar). An energy balance was chosen which is based on heat exchange between the four absorber tubes, the heat transfer fluid and glass tubes. A program Matlab was developed using the finite difference method in case implicit to simulate the performance of the concentrator. This study was done using real data from the parabolic trough collector of R'Mel Hassi hybrid power plant, Province of Laghouat, Algeria.

A gas / solar hybrid electric central was established in Algeria with German specifications in the region of Hassi R'Mel .This plant combine parabolic trough concentrating solar power of 25 MW with area coverage of 180,000 m^2, in conjunction with a gas turbine plant of 130 MW.

The optical performance of collector was higher i.e 83.61 %.The maximum value of thermal efficiency can reach up 82.80 %, because the inlet temperature of water is almost identical to the ambient temperature, which thus corresponds to a very good thermal insulation and the lower heat loss to the atmosphere. This reduction in the thermal efficiency after the maximum value, is due to thermal losses believe that with increasing water temperatures respectively at the inlet and outlet of the absorber.

This numerical study shows that the fluid temperature exceeds 488 K; they note that there is a change in the water liquid to vapour. This change is caused by a change in the pressure, in the temperature and in the volume of the heat transfer fluid. Finally, the results are very encouraging for the use of solar energy in the study area (Ghodbane and Boumeddane 2016).

- Assefa (2011) studies his master thesis on Techno-Economic Assessment of Parabolic trough Steam Generation for Hospital.

This project aims in analysing the Technical performance of parabolic trough steam generation and oil fired boiler steam generation system for Black lion general specialized hospital which is located in Addis Ababa and to perform economic assessment on both systems so as to make comparison test.

Black lion hospital uses one three pass (3p) wet back fire tube boiler, 3000 kg/hr steam generation capacity at a pressure of 12 bar, with another one standby to satisfy the daily steam demand of different services in the hospital.

The hospital uses furnace oil for the generation of the steam, consumes 245 m^3 and pays 1,593,087.41 birr (96,550.00 Dollar) in the fiscal year, 2,008/09 (Assefa,2011).

The main target of solar collector model is to generate 5,000 kg/hr saturated steam at 8 bar. The steam generated will be distributed to sterilizer, hot water generator and laundry drying machine. The total steam consumed in hot water generator reaches two-third of the total steam generated in the boiler and the remaining will be distributed to sterilizer and drying.

For different temperature difference between inlet and outlet of the trough collector area and thermal efficiency is checked using Matlab, optimal thermal efficiency of 62.76% and collector area 11000 m^2 is found for 300^oC at outlet and 150^oC at inlet to the trough.

The hospital currently uses diesel boilers for steam generation 365 days in a year and 9 hours a day, though due to several reasons usually it works for 4 to 5 hours a day.

The total capital cost of the system will be the sum of direct and indirect capital costs found as 89,447,452.88 birr. The economic analysis shows that although the initial investment of concentrated solar steam generation is high as compared to convention steam generation system, the reverse is observed in operation and maintenance cost, resulting concentrated solar steam generation break even (payback) to occur early, after 7 year the system let to operate over the conventional steam generation (Assefa,2011).

The steam generated will be distributed to sterilizer, hot water generator and laundry drying machine.

- Canuçkun (2013) develop a mathematical model of direct steam generation using parabolic trough collectors.

A parametric study for direct steam generation in parabolic trough collectors is presented for different inlet temperature, pressures and solar resources are analyzed.

The direct steam generation mathematical model is integrated into a TRNSYS model of a complete solar thermal power plant. The predictions for this model of a complete solar thermal power plant are compared with previously published and acceptable results are found.

The model is run for different inlet temperatures with two different cases.

- ❖ In the first case different working pressures are simulated.
- ❖ In the second case different solar resources are also simulated.

The results of DSG simulations show that for lower working pressures, the overall efficiency is higher due to lower saturation temperature of the water and consequently lower temperatures and thermal losses in the 2-phase part of the collector.

On the other hand, for lower working pressures the pressure drops are higher which can cause increase the required pumping power.

After the steam/liquid separation process, pure steam with a low mass flow rate is passed through the superheating collectors, and the steam can be heated up much higher than required and can be harmful the components. The DSG mathematical model programmed in Matlab is then linked to TRNSYS 17 software.

For the parametric studies, collector inlet temperatures from 20°C to 200°C are assumed with 20°C increments. Simulations are performed for these inlet temperatures for working pressures of 60 bars, 80 bars, 100 bars and 120 bars. All the other parameters are fixed. Another parametric study is done for varying DNI from 400W/m^2 to 1000W/m^2 with 200W/m^2 increments.

- ➢ Bellos and Tzivanidis (2018) develop analytical expression of parabolic trough solar Collector performance. The objective of their study is to develop analytical expressions for the determination of the thermal performance of parabolic trough collectors.

The non-linear equations of the energy balances in the parabolic trough collector device are simplified using suitable assumptions. The final equation set includes all the possible parameters which influence the system performance and it can be solved directly without computational cost. This model is validated using experimental literature results. Moreover, the developed model is tested using another model written in Engineering Equation Solver under different operating conditions.

The impact of the inlet fluid temperature, flow rate, ambient temperature, solar beam irradiation and the heat transfer coefficient between cover and ambient are the investigated parameters for testing the model accuracy. According to the final results, the thermal efficiency is found with high accuracy; the deviations are found to be up to 0.2% in the majority of the examined cases.

In every case, only one parameter is variable, while the other parameters have their default values. This technique aids to perform a suitable sensitivity analysis in the developed model and to check its behaviour with different parameters.

Eight different cases are examined. The outlet temperature and the thermal efficiency are compared for experimental results (EXP) and the results of the model (MODEL).The mean deviation in the outlet temperature is found to be 0.06% and in the thermal efficiency, 1.16%. These values are relatively low and so it is proved that the developed model is valid for various operating conditions.

2.4 Conclusions from literature review

A PTC solar power plant works best between 40° north and south latitudes regions. In these regions solar beam radiation is high.

PTC solar power plants are the most developed, proven and cheapest way to use solar energy to produce electricity and thermal energy since significant work on PTC solar power plants has been completed, including experiments and prototypes. Also PTC is currently the most commercially proven way for CSP plants, which proves its suitability.

Parabolic Trough is used for any low to medium process heat applications. It can attain a maximum temperature up to 250°C as per requirement in industries.

Therefore, developing PTC at Wenji Pulp and Paper Factory to provide process steam can solve the problem of cost of energy in the factory.

CHAPTER THREE

PAPER PRODUCTION PROCESS

3.1 Introduction

Wenji Pulp and Paper Share Company operates a paper mill and corrugated box manufacturing enterprise located near the city of Nazareth, about 100 km south east of the capital city of Addis Ababa. The mill is owned jointly, 70% by the Government of Ethiopia and 30% by the International Finance Corporation (IFC) part of the World Bank Group.

This paper plant was constructed in the late 1960's and commissioned in 1970. The mill has a single paper machine width a 2,840 mm reel trims. Presently, the factory uses imported pulp as feed stock to produce different grades of paper such as printing, writing, wrapping, corrugated, and board for book covers in the 45 to 350 gsm basis weight range.

The production start by hydra pulping of the raw materials (furnishes) with sequences of sub process. The paper production in the factory produce paper using foundries machine which is a standard machine for paper production. The company's paper machine is composed of Forming machine, Press machine, Drying section and calender/reel section.

3.2 Paper production process

3.2.1 Stock preparation

This process covers the process from hydra pulp to machine head box.

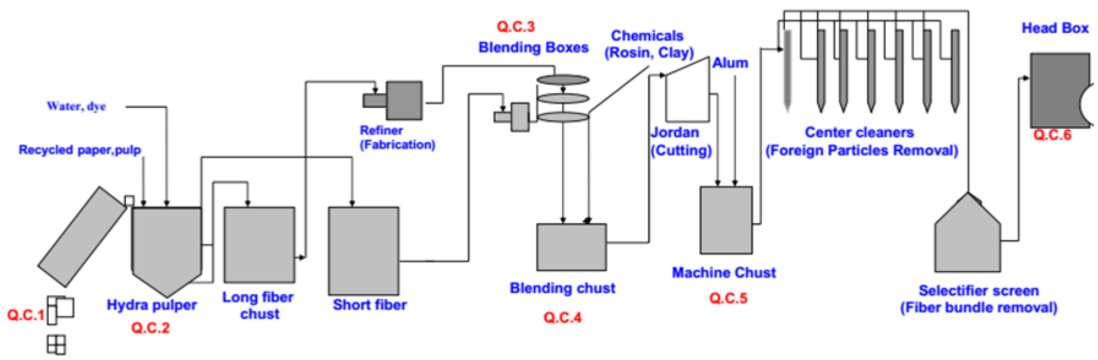

Figure 3- 1: Stock preparation flow diagram

3.2.2 Paper production

This cover from wire section to winder machine.

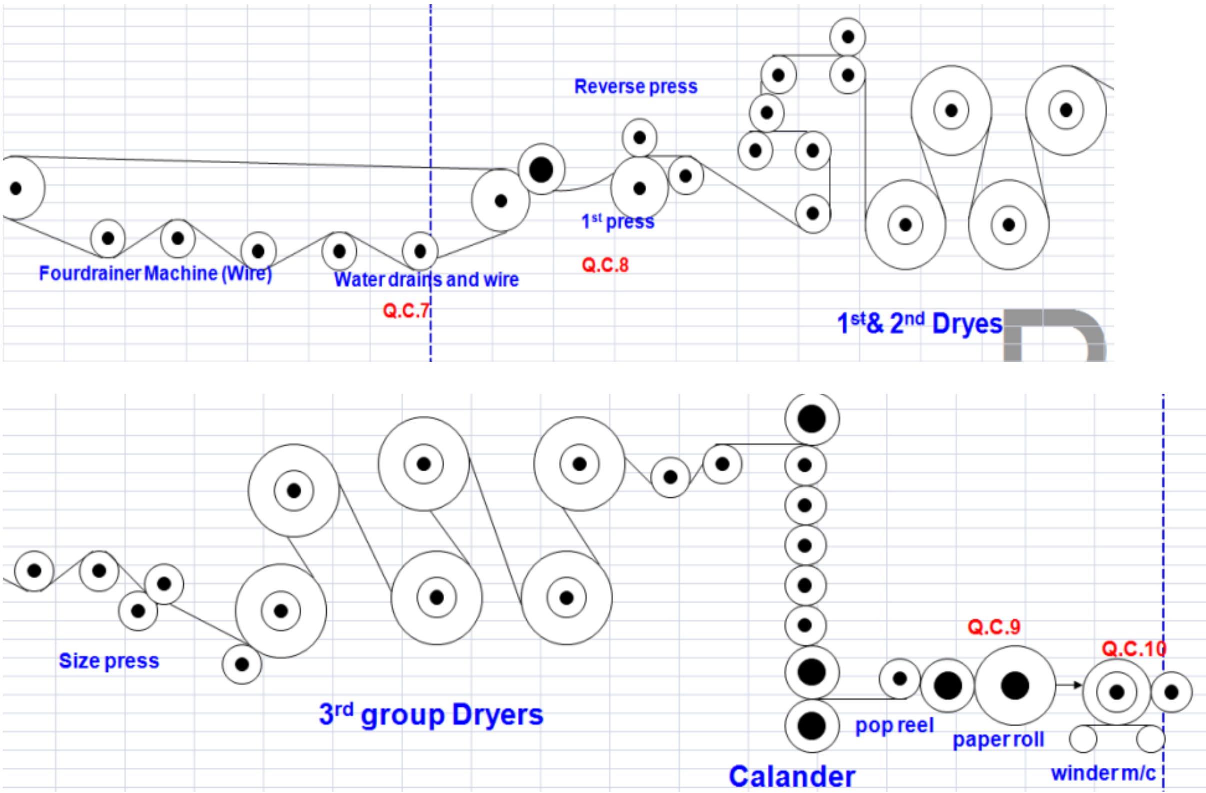

Figure 3- 2: Paper production flow diagram

3.3 Resistor electric boiler

Boiler is the main supply of steam for the industry. The higher energy source of the factory which is steam is produced by two boilers. By the principle of an electric resistors inserted into the water tanker and boil the water to generate steam.

Giving up to 660 V electric source connected to the resistor tube, since the resistor prevent the current to flow with it there exist heat on the resistor tube and also the treated water hardness is very low. So the water boils and finally steam will be generated.

Advantage: less water treatment required & less prone to explode.

Disadvantage: steam generation is somewhat less compare to electrode.

There are two resistor boilers in Wenji pulp and paper share company (WPPSC) which has different capacity.

The following two tables represent the nameplate data for the two boilers existing in WPPSC:

Table3- 1: Nameplate Data for the Smaller Electric Steam Boiler

Manufacturer	Grarini Aval
Serial №	280.11
Year	2011
Capacity	3,000 kW
Steam Production	4,302 kg/h
Safety Valve Set Pressure	20 bar
Fluid Group	2
Temperature	Min. 0 ^{o}C & Max. 215 ^{o}C
Maximum Working Pressure	20 bar
Volume	13,355 Lt
Pressure Test Date	22/11/2011
Pressure Test	36.3 bar
Voltage	660 V
Frequency	50 Hz
Empty Weight	9,920 kg
Filling Mass	10,000 kg

Table3- 2:Nameplate Data for the Larger Electric Steam Boiler

Manufacturer	Grarini Aval
Type	GEV 6000
Serial №	257.13
Design Code	VSG ED.95
Year	2013
Capacity	6,000 kW
Steam Production	8,600 kg/h
Safety Valve Set Pressure	20 bar
Fluid Group	2
Temperature	Min. 0 ^{o}C & Max. 215 ^{o}C
Maximum Allowable Pressure	20 bar
Maximum Operating Pressure	20 bar
Volume	14,070 Lt
Pressure Test Date	29/11/2013
Pressure Test	34.4 bar
Voltage	660 V
Frequency	50 Hz
Empty Weight	9,000 kg
Filling Mass	10,630 kg

3.4 Description of data analysis

The following Tables 3-3 up to 3-7 shows energy utilization reports are obtained from Wenji pulp and paper factory.

Table3- 3: Yearly Energy Utilization Report for 2014 (Tafesse,2016).

Months	Product Achieved (ton)	Utilized Energy by Electric Steam Boilers (kWh)	Utilized Energy by Motors(kWh)	Total Utilized Energy (kWh)	Utilized Energy per ton of Product(kWh /ton)	Cost per ton of Product (Birr/ton)
January	481.31	1,245,083.12	321,028.74	1,566,111.86	3,253.85	1,329.52
February	398.82	1,269,600.05	280,978.76	1,550,578.81	3,887.92	1,588.60
March	649.65	1,987,033.50	386,666.38	2,373,699.88	3,653.81	1,492.95
April	472.75	1,222,939.57	316,430.41	1,539,369.98	3,256.20	1,330.48
May	705.91	1,917,654.53	437,306.34	2,354,960.87	3,336.06	1,363.11
June	970.17	2,509,697.06	577,626.01	3,087,323.07	3,182.25	1,300.27
July	757.70	2,051,628.18	464,806.36	2,516,434.54	3,321.15	1,357.02
August	624.20	1,689,264.93	321,426.85	2,010,691.78	3,221.23	1,316.20
September	765.20	2,071,029.65	468,788.79	2,539,818.44	3,319.16	1,356.21
October	644.44	1,819,200.00	346,942.84	2,166,142.84	3,361.28	1,373.42
November	628.15	1,544,900.00	308,957.90	1,853,857.90	2,951.30	1,205.90
December	620.59	1,533,599.70	350,326.51	1,883,926.21	3,035.70	1,240.39
2014 Year	7,718.89	20,861,630.29	4,581,285.89	25,442,916.2	3,296.19	1,346.82

Table3- 4: Yearly Energy Utilization Report for 2015 (Tafesse,2016).

Months	Product Achieved (ton)	Utilized Energy by Electric Steam Boilers (kWh)	Utilized Energy by Motors(kWh)	Utilized Energy per ton of Product (kWh/ton)	Cost per ton of Product (Birr/ton)	Cost per ton of Product(Birr/ton)
January	221.75	703,614.56	220,902.98	924,517.51	4,169.19	1,703.53
February	183.27	585,691.00	195,237.22	780,928.22	4,261.08	1,741.08
March	161.28	542,491.00	194,970.15	737,461.15	4,572.55	1,868.34
April	215.59	693,571.79	214,994.32	908,566.11	4,214.32	1,721.97
May	257.90	762,550.65	243,214.65	1,005,765.27	3,899.83	1,593.47
June	315.76	856,880.99	281,806.66	1,138,687.65	3,606.18	1,473.49
July	703.56	1,920,013.46	435,850.53	2,355,863.99	3,348.49	1,368.19
August	540.35	1,497,811.52	376,228.62	1,874,040.14	3,468.20	1,417.11
September	676.96	1,851,202.90	418,433.63	2,269,636.53	3,352.69	1,369.91
October	507.91	1,413,893.68	357,916.06	1,771,809.74	3,488.43	1,425.37
November	560.11	1,548,927.94	387,383.25	1,936,311.19	3,457.02	1,412.54
December	563.85	1,558,555.58	389,494.36	1,948,049.94	3,454.91	1,411.68
2015 Year	4,908.29	13,935,205.07	3,716,432.53	17,651,637.60	3,596.29	1,469.44

Table3- 5: Yearly Energy Utilization Report for 2016 (Tafesse, 2016).

Months	Product Achieved (ton)	Utilized Energy by Electric Steam Boilers (kWh)	Utilized Energy by Motors (kWh)	Total Utilized Energy (kWh)	Utilized Energy per ton of Product (kWh/ton)	Cost per ton of Product (Birr/ton)
January	501.16	1,743,085.58	256,678.61	1,999,764.19	3,990.27	1,630.42
February	518.90	1,690,805.80	246,871.87	1,937,677.67	3,734.20	1,525.79
March	404.23	1,673,792.80	295,789.99	1,969,582.79	4,872.43	1,990.88
April	453.37	1,845,599.20	312,475.97	2,158,075.17	4,760.08	1,944.97
May	540.64	2,068,800.00	311,229.71	2,380,029.71	4,402.25	1,798.76
June	741.95	2,109,600.00	365,954.11	2,475,554.11	3,336.55	1,363.31
July	288.64	1,096,800.00	340,133.43	1,436,933.43	4,978.29	2,034.13
August	402.69	1,536,000.00	475,612.84	2,011,612.84	4,995.44	2,041.14
September	511.96	1,601,999.30	467,119.63	2,069,118.93	4,041.57	1,651.39
October	Data for these months not obtained, so that estimation will be made in this work					
November						
December						
2016 Year (for three remaining Months) estimation	1,203.29	4,234,799.3	1,282,865.9	5,517,665.2	4,585.5	1,726.56
2016 Year (Estimation)	5,566.83	19,601,281.98	3,934,332.06	23,535,614.04	4227.83	1,726.56

Table3- 6: Average Values of Product Achieved and Energy Utilized for the Three Years Yearly Energy Utilization Report (Tafesse,2016).

Year	Total Product Achieved (ton)	Utilized Energy by Electric Steam Boilers (kWh)	Utilized Energy by Motors (kWh)	Total Utilized Energy (kWh)	Utilized Energy per ton of Product (kWh/ton)
2014	7,718.89	20,861,630.29	4,581,285.89	25,442,916.18	3,296.19
2015	4,908.29	13,935,205.07	3,716,432.53	17,651,637.60	3,596.29
2016	5,818.05	20,488,643.57	4,095,821.55	24,584,465.12	4,225.55
Average	6,148.41	18,428,492.98	4,131,179.99	22,559,672.97	3,706.01

Table3- 7: Maximum and Minimum Values of Utilized Energy per ton of Product for the Three Years Yearly Energy Utilization Report (Tafesse,2016).

Year	Maximum Value of Utilized Energy per ton of Product (kWh/ton)	Minimum Value of Utilized Energy per ton of Product (kWh/ton)
2014	3,887.92	2,951.30
2015	4,572.55	3,348.49
2016	4,995.44	3,336.55

3.5 Calculation of average electric input power to electric steam boilers

From Table 3-6, it can be known that the average value of total utilized energy by electric steam boilers is 18,428,492.98 kWh. Let assume that the electric boiler is worked throughout the year except ten days left for maintenance in a year. So 355 days assumed for full running of electric boiler which is 8520 hours of working hours in a year.

$$\text{Average input power to boilers} = \frac{\text{Total Annual Utilized Energy by Boilers}}{\text{Number of Working Hours in a Year}} \quad \text{……………………..(3.1)}$$

$$\text{Average input power to boilers} = \frac{18{,}428{,}492.98\ \text{kWhr}}{8520\text{hr}} = \underline{2163\ \text{kW}}$$

CHAPTER FOUR

PARABOLIC TROUGH MODEL

4.1 Introduction.

Parabolic trough concentrator works by focusing direct sun beam onto a linear receiver. The direction of the reflector surface should be arranged according to the position of the sun at each instant in time. A heat transfer fluid (HTF) gets heated up as it flows through the receiver. The hot HTF then leaves the collector and is used to produce steam in heat exchanger. The resulting steam can be used as process steam (Heng et.al,2006).

In this section about parabolic trough system component and mathematical geometry of PTC, optical efficiency, thermal efficiency, effective area of PTC, mass flow rate and solar beam radiation that used for simulation of PTC will be discuss.

Parabolic trough system consists of large fields of parabolic trough collectors, a heat transfer fluid/steam generation system. The collector field is made up of a large field of single-axis-tracking parabolic trough solar collectors. A heat transfer fluid (HTF) is heated and it circulates through the collectors and returns to a series of heat exchangers (HX), where the fluid is used to generate saturated steam (20 bar, 215 ºC).

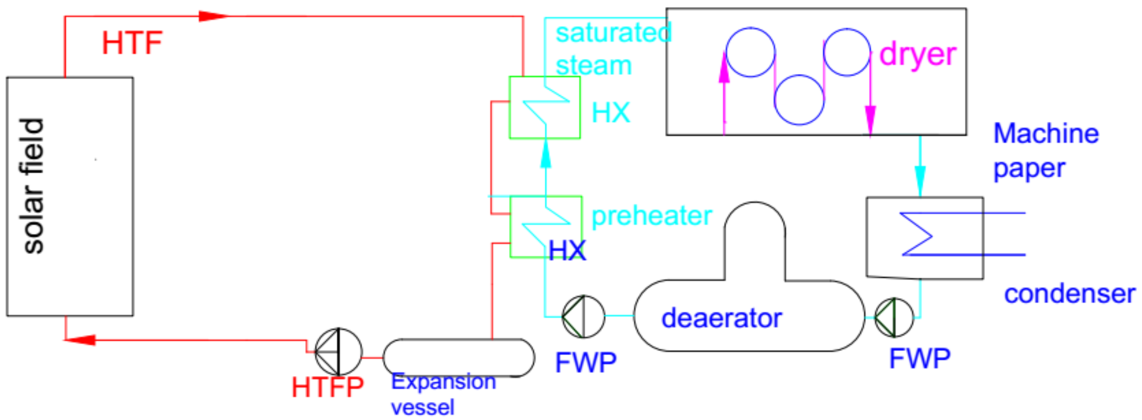

Figure 4- 1: Schematic flow diagram of a parabolic trough solar steam generator

Figure 4-1 shows a process flow schematic for a typical large-scale parabolic trough solar steam generators.

Exhaust HTF from steam generator heat exchanger is entering to preheater heat exchanger for preheating feed water. Exhaust HTF from preheater enters to expansion vessel and pumped to solar field.

The saturated steam generated is then sent to dryer section of machine paper to dry the paper. Exhaust steam from dryer section of machine paper is sent to condenser to be condensed.

- **Condenser**

The exhaust steam from dryer section is entering to condenser. The condenser is a closed shell-and-tube heat exchanger, with cooling water flowing on the tube side and condensing steam from the dryer on the shell side. The function of the condenser is to condense the dryer exhaust from vapor to liquid, so the working fluid can be pumped back to the deaerator.

- **Pump**

The pumps in the cycle serve to increase the pressure of the working fluid. There are two pumping processes on the working fluid side of the cycle. One set of pumps is located at the condenser outlet to pump the fluid from condenser to deaerator. Another set of pump is located at the deaerator outlet to pump the fluid from deaerator to preheater and saturated steam generator heat exchanger.

Finally one pump on HTF side to transport HTF from expansion vessel through the collector field.

- **Deaerator**

A deaerator is a device that is widely used for the removal of oxygen and other dissolved gases from the feedwater to steam-generating boilers. In particular, dissolved oxygen in boiler feedwaters will cause serious corrosion damage in steam systems by attaching to the walls of metal piping and other metallic equipment and forming oxides (rust).

The spray-type deaerator consists only of a horizontal (or vertical) cylindrical vessel which serves as both the deaeration section and the boiler feedwater storage tank (Saad,2015-2016).

- **Expansion Vessel**

Expansion vessel should cause positive fluid pressure to the pump's suction side during system start-up and should minimize the vapor space in the tank during normal operation.

4.2 Material for parabolic trough collector

Critical factors to be considered in the analysis of the solar concentrating collector are its material properties. When radiation strikes a body, part of it is reflected, a part is absorbed and if the material is transparent, a part is transmitted. The fraction of the incident radiation reflected is the reflectance (ρ), the fraction of the incident radiation transmitted is the transmittance (τ) and the fraction absorbed is the absorptance (α) as shown schematically in figure 4-2.

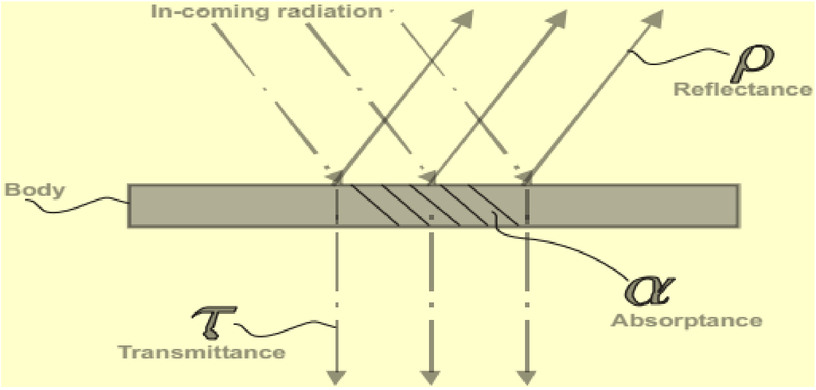

Figure 4- 2: Reflection, Absorption and Transmission of incident solar radiation by a solid body (Sintali et al.,2014).

Table 4- 1:List of material for main components module (Heng et.al,2006).

Component	Material
Absorber pipe	304L Stainless steel
Glass cover	Borosilicate glass pipe
Receiver support	Anodized aluminium
Cantilever arm	3 mm thick, 38 mm square tubular mild steel
Torque-box central frame	3 mm thick, 38 mm square tubular mild steel
Trough-base	3 mm thick aluminium sheet

4.2 Geometry of parabolic trough collector

The parabolic trough collector is a trough which has the shape of a part of a parabola. More exactly, it is a symmetrical section of a parabola around its vertex.

The following four parameters are commonly used to characterize the form and size of a parabolic trough (Günther et al.,2011).

- Focal length,
- Trough length,
- Aperture width and
- Rim angle

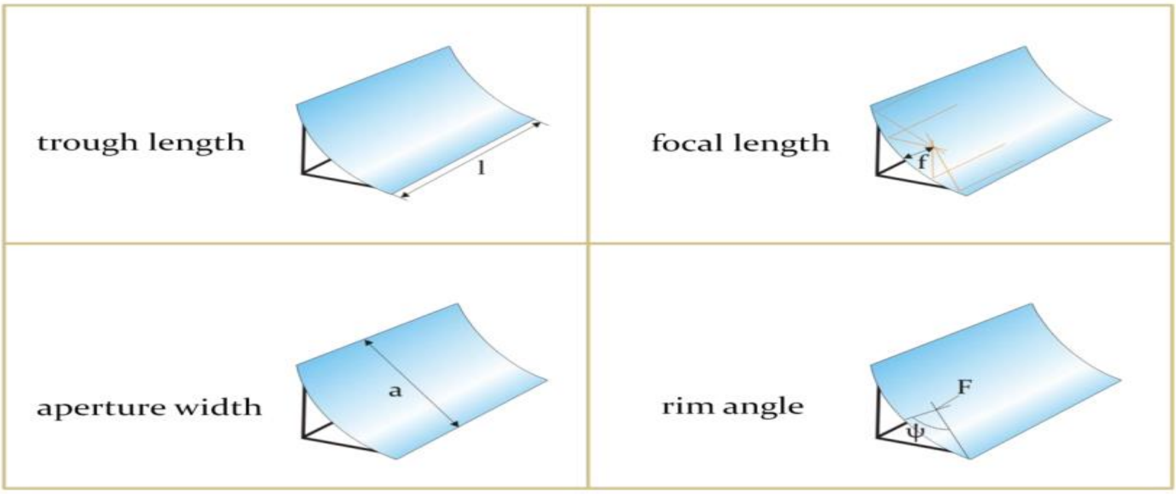

Figure 4- 3: Geometrical parabolic trough parameters (Günther et al.,2011)

4.2.1 Focal length

Parabolic troughs have a focal line, which consists of the focal points of the parabolic cross-sections. Radiation that enters in a plane parallel to the optical plane is reflected in such a way that it passes through the focal line. Focal length f is the distance between the vertex of the parabola and the focal point (Günther et al.,2011).

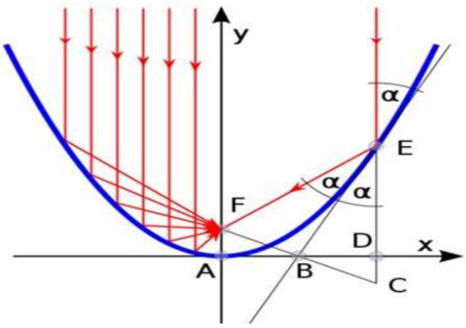

Figure 4- 4: Path of parallel rays at a parabolic mirror (Günther et al.,2011)

An appropriate analytic representation of a parabola is given by:

$$y = \frac{1}{4f}x^2 \quad \text{……………………………………..………… (4-1)}$$

Where f is the focal length

4.2.2 Rim angle

The rim angle the angle between the optical axis and the line between the focal point. The rim angle ψ can be expressed as a function of the ratio of the aperture width to the focal length (Günther et al.,2011).

$$\tan\psi = \frac{\frac{a}{f}}{2-\frac{1}{8}(\frac{a}{f})^2} \quad \text{………………………………………… (4-2)}$$

The rim angle of real parabolic troughs is around 80°.

4.2.3 Mirror area and aperture area

At a given DNI and a given Sun position aperture area determines the radiation capture. The aperture area is calculated as the product of the aperture width and the collector length (Günther et al.,2011).

$$A_{ap} = a * l \qquad (4\text{-}3)$$

The surface area of a parabolic trough may be important to determine the material need for the trough. The area is calculated as follows(Günther et al.,2011)

$$A = \left(\frac{a}{2}\sqrt{1+\frac{a^2}{16f^2}} + 2f * \ln\left(\frac{a}{4f} + \sqrt{1+\frac{a^2}{16f^2}}\right)\right) * l \qquad (4\text{-}4)$$

4.2.4 Geometrical concentration ratio

The geometrical concentration ratio is a useful approximation. It is defined as the ratio of the collector aperture area to the receiver aperture area.

$$\mathbf{C_G} = \frac{\mathbf{A_{ap,c}}}{\mathbf{A_{ap,r}}} = \frac{\mathbf{w \cdot l}}{\mathbf{d \cdot l}} = \frac{\mathbf{w}}{\mathbf{d}} \qquad (4\text{-}5)$$

In many cases, the projected area of the absorber tube is chosen. In this case the receiver aperture area is a rectangle with the area $d * l$, where d is the absorber tube diameter.

Another possibility is to take the irradiated absorber surface area as the receiver aperture area. In real parabolic troughs this would mean that the whole absorber tube surface area $\pi \cdot d \cdot l$ is the receiver aperture area.

$$\mathbf{C_G} = \frac{\mathbf{A_{ap,c}}}{\mathbf{A_{ap,r}}} = \frac{\mathbf{w \cdot l}}{\mathbf{\pi \cdot d \cdot l}} = \frac{\mathbf{w}}{\mathbf{\pi \cdot d}} \qquad (4\text{-}6)$$

This definition would lead to a lower geometrical concentration ratio. However, the concentration ratio according to the projected areas is more commonly used.

Table 4- 2: Parameters used for simulation of parabolic trough solar steam generators

Parameter	Symbol	Value	Referance
Width of the PTC	W	5.0 m	Duffie and Beckman,2005
Focal distance of the PTC	F	1.84 m	
Distance between solar row	L_{SR}	12 m	
Concentration ratio of the PTC	C	22.74	
Receiver inner diameter	D_{ri}	66×10^{-3} m	Bellos and Tzivanidis ,2018
Receiver outer diameter	D_{ro}	70×10^{-3} m	
Cover inner diameter	D_{ci}	109×10^{-3} m	
Cover outer diameter	D_{co}	115×10^{-3} m	
Receiver emittance	ε_r	0.2	
Cover emittance	ε_c	0.9	
Receiver absorptance	α	0.96	
Cover transmittance	τ	0.95	
Mirror reflectance	ρ_c	0.83	
Incident angle modifier (Zero incident angle)	K	1	
Incident angle	θ	0^o	
Receiver thermal conductivity	K	54 W/m.K	

4.3 Heat transfer fluid

A HTF has to fulfil certain requirements.

- ✓ It must be liquid
- ✓ It is not evaporated under the high temperatures that are reached in the solar field.
- ✓ Low freezing temperatures are an advantage so that no freezing protection measures are necessary if the temperatures in the solar field get low.
- ✓ It is also important that its thermal stability is sufficient to stand the high operation temperatures (so no thermal cracking).

The following table gives an overview over some properties of appropriate candidates for a usage as HTF in parabolic trough collectors.

Table 4- 3: Heat Transfer Fluids (Mesfin,2009)

Name	Type	Min HTF Temp [^{o}C]	Max Operating Temp [^{o}C]	Freeze Point	Comments
Solar Salt	Salt	260	600	220	
Caloria	Mineral Hydrocarbon	-20	300	-40	Used in first Luz trough plant, SEGS I
Hitec XL	Nitrate salt	150	500	120	New generation
Therminol VP-1	Mixture of Biphenyl and Diphenyl Oxide	50	400	12	Standard for current generation HTF systems
Hitec	Nitrate Salt	175	500	140	For high temperature systems
Dowtherm Q	Synthetic	-30	330	-50	New generation
Dowtherm RP	Synthetic	-20	350	-40	New generation

The solar field heat transfer fluid (HTF) absorbs heat as it circulates through the heat collection elements in the solar field and transports the heat to the secondary fluid where it is used to run end use devices. Several types of heat transfer fluid are used for trough systems, including hydrocarbon (mineral), synthetics, silicones and nitrate salts.

For this analysis Therminol VP-1 HTF is selected for the simulations of Wenji pulp and paper factory, due to better stability in liquid phase at elevated temperature and heat transfer properties.

Table 4- 4:Property of heat transfer fluid (Benidir et al.,2018)

HTF type	THERMINOL VP-1
HTF density (kg/m3)	-0.90797 T (°C) + 0.00078116T^2 (°C) - 2.367 × 10^{-6} T^3(°C) + 1083.25
HTF specific heat (kJ/kg K)	0.002414 T (°C) + 5.9591 × $10^{-6}T^2$ (°C) -2.9879× 10^{-8} T^3 (°C) + 1.498
HTF thermal conductivity (W/m K)	-8.19477× 10^{-5} T (°C) -1.92257× $10^{-7}T^2$ (°C) + 2.5034× $1O^{-11}T^3$(°C) +0.137743
HTF kinematic viscosity (m^2/s)	$e^{\left(\left[\frac{544.149}{T(℃)+114.43}\right]-2.59578\right)}$

When the plant operates at its rated capacity the whole volume of the absorber tube in the solar field is filled by the HTF. At this operating condition the mass of the HTF in the solar field can be found as shown below (Assefa,2011).

$$\mathbf{M_{SF}} = \frac{\pi\cdot(\mathbf{D_{HCE}})^2}{4} \cdot \mathbf{L_{sca}} \cdot \mathbf{N_{sca}} \cdot \boldsymbol{\rho}(\mathbf{T_{avg}}) \ldots\ldots\ldots\ldots\ldots\ldots\ldots\ldots\ldots\ldots\text{(4-7)}$$

Where:

M_{SF} = mass of the HTF in the solar field (kg)

D_{HCE}=inner diameter of the steel absorber tube

Lsca = length of one solar collector assembly (SCA) loop

N_{sca}= number of SCA loops in the solar field

ρ = density of heat transfer fluid (Therminol VP-1) (kg/m^3)

T_{avg}= average temperature of the HTF in the solar field = 225 (^oC)

4.4 Over-temperature protection

Overheating can cause liquid expansion or excessive pressure, which may burst piping or storage tanks (Duffie and Beckman,2005).

The solar system can be protected from overheating by a number of methods, such as:

- ✓ Stopping circulation in the collection loop until the storage temperature decreases (in air systems).
- ✓ Discharging the overheated water from the system and replacing it with cold make-up water.
- ✓ Using a heat exchanger coil for rejecting heat to the ambient air

4.5 Solar thermal performance simulation model of PTC steam generators

The parabolic trough collector based on the model of Lippke (Schwarzbözl and Eiden,2002) uses an integrated efficiency equation to account for the different fluid temperature at the field inlet and outlet of the collector field.

The net heat gain by parabolic trough is given by (Schwarzbözl and Eiden,2002)

$$\mathbf{Q_{net}} = \dot{\mathbf{m}}\mathbf{c_p}(\mathbf{T_{out}} - \mathbf{T_{in}}) \ldots\ldots\ldots\ldots\ldots\ldots\ldots\ldots\ldots\ldots\text{(4-8)}$$

Using

$$\mathbf{Q_{net}} = \mathbf{Q_{abs}} - \mathbf{Q_{pipe}} \ldots\ldots\ldots\ldots\ldots\ldots\ldots\ldots\ldots\ldots\text{(4-9)}$$

Heat absorbed by the receiver of the parabolic trough collector is given by (Schwarzbözl and Eiden,2002).

$$Q_{abs} = A_{eff} * Ib * \eta_{SF} \ldots\ldots\ldots\ldots\ldots\ldots\ldots\ldots\ldots\ldots\text{(4-10)}$$

$$\mathbf{A_{eff}} = \mathbf{w} * \mathbf{L} \quad \text{...(4-11)}$$

Where:

A_{eff} is effective area

W is width of the collector

L is length of the collector

Ib is direct beam irradiance

η_{SF} is collector efficiency and it is given by:

$$\eta_{SF} = K * EL * RS \left[A + B * \frac{\Delta T_{out} + \Delta T_{in}}{2}\right] +$$

$$(\mathbf{C} + \mathbf{C_w} * \mathbf{WS}) * \frac{\mathbf{\Delta T_{out}} + \mathbf{\Delta T_{in}}}{\mathbf{2 * Ib}} + \mathbf{D} * \frac{\mathbf{\Delta T_{out}} * \mathbf{\Delta T_{in}} + \frac{1}{3}(\mathbf{\Delta T_{out}} - \mathbf{\Delta T_{in}})^2}{\mathbf{Ib}} \quad \text{........ (4-12)}$$

The coefficients A, B, C, C_w and D are empirical factors describing the performance of the collector.

Where:

K is the incident angle modifier,

EL considers end losses

RS parallel row shading

ΔT_{in} is the difference between collector inlet and ambient temperature

ΔT_{out} is the difference between collector outlet and ambient temperature.

Ib is the beam radiation (direct normal irradiation).

Q_{pipe} accounts for losses in the piping and expansion vessel using empirical coefficients.

4.5.1 Piping and expansion vessel heat losses

In the operation of a distributed Solar Power Plant, the heat losses in all the piping are important and have to be included in the model. Additionally, the heat losses in the expansion vessel,which has a large surface area, should be included in the calculations. Both heat losses are considered to be temperature dependent. The following dependency was implemented in the model.

$$\dot{\mathbf{Q}}_{\mathbf{pipe}} = \dot{\mathbf{Q}}_{\mathbf{piping}} + \dot{\mathbf{Q}}_{\mathbf{expansion\ valve}} \quad \text{.......................... (4-13)}$$

$$\dot{\mathbf{Q}}_{\mathbf{pipe}} = \mathbf{20}\,\frac{\mathbf{W}}{\mathbf{m^2}}\,\mathbf{A_{eff}}\,\frac{\mathbf{T_{avg}}}{\mathbf{225℃}} + \mathbf{2.57} \times \mathbf{10^6 W}\,\frac{\mathbf{T_{avg}}}{\mathbf{275℃}} \quad \text{............(4-14)}$$

Here, heat losses of all the piping of 20 W per meter square aperture area, A_{eff} , are assumed at full power at a mean solar field temperature above ambient of about T_{avg} = 225. The radiation and mixed convection heat losses of the expansion vessel is estimated to be 2.57 MW at 300^{O}C field outlet temperature by assuming poor insulation conditions (Mesfin,2009).

4.5.2 Incidence angle modifier

The incident angle modifier K is the ratio of collector efficiency at any angle of incidence, to that at normal incidence. It is measured experimentally by varying the angle of incidence under noon time solar irradiance conditions with ambient temperature heat transfer fluid passing through the collector. A regression analysis of the data is used to obtain from (Duffie and Beckman,2005).

$$K=\cos(\theta)-B(\theta) - C(\theta)^{2} \quad \text{……………………………………..(4-15)}$$

Where:

K = Incident angle modifier value ranges from 0 to1

θ = Solar beam incident angle

B = Coefficient for linear term

C = Coefficient for nonlinear term

The equation is applied for temperatures between ambient and 400^{o}C, at any insolation level from 100 to 1100 W/m^{2}, and at any incident angle from 0 to 60 degrees.

$$K = \cos(\theta) - 0.0003512(\theta) - 0.00003137(\theta)^{2} \quad \text{…………………..(4-16)}$$

4.5.3 Row shading

Generally at any solar field the collectors are arranged in parallel rows. The distance between the collector rows is $L_{Spacing}$ = 12.5 m at SEGs VI. Hence, in the morning, at sunrise, when the first sunrays fall on the trough collector field, the first row may be unobstructed, but the following rows are shaded by the first. During the sun's path in the morning, partial shading of the collectors occurs until a particular zenith angle is reached.

The shading reduces the effective width of the collector and thus reduces the effective aperture area of the collector on which the solar beam radiation acts. Consequently, the absorbed solar energy is reduced as well. After a certain zenith angle is reached, there is no mutual shading of the collectors anymore as described very well in figure 4-5. The same phenomenon occurs, of course, in the evening during sunset (Assefa,2011).

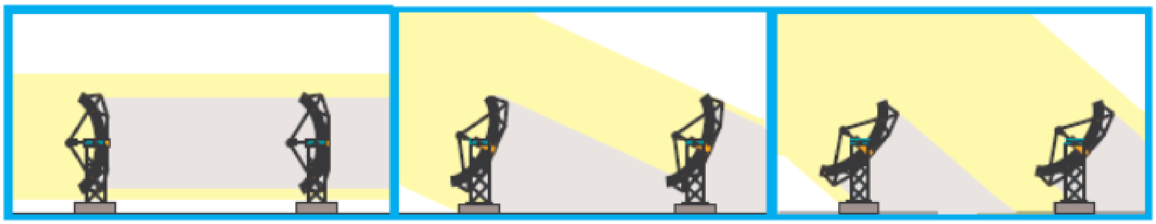

Figure 4- 5: Collector tracking through morning, showing digression of collector shading as the day progresses (Assefa,2011).

The row shadow factor is the ratio of the effective mirror aperture width to the actual mirror aperture width. This ratio can be derived from the geometry of the solar zenith angle, the incidence angle, and the layout of the collectors in a field.

$$RS=\frac{L_{Spacing}}{W}\frac{Cos(\theta_Z)}{Cos(\theta)}\text{...(4-17)}$$

Where:

RS = row shadow factor

$L_{Spacing}$ = length of spacing between troughs

w = collector aperture width (5 [m] for LS-2)

θ_Z= Zenith angle

θ = angle of incidence

Where RS ∈ [0; 1] A value of 0 for RS means complete shading where as a value of 1 for RS means no shading of the collector.

$$RS=min[max(0.0;\frac{L_{Spacing}}{W}\frac{Cos(\theta_Z)}{Cos(\theta)});1.0]\text{..............................(4-18)}$$

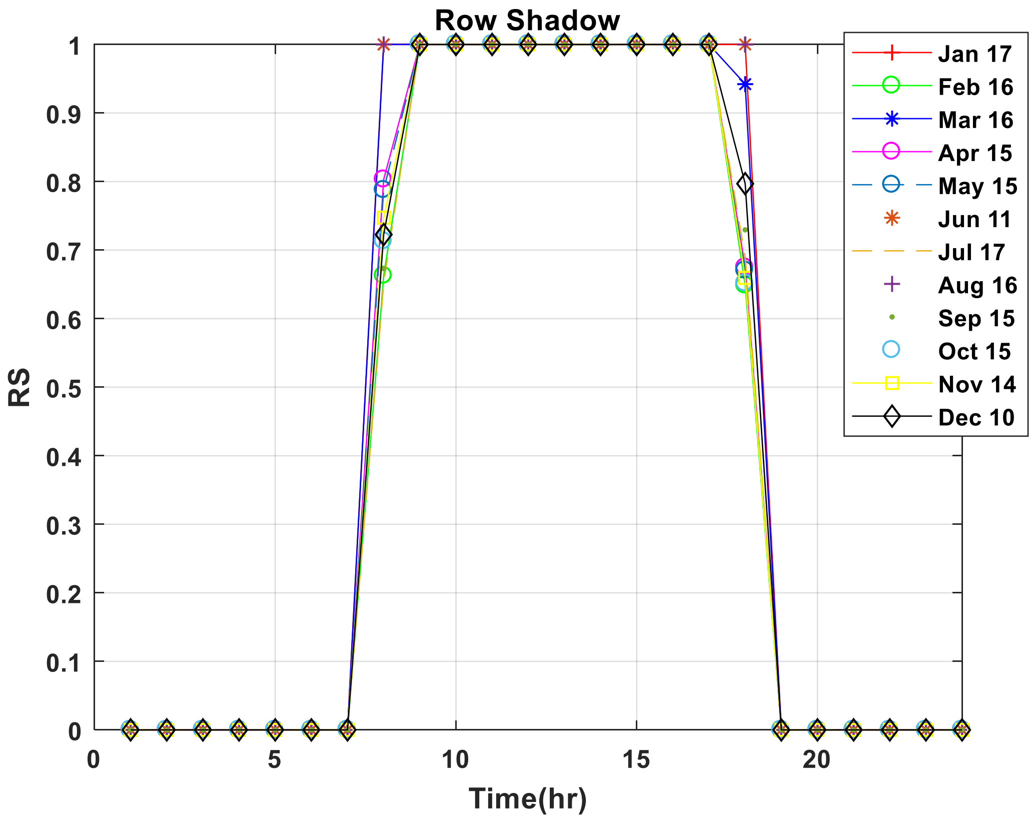

Figure 4- 6: Row shading versus time

The above equation for row shading is plotted as shown in Figure 4-6 for Adama with latitude 8.51447° east.

4.5.4 Heat gain per unit area of parabolic trough collector

A multiple linear regression of calculated heat gain over the range of insolation from zero to 1100 W/m^2, and a temperature from ambient to 400 °C produces a heat gain equation of the following form.

$$\mathbf{q} \ = \mathbf{A}(\mathbf{Ib}) - \mathbf{B}(\mathbf{Ib})(\Delta\mathbf{T}) - \mathbf{C}(\Delta\mathbf{T}) - \mathbf{D}(\Delta\mathbf{T}^{\mathbf{2}} \ldots\ldots\ldots\ldots\ldots\ldots\ldots(4\text{-}19)$$

Where:

q = Operating heat gain (W/m^2) at zero incident angle

ΔT = Average fluid temperature (°C)

Ib =Beam radiation (Direct normal insolation) (W/m^2)

In this equation, A accounts for the optical efficiency above ambient air temperature of the trough and the absorptivity of the selective coating without considering the losses at the end of a collector row. B, C and D describe the heat losses of the heat collecting element (HCE) dependent on its conditions with ΔT. The above equation is valid only at zero incident angles. An incident angle modifier term must be added to obtain collector heat gain at any other incident angle.

$$\mathbf{q} = \mathbf{kA(Ib) - B(Ib)(\Delta T) - C(\Delta T) - D(\Delta T^2)} \ldots\ldots\ldots\ldots\ldots\ldots(4\text{-}20)$$

The above equations are not complete physical models of the collector; rather they are empirical fits to experimental data. The following table summarizes the parameters as they were found in the test results.

Table 4- 5: Values of the different coefficients of collector efficiency (Mesfin,2009).

	A	B	C	D
Cermet, Vacuum	73.3	-0.007276	-0.496	-0.0691
Cermet, air	73.4	-0.004683	-14.40	-0.0637
Cermet, bare	74.7	-0.042-0.00927*Vwind/K	0	-0.000731*DNI
Black Chrome, Vacuum	73.6	-0.004206	7.44	-0.0958
Black Chrome, air	73.8	-0.006460	-12.16	-0.0641

4.5.5 End losses

End losses occur at the ends of the HCEs, where, for a nonzero incidence angle, some length of the absorber tube is not illuminated by solar radiation reflected from the mirrors.

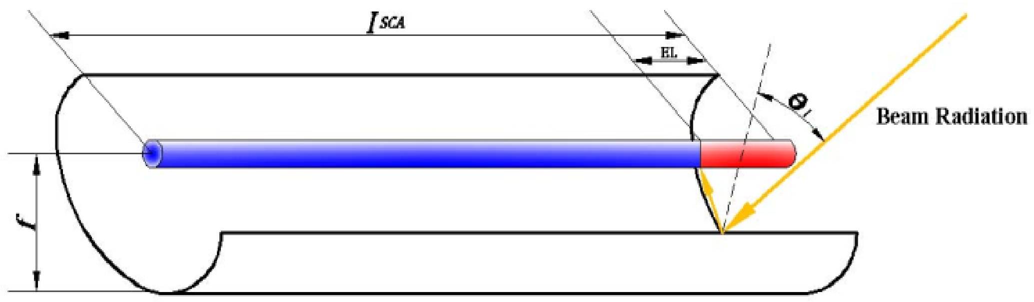

Figure 4- 7: End losses from an HCE (Mesfin,2009).

The end losses are a function of the focal length of the collector, the length of the collector, and the incident angle.

$$\mathbf{EL = 1 - \frac{f\tan\theta}{L_{SCA}}} \ldots\ldots\ldots\ldots\ldots\ldots\ldots\ldots\ldots\ldots(4\text{-}21)$$

Where:

f = focal length of the collectors =1.84 m

θ = incident angle which is varies between 20 to 30 degree

L_{sca} = length of a single solar collector assembly 47 m [LS-2]

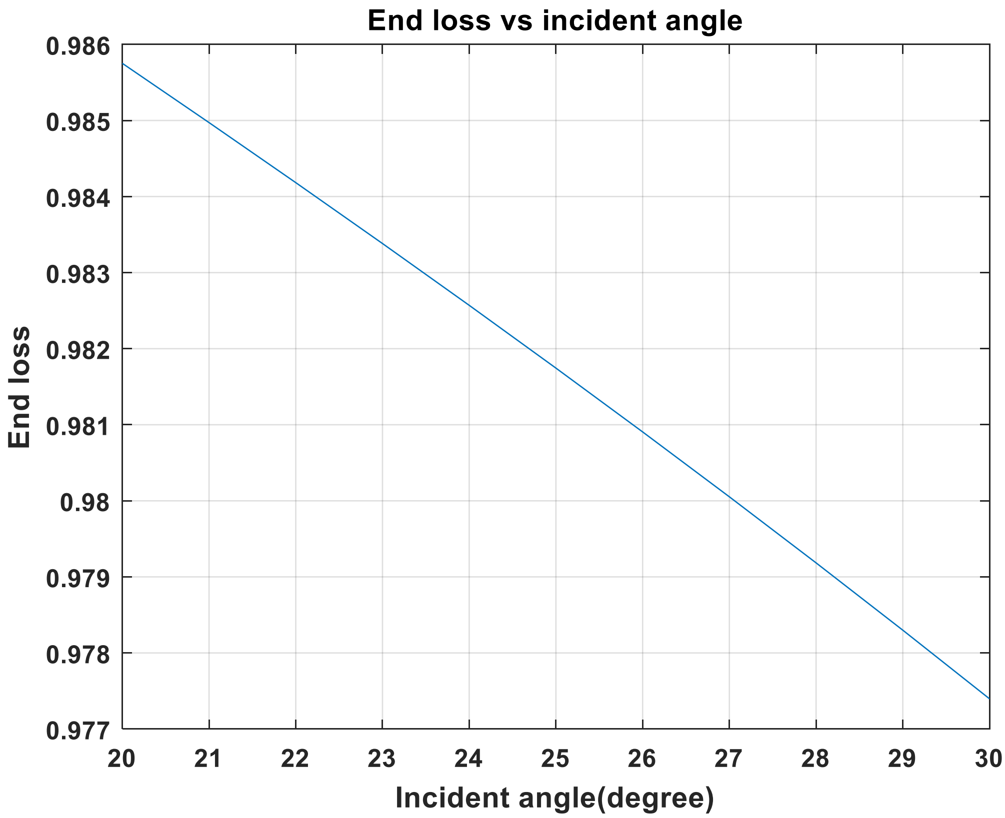

Figure 4- 8: End losses versus incident angle of East-West tracking

Figure 4-8 Indicate that end loss is varies from 0.979 to 0.986 which is very close to 1 which means almost no end loss.

4.6 Thermal analysis of parabolic trough collector

The use of the solar concentrators to focus the sun's rays can greatly reduce the size of the absorber tube, thereby reducing heat loss and allow increasing the efficiency of the system at high temperatures. In addition, the concentrators are significantly less expensive per unit area compared to flat plate collectors.

The factor (U_t) is the heat loss coefficient; it is expressed by (Ghodbane and Boumeddane 2016).

$$\mathbf{U_t}=\left(\frac{1}{C_1\left[\frac{T_r-T_{am}}{1+f}\right]^{0.25}}+\frac{D_{ri}}{D_{ro}\times h_v}\right)^{-1}+\left(\frac{\sigma\left(T_r^2+T_{am}^2\right)\left(T_r+T_{am}\right)}{\left[\varepsilon_r-0.04\left(1-\varepsilon_r\right)\left(\frac{T_r}{450}\right)\right]^{-1}-\left[\left(\frac{D_{ri}}{D_{ro}}\right)\left(\frac{1}{\varepsilon_c}\right)\left(\frac{f}{\varepsilon_c}\right)\right]}\right)\quad\text{.........(4-22)}$$

Where:

ε_r = emissivity of the absorber tube.

ε_c= emissivity of the transparent glass envelope .

σ =stefan-Boltzmann constant ($\sigma = 5.670 \times 10^{-8}$ W/m^2.K^4).

D_{ro} = receiver outside tube diameter (m).

D_{ri} = receiver inside tube diameter (m).

With the factor (f) takes into account the loss ratio of the wind, and which can be obtained by the following equation:

$$\mathbf{f = D_{ri}^{-0.4}(1.61 + 1.3\varepsilon_r)h_v^{-0.9}exp[0.00325(T_r - 273)]} \quad \text{…………} (4\text{-}23)$$

C_1 is given by the following empirical expression:

$$\mathbf{C_1} = \frac{\mathbf{1.45+0.96(\varepsilon_r-0.5)^2}}{\mathbf{D_{ri}\left(\frac{1}{D_{ri}^{0.6}-D_{ro}^{0.6}}\right)^{1.25}}} \text{……………………………….....} (4\text{-}24)$$

The term h_v is the convection coefficient of the wind; it is given by the following equation (according McAdams (1954)) (Ghodbane and Boumeddane 2016).

$$\mathbf{h_v}=2.8+3V \text{…………………………………} (4\text{-} 25)$$

Where:

V = wind speed ($m.s^{-1}$).

In this work average wind speed is assumed to be equal to 4 m/s.

Next, the overall heat transfer coefficient,U_o, needs to be estimated. This should include the tube wall because the heat flux in a concentrating collector is high. Based on the outside tube diameter, this is given by (Kalogirou,2009).

$$\mathbf{U_o} = \left[\frac{\mathbf{1}}{\mathbf{U_t}} + \frac{\mathbf{D_{ro}}}{\mathbf{h_{fi}Dr_i}} + \frac{\mathbf{D_{ro}ln(D_{ro}/Dr_i)}}{\mathbf{2k}}\right]^{-\mathbf{1}} \text{………………} (4\text{-}26)$$

Where:

h_{fi} is convective heat transfer coefficient inside the receiver tube (W/m^2-K).

k is thermal conductivity of receiver (W/m^2-K).

The convective heat transfer coefficient,h_{fi}, can be obtained from the standard pipe flow equation.

For turbulent flow (Re> 2300) the nuselt number is given by:

$$\mathbf{Nu = 0.023(Re)^{0.8}(Pr)^{0.4} = \frac{hD}{k}} \text{…………………………….} (4\text{-}27)$$

Where:

h=Convective coefficient of HTF (W/m^2K)

Presents Reynolds number which is expressed by the following relation:

$$\text{Re} = \mathbf{\rho u_m D_{ri}/\mu = u_m D_{ri}/v} \text{………..……………..………} (4\text{-}28)$$

Where:

u_m=is the mean fluid velocity over the tube cross section

For flow in a circular tube ($A_c = \frac{\pi D_{ri}^2}{4}$), the Reynolds number reduces to :

$$\mathbf{Re_{D_{ri}} = \frac{4\dot{m}}{\pi D_{ri}\mu}} \quad \text{…(4-29)}$$

The Prandtl number (Pr) is given by:

$$Pr = \mathbf{C_p\mu/k_f} \quad \text{…(4-30)}$$

Kinematic viscosity of the fluid is given by:

$$\mathbf{v = \frac{\mu}{\rho}} \quad \text{…(4-31)}$$

Where:

μ = Fluid viscosity (kg/m-s)

Because the velocity varies over the cross section and there is no well-defined free stream, it is necessary to work with a mean velocity when dealing with internal flows.

The rate of mass flow through the tube is given by:

$$\mathbf{\dot{m} = \rho u_m A_c} \quad \text{…(4-32)}$$

For steady, incompressible flow in a tube of uniform cross-sectional area, $\dot{m}$ and u_m are constants independent of x.

4.6.1 Thermal performance

Complications occur in the calculation of thermal losses from receiver/absorber due to the following reasons:

(i) Receiver shapes are widely variable and the beam radiation at the receiver is not uniform.

(ii) Due to the temperature being high, edge losses and conduction effects are significant.

Let us consider an elemental length between 'x' and '$x + dx$'. The fluid temperatures at 'x' and '$x + dx$' are $T_f(x)$ and $T_f(x)+dT_f(x)$ respectively. Here the rate of heat available per unit length at fluid, will be carried away by the working flowing fluid.

For circular conductive absorber/receiver tube:

$$\mathbf{\dot{q}'_u = \left(\frac{A_a}{L}\right) F' \left[\rho(\alpha\tau)I_b - U_t\left(\frac{A_r}{A_a}\right)(T_f - T_a)\right] = \dot{m}C_p\frac{dT_f}{dx}} \quad \text{…(4-33)}$$

After solving the one-order differential equation becomes:

$$\frac{\left[S-\left(\frac{A_r}{A_a}\right)U_t(T_{fo}-T_a)\right]}{\left[S-\left(\frac{A_r}{A_a}\right)U_t(T_{fi}-T_a)\right]} = \exp\left(-\frac{F'A_rU_t}{\dot{m}C_p}\right) \quad (4\text{-}34)$$

The initial condition T_f at $x = 0$ are equal to T_{fi} .

The outlet-fluid temperature of the tube-type concentrator absorber/receiver, T_{fo} at $x = L$ is given by:

$$\mathbf{T_{fo}}=\left[\left(\frac{A_a}{A_r}\right)\frac{1}{U_t}\mathbf{S}+\mathbf{T_a}\right]\left\{\mathbf{1}-\mathbf{exp}\left(-\frac{F'A_rU_t}{\dot{m}C_p}\right)\right\}+\mathbf{T_{fi}}\,\mathbf{exp}\left(-\frac{F'A_rU_t}{\dot{m}c_p}\right) \quad (4\text{-}35)$$

The expression for the rate of heat transfer by the fluid under forced mode for a tubular absorber can be obtained using:

$$\dot{Q}_u= \dot{m}C_p(T_{fo}-T_{fi}) = A_aF_R\left[S-U_t\left(\frac{A_r}{A_a}\right)(T_{fi}-T_a)\right] \quad (4\text{-}36)$$

Where:

$\dot{m}$=mass flow rate of HTF

C_p= Specific heat of HTF

T_{fo}= Solar field outlet temperature

T_{fi}= Solar field inlet temperature

$$\mathbf{F_R}=\frac{\dot{m}c_p}{A_rU_t}\left\{\mathbf{1}-\mathbf{exp}\left(\frac{F'A_rU_t}{\dot{m}c_p}\right)\right\} \quad (4\text{-}37)$$

which is known as the “mass flow–rate factor” for the concentrator.

To obtain the threshold intensity $(I_{b,th})$ for a single concentrator with absorber/receiver, one should have:

$$\mathbf{\dot{Q}_u}=\mathbf{A_aF_R}\left[\mathbf{S}-\mathbf{U_t}\left(\frac{A_r}{A_a}\right)(\mathbf{T_{fi}}-\mathbf{T_a})\right]\geq \mathbf{0} \quad (4\text{-}38)$$

4.7 Optical and thermal efficiency

4.7.1 Optical efficiency (η_o)

This is defined as the ratio of the rate of net thermal energy available at the absorber/receiver to the incident beam radiation available at the absorber/receiver after absorption and transmission (Duffie and Beckman,2005).It is a maximum efficiency a collector can have. It is mathematically expressed as (Tiwari et al., 2016).

$$\eta_o= \frac{\dot{q}_u}{\alpha\tau I_b} \quad (4\text{-}39)$$

Optical efficiency of parabolic trough is also given by:

$$\eta_o = \boldsymbol{\alpha} * \boldsymbol{\tau} * \boldsymbol{\rho} \ \ldots\ldots\ldots\ldots\ldots\ldots\ldots\ldots\ldots\ldots\ldots\ldots\ldots (4\text{-}40)$$

Where:

α is absorptivity of absorber coating

τ is transmittivity of glass cover

ρ is reflectivity of mirror

Net thermal energy ($\dot{q}_u$) available on receiver is given by:

$$\dot{\mathbf{q}}_{\mathbf{u}} = \eta_o \cdot \ \boldsymbol{\alpha} \cdot \boldsymbol{\tau} \cdot \mathbf{I_b} \ldots\ldots\ldots\ldots\ldots\ldots\ldots\ldots\ldots\ldots\ldots\ldots (4\text{-}41)$$

The above equation includes the effect of the shape of mirror surface, different losses (reflection, transmission, and absorption), shading by the receiver, and the solar beam incident angle.

4.7.2 Instantaneous thermal efficiency (ηth)

This is the ratio of the rate of useful energy available at the absorber/receiver (Ar) to the beam energy incident on the aperture (Aa) (Tiwari et al., 2016). It is given by:

$$\eta_{th} = \frac{\dot{\mathbf{q}}_{\mathbf{u}}}{\mathbf{I_b}} \ldots\ldots\ldots\ldots\ldots\ldots\ldots\ldots\ldots\ldots\ldots\ldots\ldots\ldots (4\text{-}42)$$

I_b=beam radiation (direct normal radiation) (W/m^2)

An instantaneous thermal efficiency of the receiver can also be calculated as follow (Tiwari et al., 2016).

$$\eta_{th} = \left[\mathbf{1} - \frac{\boldsymbol{\varepsilon\sigma}\mathbf{T_r^4}}{\boldsymbol{\eta_o}\ \boldsymbol{\alpha\tau}\mathbf{CI_b}}\right] \ldots\ldots\ldots\ldots\ldots\ldots\ldots\ldots\ldots (4\text{-}43)$$

Where:

C is concentration ratio

I_b is beam radiation (W/m^2)

σ is Stefan–Boltzmann constant =5.67× 10^{-8} W/m^2 K^4

T_r is receiver temperature in kelvin

4.8 Solar Concentrators with a tube absorber/receiver

The outlet-fluid temperature at Nth concentrator can be written as follows:

$$\mathbf{T_{foN}} = \left[\left(\frac{\mathbf{A_a}}{\mathbf{A_r}}\right)\frac{\mathbf{1}}{\mathbf{U_t}}\mathbf{S} + \mathbf{T_a}\right]\left\{\mathbf{1} - \mathbf{exp}\left(-\frac{\mathbf{NF'A_rU_t}}{\dot{\mathbf{m}}\mathbf{c_p}}\right)\right\} + \mathbf{T_{fi}}\mathbf{exp}\left(-\frac{\mathbf{NF'A_rU_t}}{\dot{\mathbf{m}}\mathbf{c_p}}\right) \ldots\ldots\ldots (4\text{-}44)$$

For parabolic trough concentrators the mass flow rate to maintain a constant-collection temperature at $T_{foN} = T_0$ is given by:

$$\dot{m}_f = -\frac{NF'A_rU_t}{c_p}\left[\ln\frac{T_0-\left(\frac{S}{U_t}\frac{A_a}{A_r}+T_a\right)}{T_{fi}-\left(\frac{A_a}{A_r}\frac{S}{U_t}+T_a\right)}\right]^{-1} \quad \ldots\ldots\ldots\ldots(4\text{-}45)$$

4.9 Estimation of average solar radiation

Beam Radiation is the solar radiation received from the sun without having been scattered by the atmosphere.

Diffuse Radiation is the solar radiation received from the sun after its direction has been changed by scattering by the atmosphere.

Total Solar Radiation is the sum of the beam and the diffuse solar radiation on a surface. The most common measurements of solar radiation are total radiation on a horizontal surface, often referred to as **global radiation** on the surface (Duffie and Beckman,2005).

Radiation data are the best source of information for estimating average incident radiation. Lacking these data from nearby locations of similar climate, it is possible to use empirical relationships to estimate radiation from hours of sunshine or cloudiness.

In this paper empirical model to predict solar radiation is used and compared with result obtained from global radiation measured data in Adama meteorology for see the validation of the result.

4.9.1Total radiation on ground surface clear day

The effects of the atmosphere in scattering and absorbing radiation are variable with time as atmospheric conditions and air mass change.

Total radiation received on horizontal surface at ground surface is given by (Duffie and Beckman,2005).

$$\mathbf{I = I_b + I_d} \quad \ldots\ldots\ldots\ldots(4\text{-}46)$$

Where:

I_b= beam radiation on horizontal surface

I_d= diffuse radiation on horizontal surface

4.9.2 Beam radiation on moving surfaces

It is also of interest to estimate the radiation on surfaces that move in various prescribed ways. Most concentrating collector utilize beam radiation only and move to ‘‘track’’ the sun.

The correlation to predict direct normal irradiance (solar radiation) in the terrestrial region, which is given by Hottel model(Tiwari et.al, 2016).

$$I_{bn}=\mathbf{I_{on}\tau_b} \ldots\ldots\ldots\ldots(4\text{-}47)$$

At any time the beam radiation on a surface is a function of I_{bn}, the beam radiation on a plane normal to the direction of propagation of the radiation (Duffie and Beckman,2005).

$$\mathbf{I_b = I_{bn}}\cos\theta = \mathbf{I_{on}\tau_b\cos\theta} \ldots\ldots\ldots\ldots\ldots\ldots\ldots\ldots (4\text{-}48)$$

Where:

I_b = beam radiation on horizontal surface

I_{bn} = beam radiation normal to the surface

θ = incident angle for various modes of tracking of the angles calculated for the midpoint of the hour.

The atmospheric transmittance for beam radiation $\boldsymbol{\tau}_b$ is a function of air mass and its given by (Duffie and Beckman,2005).

$$\boldsymbol{\tau}_b = \mathbf{a_o + a_1 exp(\frac{-k}{cos\theta_z})} \ldots\ldots\ldots\ldots\ldots\ldots\ldots\ldots\ldots\ldots\ldots\ldots (4\text{-}49)$$

The constants a_o, a_1 and k for the standard atmosphere with 23 km visibility are found from the following equation which are given for altitudes less than 2.5 km.

$$a_o = r_o \cdot (0.4237 - 0.00821(6 - A)^2)$$

$$a_1 = r_1 \cdot (0.5055 + 0.00595(6.5 - A)^2)$$

$$k = r_k \cdot (0.2711 + 0.01858(2.5 - A)^2)$$

Where A is the altitude of the observer in kilometres.

Table 4- 6: Correction factors for climate Types (Duffie and Beckman,2005).

Climate Type	r_o	r_1	r_k
Tropical	0.95	0.98	1.02
Mid latitude summer	0.97	0.99	1.02
Subarctic summer	0.99	0.99	1.01
Mid latitude winter	1.03	1.01	1.00

From Hottel(1976)

For a solar collector array rotated about a North-South axis with continuous adjustments, the angle of incidence is calculated as,

$$\mathbf{cos}\theta = (\mathbf{cos^2}\theta_Z + \mathbf{cos^2}\delta\,\mathbf{sin^2}\omega)^{\mathbf{1/2}} \ldots\ldots\ldots\ldots\ldots (4\text{-}50)$$

The slope of this surface is given by:

$$\tan \boldsymbol{\beta} = \tan \boldsymbol{\theta_z}|\mathbf{cos}(\boldsymbol{\gamma} - \boldsymbol{\gamma_s})| \ldots\ldots\ldots\ldots\ldots\ldots\ldots\ldots\ldots (4\text{-}51)$$

The surface azimuth angle γ will be 90^o or -90^o depending on the sign of solar azimuth angle(γ_s): `

$$\gamma = \begin{cases} 90^o & \text{if } \gamma_s > 0 \\ -90^o & \text{if } \gamma_s \le 0 \end{cases} \qquad \text{...(4-52)}$$

For a solar collector array rotated about an East-West axis with continuous adjustments, the angle of incidence is calculated as,

$$\cos\theta = (1 - \cos^2\delta \sin^2\omega)^{1/2} \qquad \text{...(4-53)}$$

The slope of this surface is given by:

$$\tan\beta = \tan\theta_z |\cos\gamma_s| \qquad \text{...(4-54)}$$

The surface azimuth angle(γ) for this mode of orientation will change between 0^o and 180^o if the solar azimuth angle(γ_s) passes through $\pm 90^o$.For either hemisphere,

$$\gamma = \begin{cases} 0^o & \text{if} |\gamma_s| < 90 \\ 180^o & \text{if} |\gamma_s| \ge 90 \end{cases} \qquad \text{...(4-55)}$$

4.9.3 Diffuse Radiation

The atmospheric transmittance for diffuse radiation is the ratio of the transmitted diffuse radiation to the total radiation incident at the top of atmosphere.

Liu and Jordan (1960) developed an empirical relationship between the transmission coefficients for beam and diffuse radiation for clear days (Duffie and Beckman,2005).

$$\tau_d = 0.271 - 0.294 \cdot \tau_b \qquad \text{... (4-56)}$$

$$I_d = \tau_d \cdot I_{on} \cdot (\cos\phi \cdot \cos\delta \cdot \cos\omega + \sin\phi \cdot \sin\delta) \qquad \text{...(4-57)}$$

$$I_d = I_{on}\, \tau_d \cos\theta_z \qquad \text{...(4-58)}$$

4.10 Solar time

In solar energy study there is an important distinction between standard time and solar time. Solar time is a time based on the apparent angular motion of the sun across the sky, with solar noon the time with the sun crosses the meridian of the observer. Standard time is described on longitudes and is dependent on the standard meridian for each country. The relation between solar time and standard time in min is given by (Duffie and Beckman,2005).

$$\text{solar time} = \text{Standard time} + 4(L_{st} - L_{Loc}) + E \qquad \text{...(4-59)}$$

$$E = 229.2(0.000075 + 0.001868\cos B - 0.032077\sin B - 0.014615\cos 2B - 0.04089\sin 2B) \qquad \text{...(4-60)}$$

$$B = (N-1)\frac{360}{365} \qquad \text{...(4-61)}$$

Where:

L_{st} = standard meridian for the local time zone.

L_{Loc} = longitude of the location in question.

E = equation of time in minutes, accounts for the small irregularities in day length that occur due to the Earth's elliptical path around the sun.

The equation of time as a function of each day of the year is shown in Figure 4-19. Minimum irregularities occur in February 14 and maximum in November 2.

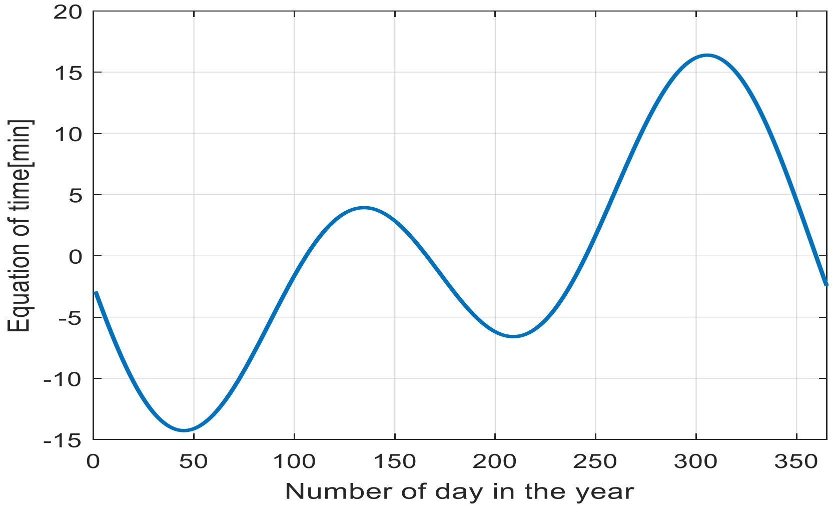

Figure 4- 9: Equation of time in minutes as a function of Day of the year

4.11 Hour angle (ω)

The hour angle is the sun's angular deviation from south.

Hour angle is given by the following equation (Tiwari, 2016).

$$\omega = (\mathbf{ST} - \mathbf{12}) * \mathbf{15^o} \quad \text{(4-62)}$$

Where:

ST is solar time

-180°≤ω≤180°, negative before solar noon

4.12 Solar altitude angle (α)

The angle specified between the ray from the sun and a horizontal plane is named as solar altitude angle.

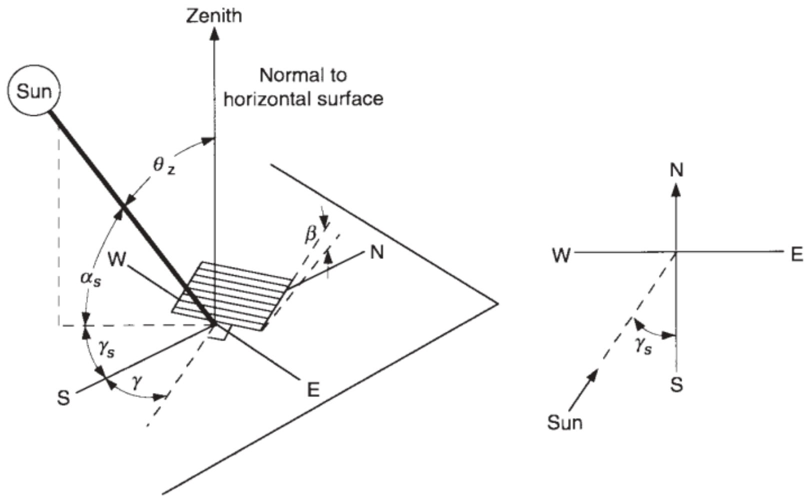

Figure 4- 10: Zenith angle, slope, surface azimuth angle and Plan view showing solar azimuth angle (Duffie and Beckman,2005).

Solar altitude angle (α) can be calculated by:

$$\sin\alpha = \sin\delta \sin\phi + \cos\delta \cos\omega \cos\phi \text{.........................(4-63)}$$

4.13 Solar azimuth angle (γ_s)

The additional angle which is most important to describe the position of the sun is the solar azimuth angle. Solar azimuth angle,the angular displacement from south of the projection of beam radiation on the horizontal plane. Displacements east of south are negative and west of south are positive.

$$\boldsymbol{\gamma_s = \mathrm{sign}(\omega) \left|\cos^{-1}\left(\frac{\cos\theta_z \sin\phi - \sin\delta}{\sin\theta_z \cos\phi}\right)\right|} \text{..........................(4-64)}$$

The sign function is equal to +1 if ω is positive and is equal to -1 if ω is negative:

4.14 Surface azimuth angle (γ)

The deviation of the projection on a horizontal plane of the normal to the surface from the local meridian, with zero due south, east negative, and west positive; $-180^o \leq \gamma \leq 180^o$.

4.15 Angle of incidence (θ)

The angle between the sun's rays and a vector normal (perpendicular) to the aperture or surface of the collector is the angle of incidence (θ). Knowing this angle is of critical importance to the solar designer, since the maximum amount of solar radiation energy that could reach a collector is reduced by the cosine of this angle (Canuçkun, 2013).

The angle of incidence of beam radiation on a collector surface is calculated as,

$$\cos\theta = \sin\delta \sin\phi \cos\beta - \sin\delta \cos\phi \sin\beta \cos\gamma + \cos\delta \cos\phi \cos\beta \cos\omega + \cos\delta \sin\phi \sin\beta \cos\gamma \cos\omega + \cos\delta \sin\beta \sin\gamma \sin\omega \text{.......................(4-65)}$$

For a horizontal surface, $\beta=0°$, and in this case the angle of incident becomes equal to zenith angle. Its value must be between 0^o and 90^o when the sun is above the horizon (Duffie and Beckman,2005).

$$\cos \theta_Z = \cos \phi \cos \delta \cos \omega + \sin \phi \sin\delta \text{......................(4-66)}$$

Relation between zenith angle and altitude angle is given by:

$$\theta_Z + \alpha = 90^o \text{..(4-67)}$$

During the same day, zenith angle determines amount of radiation received by surface.

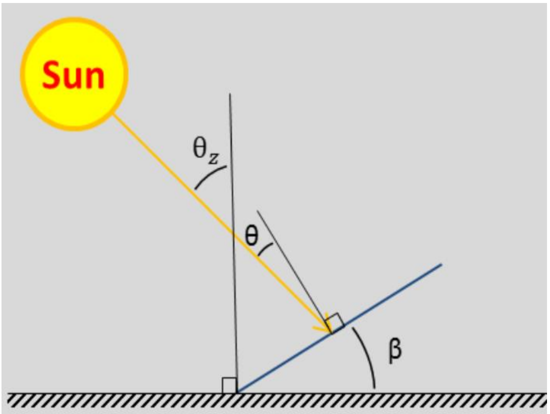

Figure 4- 11: Angle of Incidence and Zenith Angle (Canuçkun, 2013).

Certain types of concentrating collector such as parabolic trough collectors are designed to operate with tracking rotation about only one axis to minimize the angle of incidence and thus maximize the incident beam radiation. Here a tracking drive system rotates the collector about an axis of rotation until the sun central ray and the aperture normal are coplanar.

4.16 Solar collecting assembly (SCA)

The basic component of the solar field is the solar collector assembly (SCA). Each SCA is an independently tracking parabolic trough solar collector made up of parabolic reflectors (mirrors), the metal support structure, the receiver tubes, and the tracking system that includes the drive, sensors, and controls (Kalogirou,2009).

Table (4-7) shows the design characteristics of the Luz collectors used in the California plants and Euro trough.

Table 4- 7:Luz and Euro trough Solar Collector Characteristics (Kalogirou,2009).

Collector	LS-1	LS-2		LS-3	Euro trough
Year	1984	1985	1988	1989	2004
Area (m^2)	128	235		545	545/817.5
Aperture (m)	2.5	5		5.7	5.77
Length (m)	50	48		99	99.5/148.5
Receiver diameter (m)	0.042	0.072		0.07	0.07
Concentration ratio	61	71		82	82
Optical efficiency	0.734	0.734	0.764	0.8	0.78
Receiver absorptance	0.94	0.94	0.99	0.96	0.95
Receiver emittance at(^{o}C)	0.3(300)	0.2(300)	0.1(350)	0.1(350)	0.14(400)
Mirror reflectance	0.94	0.94	0.94	0.94	0.94
Operating temperature (^{o}C)	307	349	390	390	390

4.17 Extraterrestrial radiation on a horizontal surface

Extraterrestrial solar radiation follows a direct line from the sun to the Earth. Since the earth's orbit is slightly elliptical, the intensity of solar radiation received outside the earth's atmosphere varies as the square of the earth-sun distance and due to this variation Extraterrestrial solar radiation flux varies (Vasquez,2011).

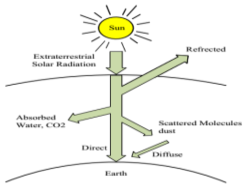

Figure 4- 12: Attenuation of solar radiation as it passes through the atmosphere (Vasquez,2011)

Extraterrestrial radiation measured on the plane normal to the radiation on the Nth day of the year,I_{on} is given by (Duffie and Beckman,2005).

$$\mathbf{I_{on}} = \mathbf{I_{sc}}\left[\mathbf{1 + 0.033cos}\left(\frac{\mathbf{360N}}{\mathbf{365}}\right)\right]\text{……………………………..(4-68)}$$

I_{sc} =1367 $\frac{W}{m^2}$, (Solar constant)

For a horizontal surface at any time between sunrise and sunset the rate solar radiation is given by (Duffie and Beckman,2005).

$$\mathbf{I_o} = \mathbf{I_{on}}\,\mathbf{cos}\,\boldsymbol{\theta}_\mathbf{z} = \mathbf{I_{sc}}(\mathbf{1 + 0.033cos}\,(\frac{\mathbf{360N}}{\mathbf{365}})\;\cos\boldsymbol{\theta}_\mathbf{z}\text{……………(4-69)}$$

$$\mathbf{I_o} = \mathbf{I_{sc}}(\mathbf{1} + \mathbf{0.033cos}\ (\frac{\mathbf{360N}}{\mathbf{365}})\ (\cos\phi\ \cos\boldsymbol{\delta}\cos\boldsymbol{\omega}+\sin\boldsymbol{\phi}\ \mathbf{sin}\ \boldsymbol{\delta}\ ) \ldots\ldots(4\text{-}70)$$

Daily extraterrestrial radiation on a horizontal surface, H_o can be calculated as follow (Duffie and Beckman,2005).

$$\mathbf{H_o} = \frac{\mathbf{24\times3600I_{sc}}}{\boldsymbol{\pi}}(1+0.033\cos\frac{\mathbf{360}\boldsymbol{N}}{\mathbf{365}})\times(\cos\phi\cos\boldsymbol{\delta}\sin\boldsymbol{\omega_s}+\frac{\boldsymbol{\pi\omega_s}}{\mathbf{180}}\sin\boldsymbol{\phi}\mathbf{sin}\boldsymbol{\delta}\ ) \ldots\ldots(4\text{-}71)$$

Where:

N=Number of days in the year

H_o= Daily extraterrestrial radiation on a horizontal surface (J/day.m^2)

ω_s =Sunset hour angle, in degrees

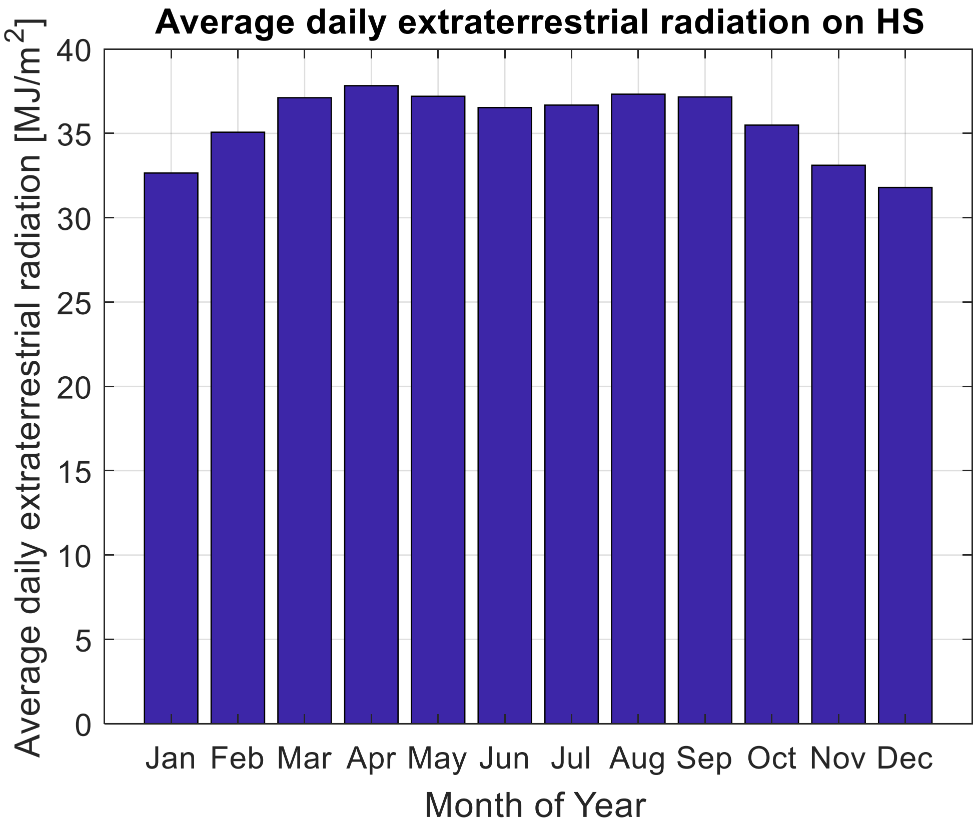

Figure 4- 13:Average daily extraterrestrial radiation

Extraterrestrial radiation on a horizontal surface for an hour period between hour angles ω_1 and ω_2 which define an hour (where ω_2 is the larger) is given by (Duffie and Beckman,2005).

$$\mathbf{I_o} = \frac{\mathbf{12\times3600I_{sc}}}{\boldsymbol{\pi}}\left(\mathbf{1}+\mathbf{0.033cos}\frac{\mathbf{360N}}{\mathbf{365}}\right)\times[\cos\phi\cos\boldsymbol{\delta}(\mathbf{sin}\boldsymbol{\omega_2}-\mathbf{sin}\boldsymbol{\omega_1})+\frac{\boldsymbol{\pi(\omega_2-\omega_1)}}{\mathbf{180}}\sin\boldsymbol{\phi}\mathbf{sin}\boldsymbol{\delta}]\ (\text{J}/\mathbf{m^2})\ldots\ldots\ldots\ldots(4\text{-}72)$$

Radiation data are the best source of information for estimating average incident radiation. Lacking these or data from nearby locations of similar climate, it is possible to use empirical relationships to estimate radiation from hours of sunshine or cloudiness.

4.17.1 Evaluation of the monthly average of daily total radiation on ahorizontal surface

The original Angstrom type regression equation related monthly average daily radiation to clear-day radiation at the location in question and average fraction of possible sunshine hours.

Page (1964) and others have modified the method to base it on extraterrestrial radiation on a horizontal surface rather than on clear-day radiation (Duffie and Beckman,2005).

It is the most widely used method because of its simplicity and the fact that many meteorological stations measure the sunshine duration.

$$\frac{\overline{H}}{\overline{H}_o} = a + b\,\frac{\overline{n}_s}{\overline{N}_s} \quad \text{...(4-73)}$$

Where:

$\overline{H}$= monthly average daily solar radiation on horizontal surface

$\overline{H}_o$= extraterrestrial radiation for the location averaged over the time period which is obtain using representative days of the month

a and b are constants depending on location

$\overline{n}_s$= monthly average daily hours of bright sunshine

$\overline{N}_s$= monthly average of maximum possible daily hours of bright sunshine (i.e., day length of average day of month)

The regression coefficients can be determined as follows (Tiwari et.al,2016).

$$a = -0.110 + 0.235cos\phi + 0.323\left(\frac{\overline{n}_s}{\overline{N}_s}\right)$$

$$b = 1.449 - 0.533cos\phi - 0.694\left(\frac{\overline{n}_s}{\overline{N}_s}\right)$$

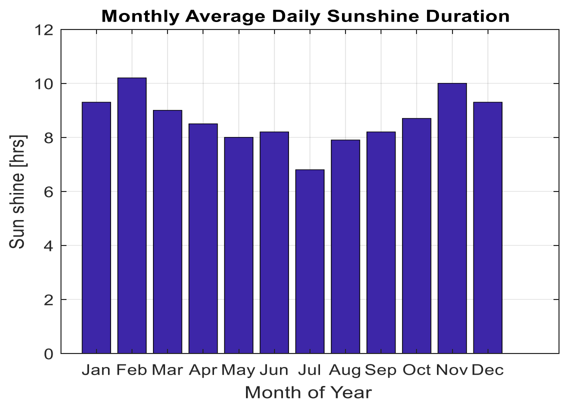

Figure 4- 14:Monthly average daily sunshine duration

- Sunset, sunrise & day length

The sunset hour angle is the hour angle when θz=90°.

$$\boldsymbol{\omega_s} = \boldsymbol{cos^{-1}}(-\tan \boldsymbol{\phi} \tan \delta) \ldots\ldots\ldots\ldots\ldots\ldots\ldots\ldots\ldots\ldots\ldots\ldots (4\text{-}74)$$

The sunrise hour angle is the negative of the sunset hour angle. It also follows that the number of daylight hours (sun shine hour) is given by (Duffie and Beckman,2005).

$$\overline{\boldsymbol{N}}_{\boldsymbol{s}} = \frac{\mathbf{2}}{\mathbf{15}}\boldsymbol{\omega_s} \ldots\ldots\ldots\ldots\ldots\ldots\ldots\ldots\ldots\ldots\ldots\ldots (4\text{-}75)$$

$$\overline{\boldsymbol{N}}_{\boldsymbol{s}} = \frac{\mathbf{2}}{\mathbf{15}} \cdot \boldsymbol{cos^{-1}}(-\mathbf{tan}\boldsymbol{\phi} \cdot \mathbf{tan}\boldsymbol{\delta}) \ldots\ldots\ldots\ldots\ldots\ldots\ldots\ldots (4\text{-}76)$$

Declination (δ) is important to calculate incident angle and sunset hour angle and its given by:

$$\delta = 23.45\sin\left(360\frac{\mathbf{284+N}}{\mathbf{365}}\right) \ldots\ldots\ldots\ldots\ldots\ldots\ldots\ldots\ldots\ldots (4\text{-}77)$$

Where: N= representative days of the month

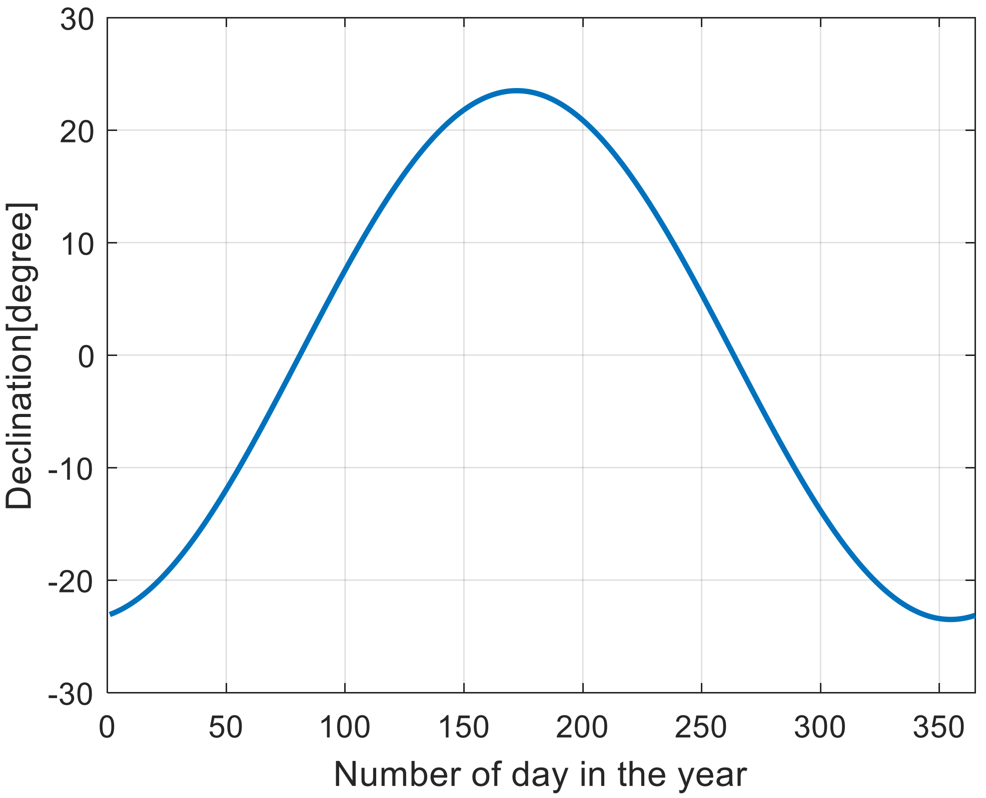

Figure 4- 15:Declination angle

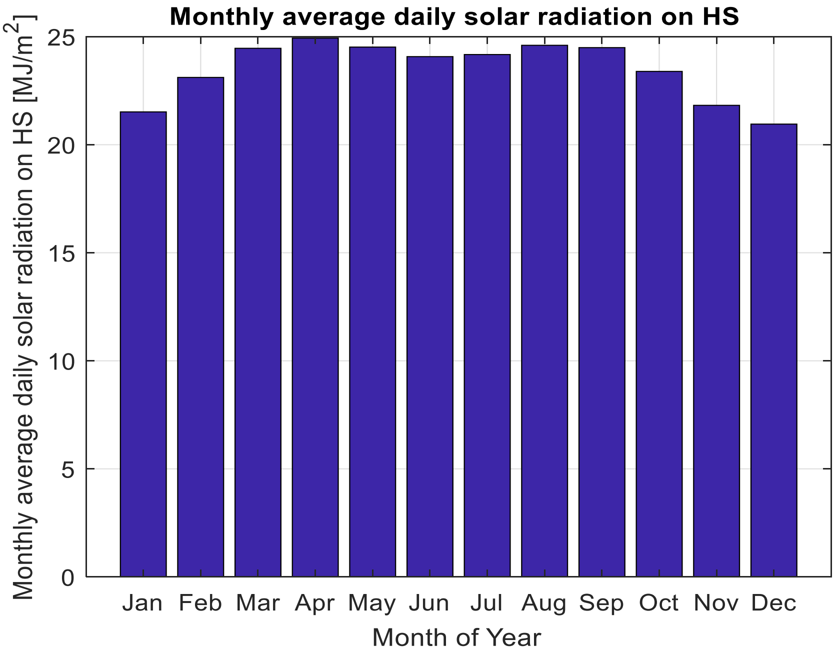

Figure 4- 16:Monthly average daily global radiation on horizontal surface

4.17.2 Estimation of the monthly average of daily diffuse solar radiation on a horizontal surface

The monthly average daily diffuse radiation on a horizontal surface can be determined from the monthly average daily global radiation on a horizontal surface and the number of bright sunshine hours (Bekele, 2007).

$$\frac{\overline{H}_d}{\overline{H}} = \mathbf{0.931 - 0.814}\left(\frac{\overline{n}_s}{\overline{N}_s}\right) \ldots\ldots\ldots\ldots\ldots\ldots\ldots\ldots\ldots\ldots..(4\text{-}78)$$

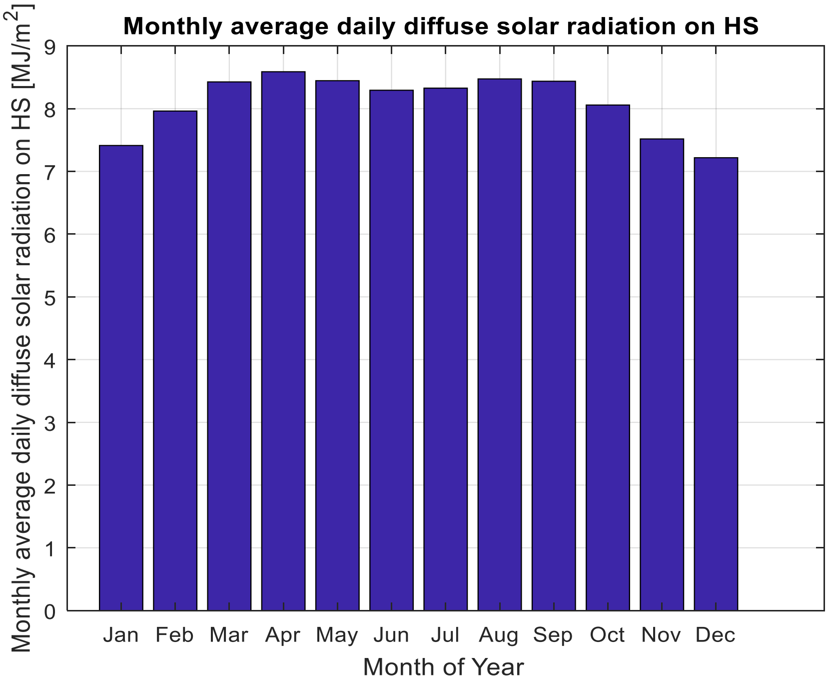

Figure 4- 17: Monthly average daily diffuse solar radiation on horizontal surface

4.17.3 Monthly average hourly global radiation on a horizontal surface

The monthly average hourly global radiation on a horizontal surface can be calculated from the knowledge of the monthly average daily global radiation on a horizontal surface.

$$\frac{\bar{I}}{\bar{\bar{H}}} = \frac{\pi}{24}(\boldsymbol{a} + \boldsymbol{b}\cos\boldsymbol{\omega})\frac{cos\omega - cos\omega_s}{sin\omega_s - \frac{\pi}{180}\omega_s cos\omega_s} \quad \text{......................(4-79)}$$

Where:

$$a = 0.409 + 0.5016\sin(\omega_s - 60)$$

$$b = 0.6609 - 0.4767sin(\omega_s - 60)$$

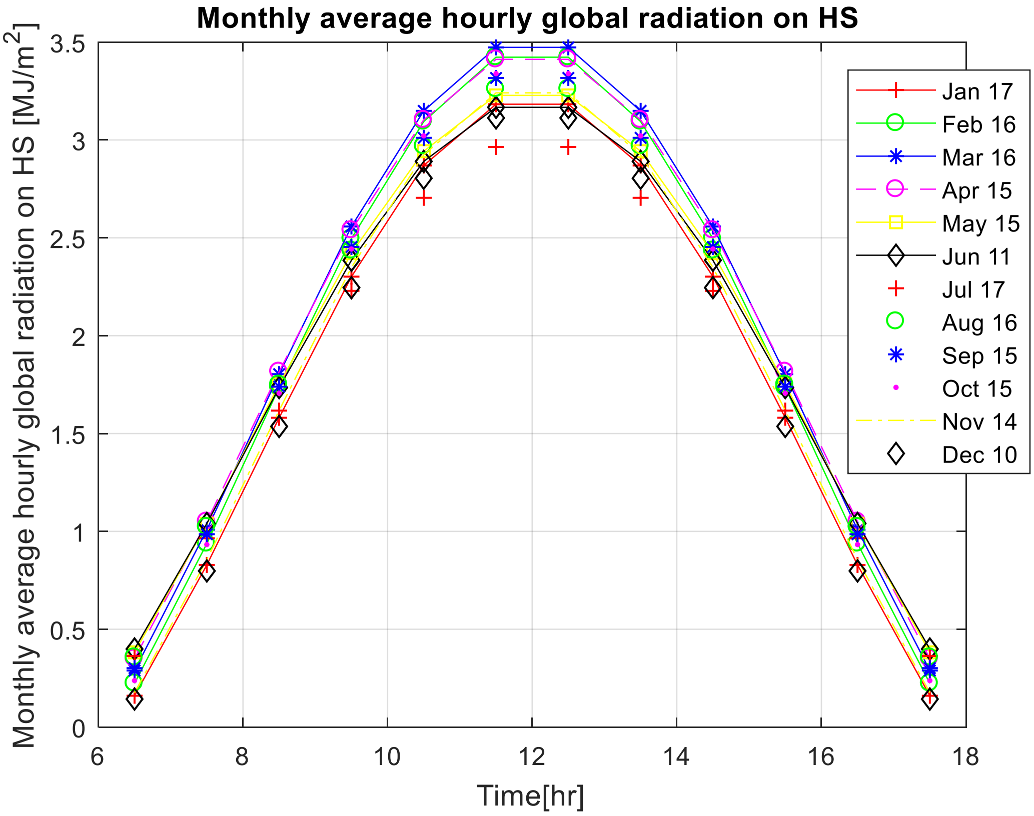

Figure 4- 18: Monthly average hourly global radiation on horizontal surface

4.17.4 Monthly average hourly diffuse radiation on a horizontal surface

The monthly average hourly diffuse radiation on a horizontal surface can be calculated from the knowledge of the monthly average daily diffuse radiation on a horizontal surface (Bekele, 2007).

$$\frac{\bar{I}_d}{\bar{\bar{H}}_d} = \frac{\pi}{24}\frac{\cos\omega - \cos\omega_s}{\sin\omega_s - \frac{\pi}{180}\omega_s\cos\omega_s} \quad \text{.............................(4-80)}$$

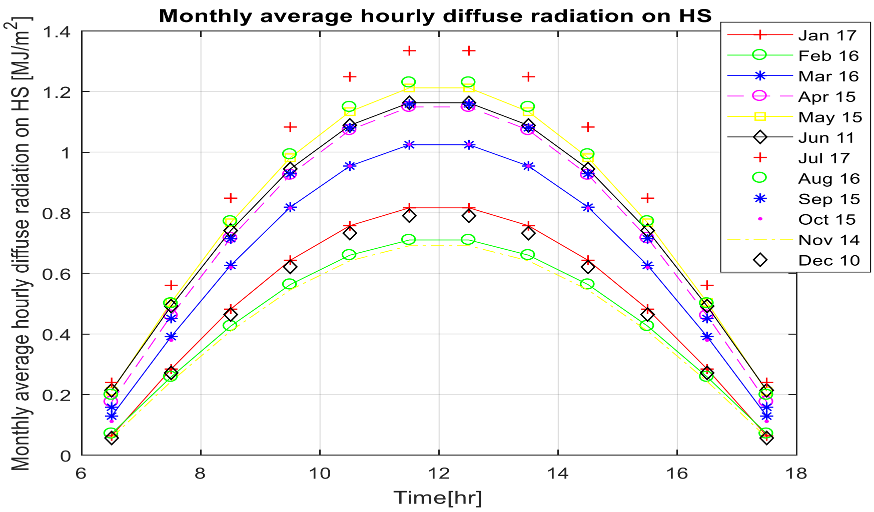

Figure 4- 19:Monthly average hourly diffuse radiation on horizontal surface

4.18 Pressure gradient and friction factor in fully developed flow

The engineer is frequently interested in the pressure drop needed to sustain an internal flow because this parameter determines pump or fan power requirements (Bergman.et.al).

A correlation for the smooth surface condition that encompasses a large Reynolds number range has been developed by Petukhov and is of the form.

$$\mathbf{f = (0.790 \ln Re_D - 1.64)^{-2}} \qquad 3000 \leq 5\times \mathbf{Re_D \leq 10^6} \text{……..} \ (4\text{-}81)$$

The pressure drop $\Delta p = p_1 - p_2$ associated with fully developed flow from the axial position x_1 to x_2 may then be expressed as:

$$\boldsymbol{\Delta p = -\int_{p_1}^{p_2} dp = f\frac{\rho u_m^2}{2D}\int_{x_1}^{x_2} dx = f\frac{\rho u_m^2}{2D}(x_2 - x_1)} \ \text{………………......}(4\text{-}82)$$

4.19 Pump power

The pump power is required to overcome the resistance to flow associated with pressure drop may be expressed as (Bergman.et.al).

$$\mathbf{P = (\Delta p)\dot{V}} \ \text{……………………………………………………..}(4\text{-}83)$$

Where the volumetric flow rate $\dot{V}$ is expressed as $\dot{V} = \dot{m}/\rho$ for an incompressible fluid.

4.20 Heat exchangers

A schematic of an adiabatic counter current exchanger with inlet and outlet temperatures and capacitance rates of the hot and cold fluids is shown (Duffie and Beckman,2005).

Figure 4- 20: Heat exchanger (Duffie and Beckman,2005).

The maximum possible temperature drop of the hot fluid is from T_{hi} to T_{ci} the heat transfer for this situation would be:

$$\mathbf{Q_{max}} = (\dot{\mathbf{m}}\mathbf{C_p})_{\mathbf{h}}(\mathbf{T_{hi}} - \mathbf{T_{ci}}) \text{ ....(4-84)}$$

Where:

$(\dot{m}C_p)_h$ = Capacitance rate of the hot side fluid (HTF) (kW/K)

T_{hi} = Temperature of heat transfer fluid inlet to heat exchanger

T_{ci} = Temperature of feed water inlet to heat exchanger

The maximum possible temperature rise of the cold fluid would be from T_{ci} to T_{hi}. The corresponding maximum heat exchange would be:

$$\mathbf{Q_{max}} = \left(\dot{\mathbf{m}}\mathbf{C_p}\right)_{\mathbf{c}}(\mathbf{T_{hi}} - \mathbf{T_{ci}}) \text{ ....(4-85)}$$

Where:

$\left(\dot{m}C_p\right)_c$ = Capacitance rate of the cold side water fluid (kW/K)

The maximum heat transfer that could occur in the exchanger is thus fixed by the lower of the two capacitance rates:

$$\mathbf{Q_{max}} = \left(\dot{\mathbf{m}}\mathbf{C_p}\right)_{\mathbf{min}}(\mathbf{T_{hi}} - \mathbf{T_{ci}}) \text{ ....(4-86)}$$

The actual heat exchange Q is given by:

$$\mathbf{Q} = \left(\dot{\mathbf{m}}\mathbf{C_p}\right)_{\mathbf{c}}(\mathbf{T_{co}} - \mathbf{T_{ci}}) = \left(\dot{\mathbf{m}}\mathbf{C_p}\right)_{\mathbf{h}}(\mathbf{T_{hi}} - \mathbf{T_{ho}}) \text{ ....(4-87)}$$

The actual heat exchanger Q can also relate with overall heat transfer coefficient U and mean temperature difference ΔT_m which can be written as:

$$\boldsymbol{Q = UA\Delta T_m} \text{ ....(4-88)}$$

Where:

A = total surface area for heat exchange.

Effectiveness ε is defined as the ratio of the actual heat exchange that occurs to the maximum possible, Q/Q_{max}, so

$$\varepsilon = \frac{\mathbf{Q}}{\mathbf{Qmax}} = \frac{(\dot{\mathbf{m}}\mathbf{C_p})_{\mathbf{h}}(\mathbf{T_{hi}} - \mathbf{T_{ho}})}{(\dot{\mathbf{m}}\mathbf{C_p})_{\mathbf{min}}(\mathbf{T_{hi}} - \mathbf{T_{ci}})} = \frac{(\dot{\mathbf{m}}\mathbf{C_p})_{\mathbf{c}}(\mathbf{T_{co}} - \mathbf{T_{ci}})}{(\dot{\mathbf{m}}\mathbf{C_p})_{\mathbf{min}}(\mathbf{T_{hi}} - \mathbf{T_{ci}})} \text{ ....(4-89)}$$

Since either the hot or cold fluid has the minimum capacitance rate, the effectiveness can always be expressed in terms of the temperatures only. The working equation for the heat exchanger is (Duffie and Beckman,2005).

$$Q = \boldsymbol{\varepsilon}\left(\dot{\mathbf{m}}\mathbf{C_p}\right)_{\mathbf{min}}(\mathbf{T_{hi}} - \mathbf{T_{ci}}) \qquad (4\text{-}90)$$

The dimensionless capacitance rate is given by:

$$\mathbf{c_r} = \frac{(\dot{\mathbf{m}}\mathbf{C_p})_{\mathbf{min}}}{(\dot{\mathbf{m}}\mathbf{C_p})_{\mathbf{max}}} \qquad (4\text{-}91)$$

Once Q_{max} and the effectiveness have been calculated, the actual heat transfer between fluid streams is determined as:

$$\mathbf{h_{steam,out}} = \mathbf{h_{steam,in}} + \frac{\dot{\mathbf{Q}}}{\dot{\mathbf{m}}_{\mathbf{steam}}} \qquad (4\text{-}92)$$

The exit enthalpy of the HTF is determined from an energy balance on the fluid:

$$\mathbf{h_{HTF,out}} = \mathbf{h_{HTF,in}} + \frac{\dot{\mathbf{Q}}}{\dot{\mathbf{m}}_{\mathbf{HTF}}} \qquad (4\text{-}93)$$

Continuity requires the mass flow rates of the HTF and steam at the respective outlets to equal the mass flow rates of each steam at their inlet.

$$\dot{\mathbf{m}}_{\mathbf{steam,in}} = \dot{\mathbf{m}}_{\mathbf{steam,out}} \qquad (4\text{-}94)$$

$$\dot{\mathbf{m}}_{\mathbf{HTF,in}} = \dot{\mathbf{m}}_{\mathbf{HTF,out}} \qquad (4\text{-}95)$$

The UA for the heat exchanger at the reference state is provided as a parameter to the exchanger model. At partial loads, the UA will decrease with the decreasing flow rates of the streams. The relationship between the reference UA/flow rate and a reduced UA/flow rate can be derived as follows. The UA of an un-finned, tubular heat exchanger is defined as the total thermal resistance to heat transfer between two fluids.

$$\frac{\mathbf{1}}{\mathbf{UA}} = \frac{\mathbf{1}}{\mathbf{h_i A_i}} + \frac{\mathbf{R''_{fi}}}{\mathbf{A_i}} + \frac{\mathbf{\ln D_o/D_i}}{\mathbf{2\pi kL}} + \frac{\mathbf{R''_{fo}}}{\mathbf{A_o}} + \frac{\mathbf{1}}{\mathbf{h_o A_o}} \qquad (4\text{-}96)$$

Where:

h = convection heat transfer coefficient (W/m^2-K)

A = surface area (m^2)

R'' = fouling factor, per unit area (m^2-K/W)

D= diameter (m)

k = thermal conductivity of the material between the fluids (W/m-K)

L = length of the heat exchanger (m)

Where subscripts i and o refer to inner and outer tube surfaces ($A_i = \pi \cdot D_i \cdot L$, $A_o = \pi \cdot D_o \cdot L$), which may be exposed to either the hot or the cold fluid.

If it is assumed that there is negligible fouling in the heat exchangers and that the thermal resistance through the tubes can be neglected. With these assumptions,Equation above is reduces to:

$$\frac{1}{UA} = \frac{1}{h_i A_i} + \frac{1}{h_o A_o} \quad \text{.....................................(4-97)}$$

UA is a function of the inner and outer surface areas of the tubes and the heat transfer coefficient of each fluid. The surface area of the tubes will not change with partial load conditions.

CHAPTER FIVE

HEAT COLLECTOR ELEMENT PERFORMANCE MODEL

The Heat collector element **(**HCE) performance model is based on an energy balance about the collector and the HCE. The energy balance includes the direct normal solar irradiation incident on the collector, optical losses from both the collector and HCE, thermal losses from the HCE, and the heat gain into the HTF. For short receivers (< 100 m) a one-dimensional energy balance gives reasonable results; for longer receivers a two dimensional energy balance becomes necessary (Forristal,2003).

5.1 One-dimensional energy balance model

The HCE performance model uses an energy balance between the HTF and the atmosphere, and includes all equations and correlations necessary to predict the terms in the energy balance, which depend on the collector type, HCE condition, optical properties, and ambient conditions.

Figure 5.1a shows the one-dimensional steady-state energy balance for a cross-section of an HCE, with and without the glass envelope and Figure 5.1b shows the thermal resistance model and subscript definitions. For clarity, the incoming solar energy and optical losses have been omitted from the resistance model.

The effective incoming solar energy (solar energy minus optical losses) is absorbed by the glass envelope ($\dot{q}'_{5SolAbs}$) and absorber selective coating ($\dot{q}'_{3SolAbs}$). Some energy that is absorbed into the selective coating is conducted through the absorber ($\dot{q}'_{23cond}$) and transferred to the HTF by convection ($\dot{q}'_{12conv}$); remaining energy is transmitted back to the glass envelope by convection ($\dot{q}'_{34conv}$) and radiation ($\dot{q}'_{34rad}$) and lost through the HCE support bracket through conduction ($\dot{q}'_{cond,bracket}$).

The energy from the radiation and convection then passes through the glass envelope by conduction ($\dot{q}'_{45cond}$) and along with the energy absorbed by the glass envelope ($\dot{q}'_{5'SolAbs}$) is lost to the environment by convection ($\dot{q}'_{56conv}$) and radiation ($\dot{q}'_{57\,rad}$).

If the glass envelope is missing, the heat loss from the absorber is lost directly to the environment. The model assumes all temperatures, heat fluxes, and thermodynamic properties are uniform around the circumference of the HCE.

With the glass envelope:

$$\dot{\mathbf{q}}'_{12conv}=\dot{\mathbf{q}}'_{23cond} \qquad (5\text{-}1)$$

$$\dot{\mathbf{q}}'_{3SolAbs} = \dot{\mathbf{q}}'_{34conv} + \dot{\mathbf{q}}'_{34\,rad} + \dot{\mathbf{q}}'_{23cond} + \dot{\mathbf{q}}'_{cond,bracket} \qquad (5\text{-}2)$$

$$\dot{\mathbf{q}}'_{34conv} + \dot{\mathbf{q}}'_{34\,rad} = \dot{\mathbf{q}}'_{45cond} \qquad (5\text{-}3)$$

$$\dot{\mathbf{q}}'_{45cond} + \dot{\mathbf{q}}'_{5SolAbs} = \dot{\mathbf{q}}'_{56conv} + \dot{\mathbf{q}}'_{57\,rad} \qquad (5\text{-}4)$$

$$\dot{q}'_{heat\ loss} = \dot{q}'_{56conv} + \dot{q}'_{57\ rad} + \dot{q}'_{cond,bracket} \ldots\ldots\ldots\ldots\ldots\ldots\ldots\ldots (5\text{-}5)$$

Without the glass envelope

$$\dot{q}'_{12conv} = \dot{q}'_{23cond} \ldots\ldots\ldots\ldots\ldots\ldots\ldots\ldots\ldots\ldots\ldots\ldots\ldots\ldots (5\text{-}6)$$

$$\dot{q}'_{3Sol\ Abs} = \dot{q}'_{36conv} + \dot{q}'_{37\ rad} + \dot{q}'_{23cond} + \dot{q}'_{cond\ bracket} \ldots\ldots\ldots (5\text{-}7)$$

$$\dot{q}'_{heat\ loss} = \dot{q}'_{36conv} + \dot{q}'_{37\ rad} + \dot{q}'_{cond,bracket} \ldots\ldots\ldots\ldots\ldots\ldots\ldots\ldots (5\text{-}8)$$

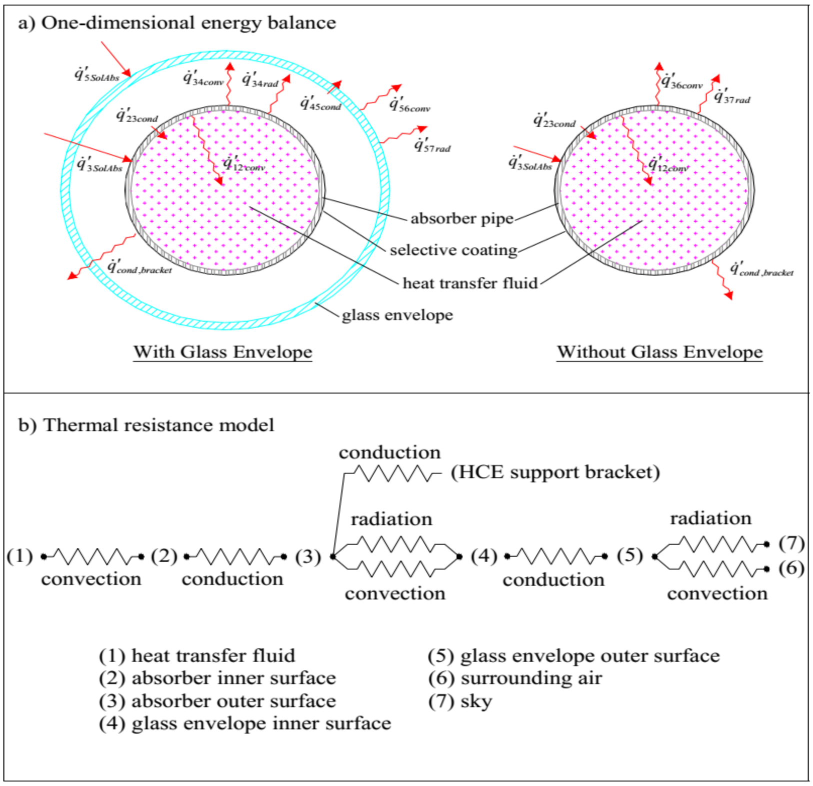

Figure 5- 1:a)One-dimensional steady-state energy balance and b)thermal resistance model for a cross-section of HCE (Forristal,2003).

5.2 Convection heat transfer between the HTF and the absorber

Considering convection for internal flow, the heat transfer per unit length (q'_{12conv}) is calculated through the Dittus-Boelter equation assuming fully developed (hydro dynamically and thermally) turbulent flow in a smooth circular tube (Mesfin ,2009).

$$\mathbf{q'_{12conv} = h_1 D_2 \pi (T_2 - T_1)} \ldots\ldots\ldots\ldots\ldots\ldots\ldots\ldots\ldots (5\text{-}9)$$

$$\mathbf{h_1 = Nu_{D2} \frac{K_1}{D_2}} \ldots\ldots\ldots\ldots\ldots\ldots\ldots\ldots\ldots\ldots\ldots (5\text{-}10)$$

Where:

h_1 = HTF convection heat transfer coefficient at T_1 (W/m^2-K)

D_2 = inside diameter of the absorber pipe (m)

T_1= mean (bulk) temperature of the HTF (℃)

T_2= inside surface temperature of absorber pipe (℃)

The local Nusselt number (Nu_{D2}) is given by:

$$Nu_{D2} = 0.023(\mathbf{Re_{D2}})^{\mathbf{0.8}}(\mathbf{pr_1})^{\mathbf{n}} \quad \text{……………………….(5-11)}$$

Where: n = 0.4 for heating ($T_2 > T_1$) and 0.3 for cooling ($T_2 < T_1$).

The Reynolds number, Re_{D2} for flow in a circular tube, is given by:

$$Re_{D2}=\frac{\mathbf{4\dot{m}}}{\mathbf{\pi D_2 \mu_1}} \quad \text{……………………………………….(5-12)}$$

With $\mu_1$as the viscosity of the HTF, the Prandtl number, P_{r1} is determined by:

$$P_{r1} = \frac{\mathbf{v_1}}{\mathbf{\alpha_1}} \quad \text{……………………………………………..(5-13)}$$

The kinematic viscosity of the HTF, v_1 is defined by:

$$\mathbf{v_1}=\frac{\mathbf{\mu_1}}{\mathbf{\rho_1}} \quad \text{………………………………………….…(5-14)}$$

and the thermal diffusivity of HTF, α_1, is given by:

$$\boldsymbol{\alpha_1}=\frac{\mathbf{k_1}}{\mathbf{\rho_1 C_1}} \quad \text{……………………………………………..(5-15)}$$

k_1 is the thermal conductivity of the HTF.

The heat transfer coefficient, h_{12} is calculated by using the local Nusselt number, Nu_{D2} through:

$$\mathbf{h_{12}}=\frac{\mathbf{Nu_{D2} k_1}}{\mathbf{D_2}} \quad \text{……………………………………(5-16)}$$

Where:

D_2 is the inside diameter of the absorber tube.

The HTF properties,C_1 ,k_1, μ_1 and ρ_1 are functions of the HTF film temperature T_f.

5.3 Conduction heat transfer through the absorber wall

Fourier's law of conduction through a hollow cylinder describes the conduction heat transfer through the absorber wall.

$$\mathbf{q'_{23cond}} = \mathbf{2\pi k_{23}}\,(\mathbf{T_2}-\mathbf{T_3})/\mathbf{ln}(\mathbf{D_3}/\mathbf{D_2}) \quad \text{……………..(5-17)}$$

Where:

k_{23}= thermal conductance at the average absorber temperature $(T_2+T_3)/2$ (W/m-K)

T_2 = absorber inside surface temperature (K)

T_3 = absorber outside surface temperature (K)

D_2 = absorber inside diameter (m)

D_3 = absorber outside diameter (m)

The conduction coefficient depends on the absorber material type. The HCE performance model includes three stainless steels: 304L, 316L, and 321H, and one copper: B42. If 304L or 316L is chosen, the conduction coefficient is calculated with the following equation.

$$\mathbf{k_{23} = (0.013)T_{23} + 15.2} \qquad \text{(5-18)}$$

If 321H is chosen,

$$\mathbf{k_{23} = (0.0153)T_{23} + 14.775} \qquad \text{(5-19)}$$

If copper is chosen, the conduction coefficient is a constant of 400 W/m-K.

5.4 Heat transfer from the absorber to the glass envelope

5.4.1 Convection heat transfer

Two heat transfer mechanisms are evaluated to determine the convection heat transfer between the absorber and glass envelope ($\dot{q}'_{34conv}$), free-molecular and natural convection.

a) Convection heat transfer for vacuum in annulus

When the HCE annulus is under vacuum (pressure < ~1 torr), the convection heat transfer between the absorber and glass envelope occurs by free-molecular convection (Forristall,2003).

$$\mathbf{\dot{q}'_{34conv} = \pi D_3 h_{34}(T_3 - T_4)} \qquad \text{(5-20)}$$

With:

$$\mathbf{h_{34} = \frac{K_{std}}{\left(\frac{D_3}{2ln\left(\frac{D_4}{D_3}\right)+b\lambda\left(\frac{D_3}{D_4}+1\right)}\right)}} \qquad \text{(5-21)}$$

$$\mathbf{b = \frac{(2-a)(9\gamma-5)}{2a(\gamma+1)}} \qquad \text{(5-22)}$$

$$\mathbf{\lambda = \frac{2.331E(-20)(T_{34}+273.15)}{P_a\delta^2}} \qquad \text{(5-23)}$$

Where:

D_3 = outer absorber surface diameter (m)

D_4 = inner glass envelope surface diameter (m)

h_{34}=convection heat transfer coefficient for the annulus gas at T_{34} (W/m^2-K)

T_3=outer absorber surface temperature (°C)

T_4=inner glass envelope surface temperature (°C)

K_{std} = thermal conductance of the annulus gas at standard temperature and pressure (W/m-K)

b = interaction coefficient

λ = mean-free-path between collisions of a molecule (cm)

a = accommodation coefficient

γ = ratio of specific heats for the annulus gas

T_{34} = average temperature $(T_3 + T_4)/2$ (°C)

P_a = annulus gas pressure (mmHg)

δ = molecular diameter of annulus gas (cm)

This correlation is valid for $R_{aD4} < (D_4/(D_4 - D_3))^4$

The table also compares the convection heat transfer coefficients (h_{34}) and other parameters that are used in the calculation for each of the three gases included in the HCE performance model.

Table 5- 1: Heat Transfer Coefficients and Constants for Each Annulus Gas (Forristall,2003).

Annulus Gas	k_{std} [W/m-K]	B	λ [cm]	Γ	δ[cm]	h_{34}[W/m^2-K]
Air	0.02551	1.571	88.67	1.39	3.53E-8	0.0001115
Hydrogen	0.1769	1.581	191.8	1.398	2.4E-8	0.0003551
Argon	0.01777	1.886	76.51	1.677	3.8E-8	0.00007499

b) Convection heat transfer between absorber and glass envlope

When the HCE annulus loses vacuum (pressure > ~1 torr (133.32pa)), the convection heat transfer mechanism between the absorber and glass envelope occurs by natural convection. Raithby and Holland's correlation for natural convection in an annular space between horizontal cylinders is used for this case (Forristall,2003).

$$\mathbf{q'_{34conv}} = \frac{2.425k_{34}(T_3 - T_4)\left(PrRa_{D3}/(0.861 + Pr_{34})\right)^{1/4}}{\left(1 + (D_3/D_4)^{3/5}\right)^{5/4}} \quad \text{(5-24)}$$

$$\mathbf{Ra_{D3}} = \frac{g\beta(T_3 - T_4)D_3^3}{\alpha\nu} \quad \text{(5-25)}$$

For an ideal gas:

$$\boldsymbol{\beta} = \frac{1}{T_{avg}} \quad \text{(5-26)}$$

$$\mathbf{Pr_{34}} = \frac{\nu_{34}}{\alpha_{34}} \quad \text{(5-27)}$$

Where:

k_{34} = thermal conductance of annulus gas at T_{34} (W/m-K)

T_3 = outer absorber surface temperature (^oC)

T_4 = inner glass envelope surface temperature (^oC)

D_3 = outer absorber diameter (m)

D_4 = inner glass envelope diameter (m)

Pr_{34} = Prandtl number

Ra_{D3} = Rayleigh number evaluated at D_3

β = volumetric thermal expansion coefficient (1/K)

T_{34} = average temperature, $(T_3 + T_4)/2$ (^oC)

This correlation assumes long, horizontal, concentric cylinders at uniform temperatures, and is valid for $Ra_{D4} > (D_4 /(D_4 - D_3))^4$. All physical properties are evaluated at the average temperature $(T_3 + T_4)/2$.

5.4.2 Radiation heat transfer

The radiation heat transfer between the absorber and glass envelope (q'_{34rad}) is estimated with the following equation.

$$\mathbf{q'_{34rad}} = \frac{\sigma\pi D_3(T_3^4 - T_4^4)}{(1/\varepsilon_3 + (1-\varepsilon_4)D_3/(\varepsilon_4 D_4))} \quad \text{(5-28)}$$

Where:

σ = Stefan-Boltzmann constant (W/m^2-K^4)

D_3 = outer absorber diameter (m)

D_4 = inner glass envelope diameter (m)

T_3 = outer absorber surface temperature (K)

T_4 = inner glass envelope surface temperature (K)

ε_3 = Absorber selective coating emissivity

ε_4 = glass envelope emissivity

5.5 Heat transfer from the glass envelope to the atmosphere

5.5.1 Convection Heat Transfer

The convection heat transfer from the glass envelope to the atmosphere (q'_{56conv}) is the largest source of heat loss, especially if there is a wind.

From Newton's law of cooling

$$\mathbf{q'_{56conv} = h_{56}\pi D_5(T_5 - T_6)} \text{.................................(5-29)}$$

$$\mathbf{h_{56} = \frac{k_{56}}{D_5} Nu_{D5}} \text{..(5-30)}$$

Where:

T_5 = glass envelope outer surface temperature (^oC)

T_6 = ambient temperature (^oC)

h_{56} = convection heat transfer coefficient for air at $(T_5 – T_6)/2$ (W/m^2-K)

k_{56} = thermal conductance of air at $(T_5 – T_6)/2$ (W/m-K)

D_5 = glass envelope outer diameter (m)

Nu_{D5} = average Nusselt number based on the glass envelope outer diameter

The Nusselt number depends on whether the convection heat transfer is natural (no wind) or forced (with wind).

a) No Wind Case

If there is no wind, the convection heat transfer from the glass envelope to the environment will be by natural convection. For this case, the correlation developed by Churchill and Chu will be used to estimate the Nusselt number.

$$\mathbf{\bar{N}u_{D5} = \left\{0.60 + \frac{0.387Ra_{D5}^{1/6}}{\left[1+(0.559/Pr_{56})^{9/16}\right]^{8/27}}\right\}^2} \text{........................(5-31)}$$

$$\mathbf{Ra_{D5} = \frac{g\beta(T_5 - T_6)D_5^3}{(\alpha_{56}\nu_{56})}} \text{..(5-32)}$$

$$\mathbf{\beta = \frac{1}{T_{56}}} \text{..(5-33)}$$

$$\mathbf{Pr_{56} = \frac{\nu_{56}}{\alpha_{56}}} \text{...(5-34)}$$

Where:

Ra_{D5}=Rayleigh number for air based on the glass envelope outer diameter, D_5

g=gravitational constant (9.81 m/s^2)

α_{56} = thermal diffusivity for air at T_{56} (m^2/s)

β = volumetric thermal expansion coefficient (ideal gas) (1/K)

Pr_{56} = Prandtl number for air at T_{56}

ν_{56} = kinematic viscosity for air at T_{56} (m^2/s)

T_{56}= film temperature $(T_5 + T_6)/2$ (K)

This correlation is valid for $10^5 < Ra_{D5} < 10^{12}$, and assumes a long isothermal horizontal cylinder. Also, all the fluid properties are determined at the film temperature,$(T_5 + T_6)/2$.

b) Wind case

If there is wind, the convection heat transfer from the glass envelope to the environment will be forced convection. The Nusselt number in this case is estimated with Zhukauskas' correlation for external forced convection flow normal to an isothermal cylinder.

$$\mathbf{\bar{N}u_{D5} = CRe_{D5}^{m}Pr_{6}^{n}\left(\frac{Pr_6}{Pr_5}\right)^{1/4}} \quad \text{.....(5-35)}$$

Table 5- 2:Reynolds number (Forristall,2003)

Re_D	C	m
1-40	0.75	0.4
40-1000	0.51	0.5
1000-200000	0.26	0.6
200000-1000000	0.076	0.7

Where:

n = 0.37, for Pr <=10

n = 0.36, for Pr >10

This correlation is valid for $0.7 < Pr_6 < 500$, and $1 < Re_{D5} < 10^6$. All fluid properties are evaluated at the atmospheric temperature, T_6, except Pr_5, which is evaluated at the glass envelope outer surface temperature.

5.5.2 Radiation heat transfer

The net radiation transfer between the glass envelope and sky becomes.

$$\mathbf{q'_{57rad}} = \sigma D_5 \pi \varepsilon_5 (T_5 - T_7) \quad \text{.....(5-36)}$$

Where:

σ = Stefan-Boltzmann constant (5.670E-8 W/m^2-K^4)

D_5 = glass envelope outer diameter (m)

ε_5 = emissivity of the glass envelope outer surface

T_5 = glass envelope outer surface temperature (K)

T_7 = effective sky temperature (K)

CHAPTER SIX

SIMULATION OF PARABOLIC TROUGH SYSTEM

In this section mathematical equation developed in chapter four is used for simulation. The geometry of the collector will be determined and model will be conducted using MATLAB for representative days of the month.

This model is used to determine all overall heat transfer coefficients of shell and tube heat exchangers, mass flow rate of the HTF, effective area required to fulfil steam demand by the factory, mass flow rate of steam and efficiency of parabolic trough collector. The following chart indicates how the efficiency of the collector is obtained.

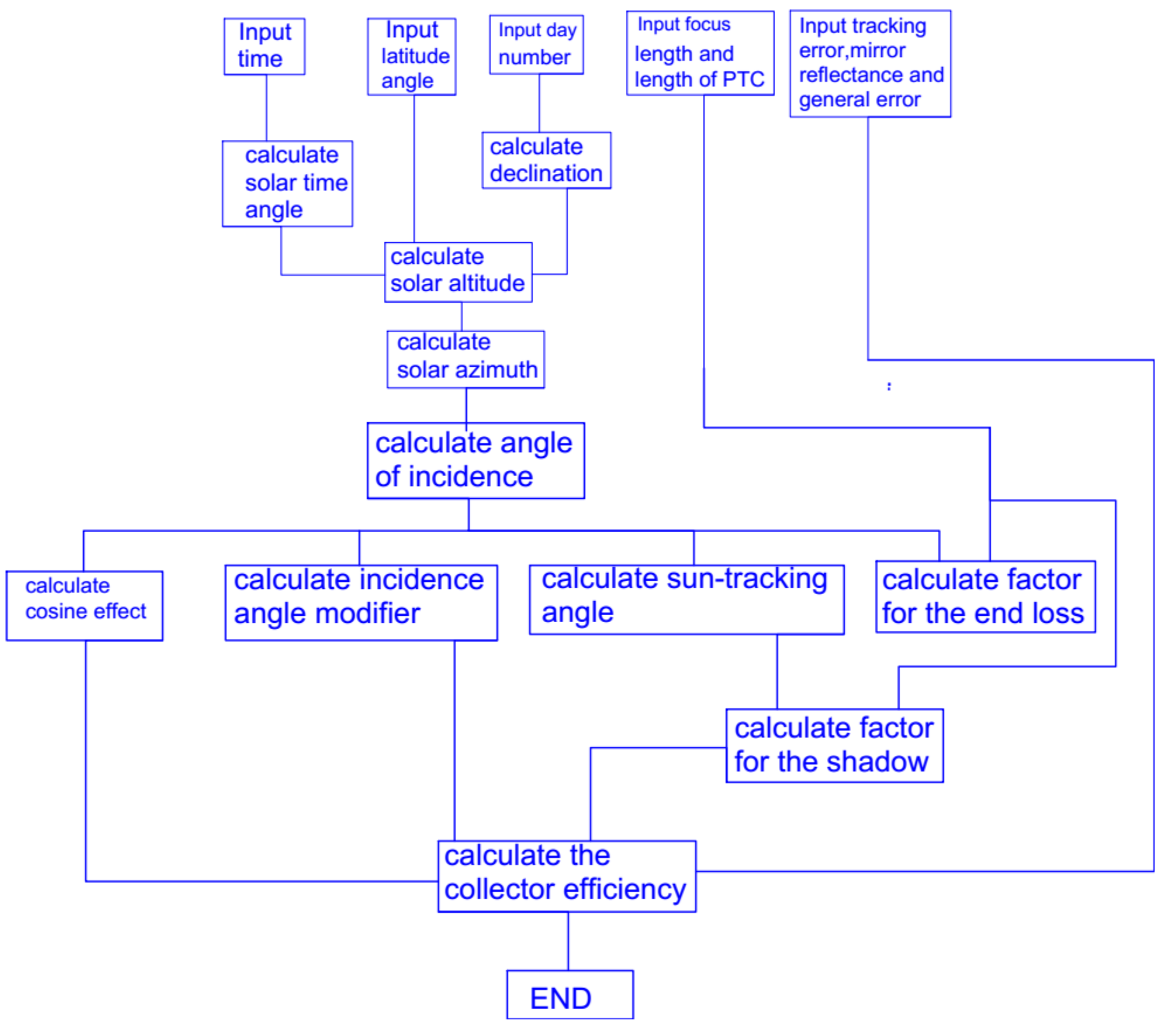

Figure 6- 1: Flow chart of calculating the endless factor, shadowing factor, cosine effect and efficiency.

- Rim angle

$$\tan\psi = \frac{\frac{a}{f}}{2-\frac{1}{8}(\frac{a}{f})^2} = \frac{\frac{5}{1.84}}{2-\frac{1}{8}(\frac{5}{1.84})^2} = \frac{2.72}{1.0752} = \underline{2.5298}$$

$$\psi = \tan^{-1}(2.5298) = \underline{68.43^o}$$

- Surface area

Surface area of parabolic trough is equal to:

$$A = \left(\frac{a}{2}\sqrt{1+\frac{a^2}{16f^2}} + 2f * \ln\left(\frac{a}{4f} + \sqrt{1+\frac{a^2}{16f^2}}\right)\right)*l$$

$$= \left(\frac{5}{2}\sqrt{1+\frac{5^2}{16*1.84^2}} + 2*1.84 * \ln\left(\frac{5}{4*1.84} + \sqrt{1+\frac{5^2}{16*1.84^2}}\right)\right)*12$$

$$= (3.0223+\ln(3.68+1.20893))*12 = \underline{55.3113}\ m^2$$

- **Beam radiation**

Wenji pulp and paper factory is located at a distance 10 km from Adama town so area contains almost approximate weather condition with Adama. Because of there is no measured beam radiation data for Wenji pulp and paper factory; in this paper Adama beam radiation is used.

For clear day the beam radiation is calculated based on three important parameter.

These are:

i. Longitude $= 39^o16'9.3252'' = 39.269257^o$East
ii. Latitude $= 8^o30'52.1172'' = 8.51447^o$North
iii. Altitude= 1869 m

The result of the simulation for two different beam radiations is considered in this paper. One is calculated beam radiation for clear representative day of the year and the other is beam radiation obtain from measured global radiation in *Adama* meteorology 2014. The results are given in the next pages.

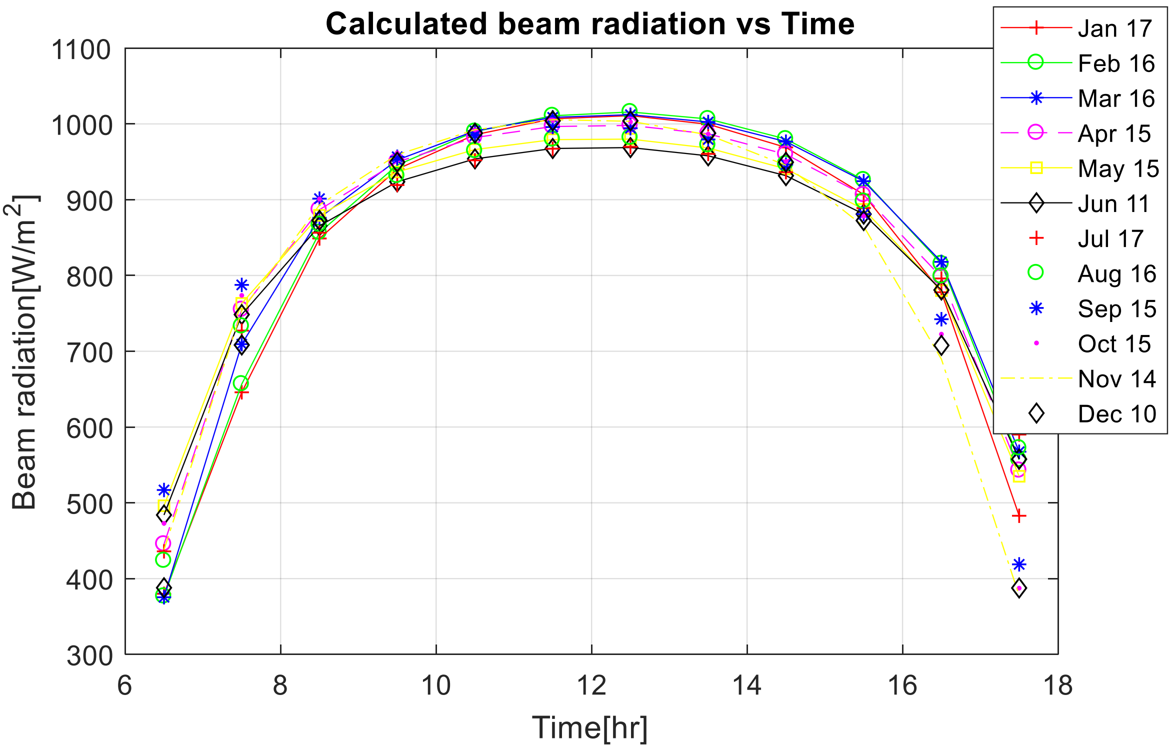

Figure 6- 2: Beam radiation for clear day.

Figure 6-2 indicate that beam radiation calculated for clear day. It is indicates that there is a good solar intensity in a clear day in all months. So that *Adama* is suitable for solar system practical applications.

It is observed that maximum beam radiations are obtain in February 16, March16, November14 and December 10.This maximum values are attain at noon time and its values are around 1000 W/m^2.The minimum values are attaining in June 11 and July 17.

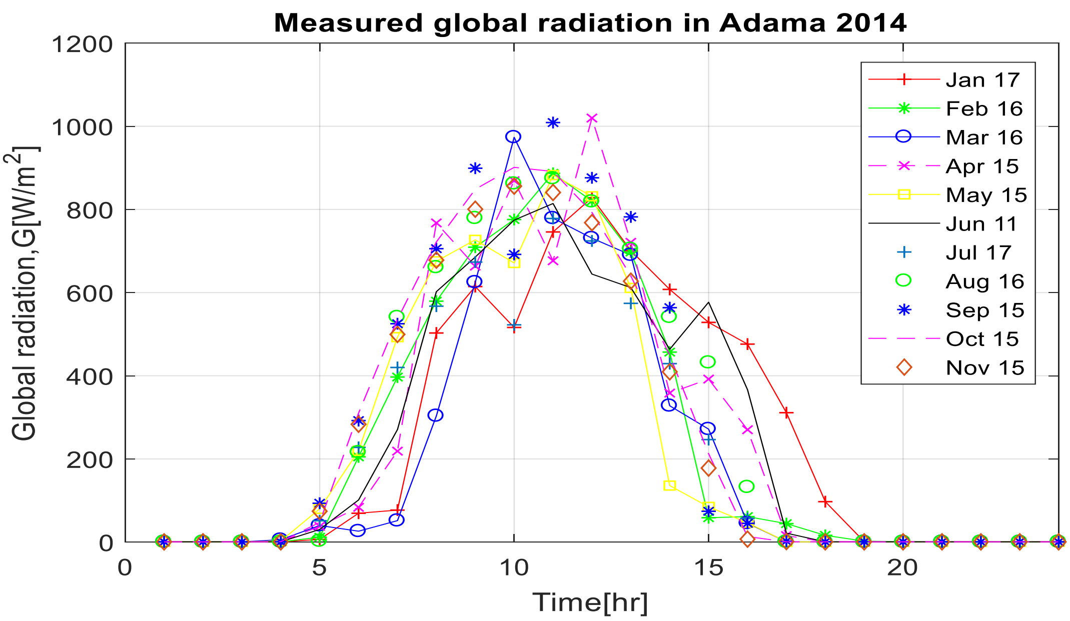

Figure 6- 3: Measured global radiation

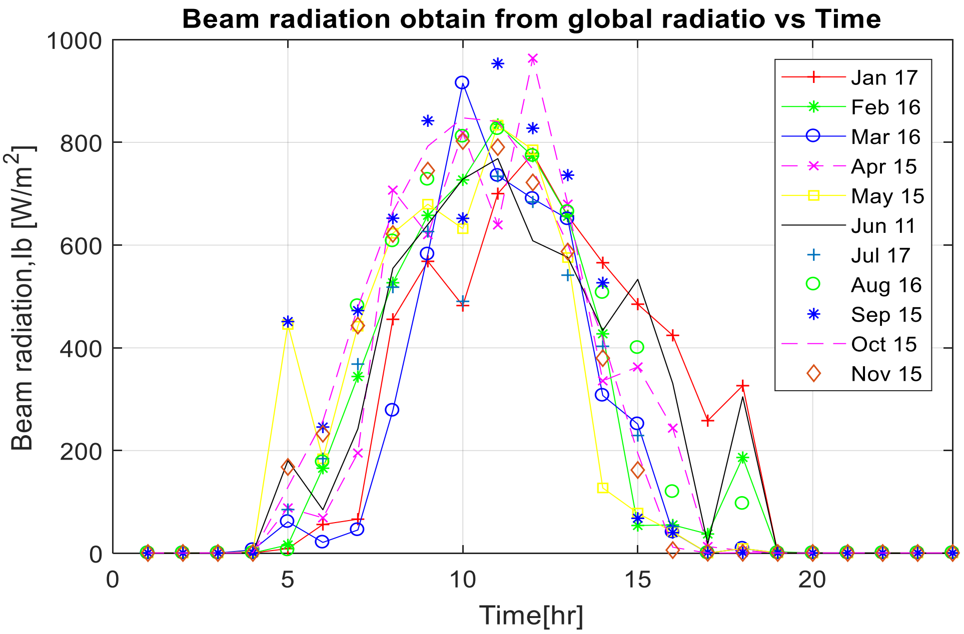

Figure 6- 4:Beam radiation obtain from measured global radiation

The maximum value is obtained in April 15 and September 15.Whereas the minimum value is exist in January 17 and July 17.

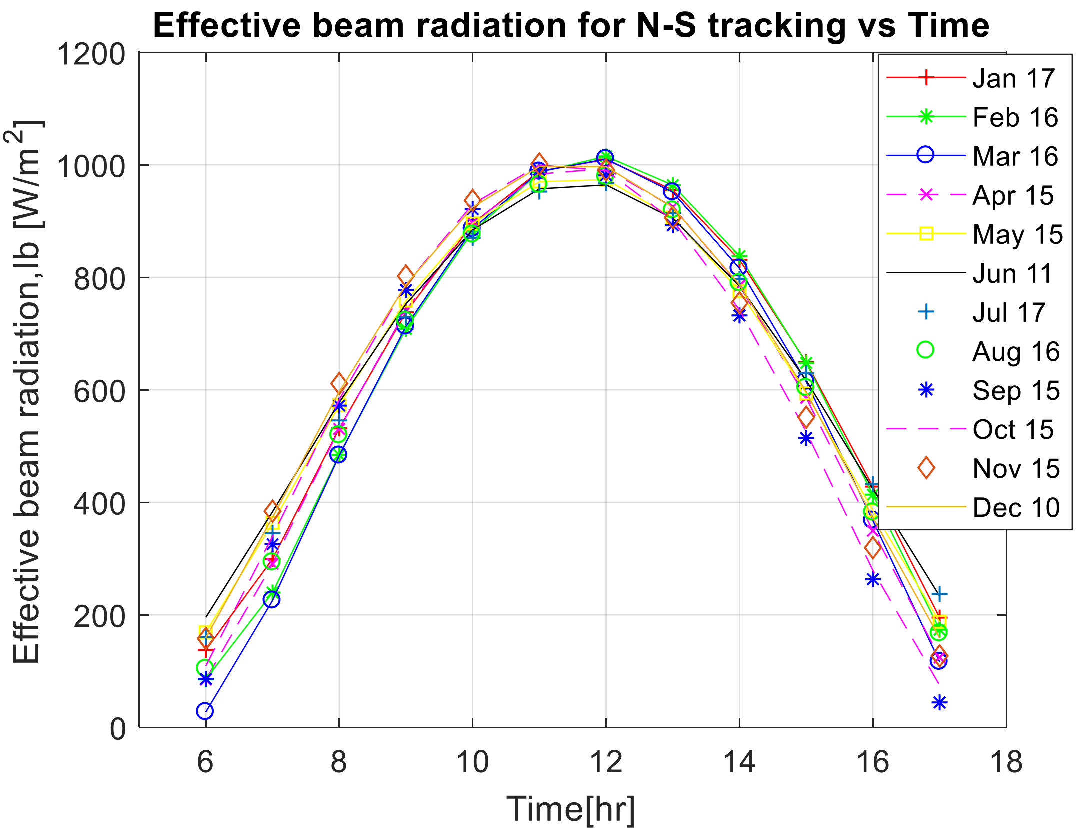

Figure 6- 5:Effective beam radiation for north-south tracking.

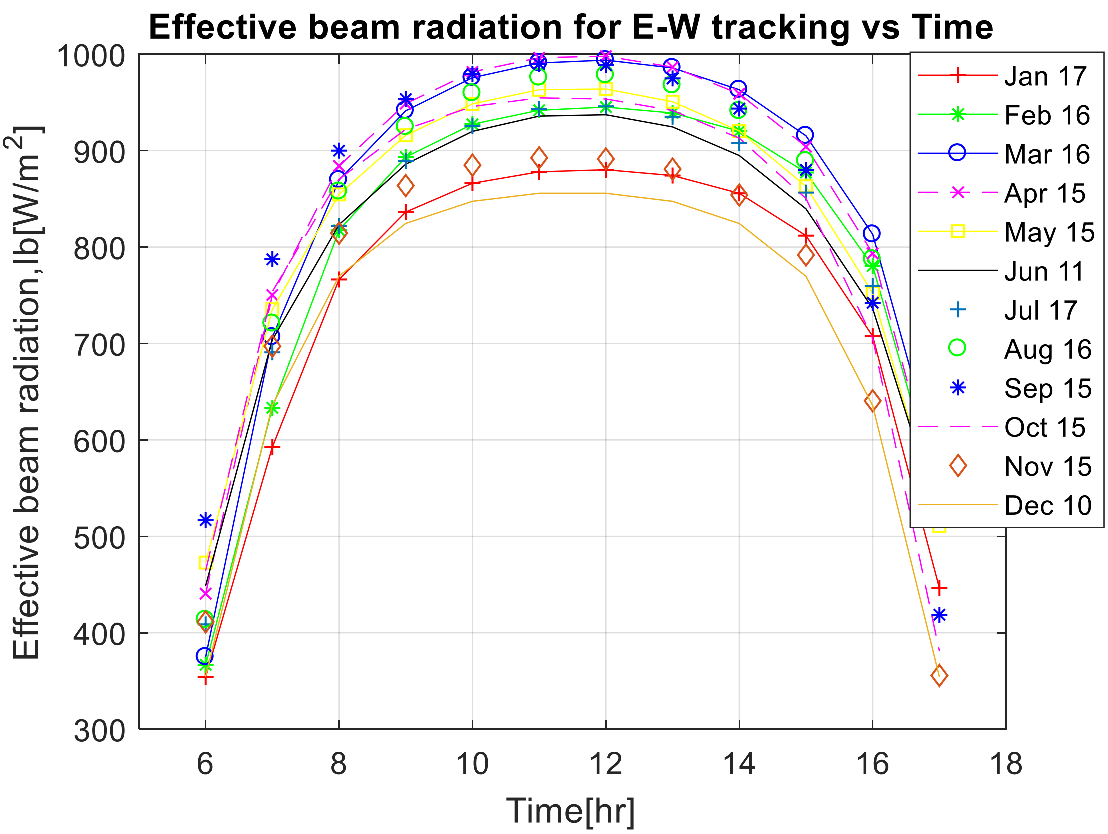

Figure 6- 6: Effective beam radiation for east-west tracking.

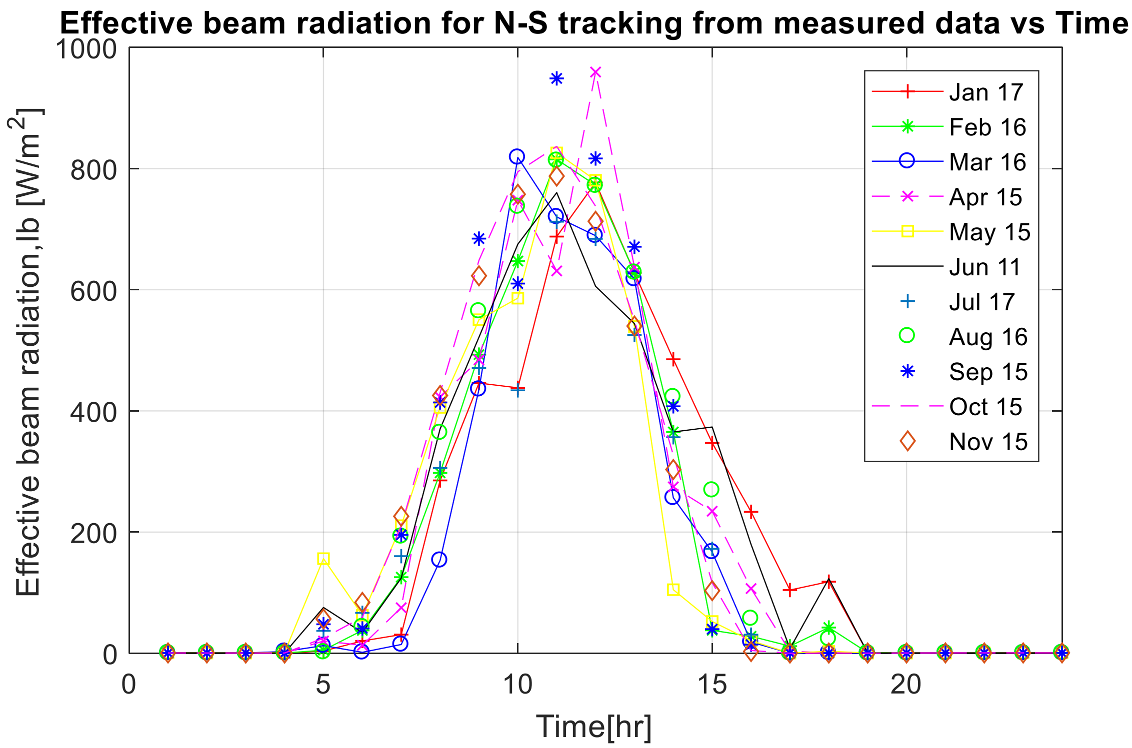

Figure 6- 7: Effective beam radiation for North-South tracking

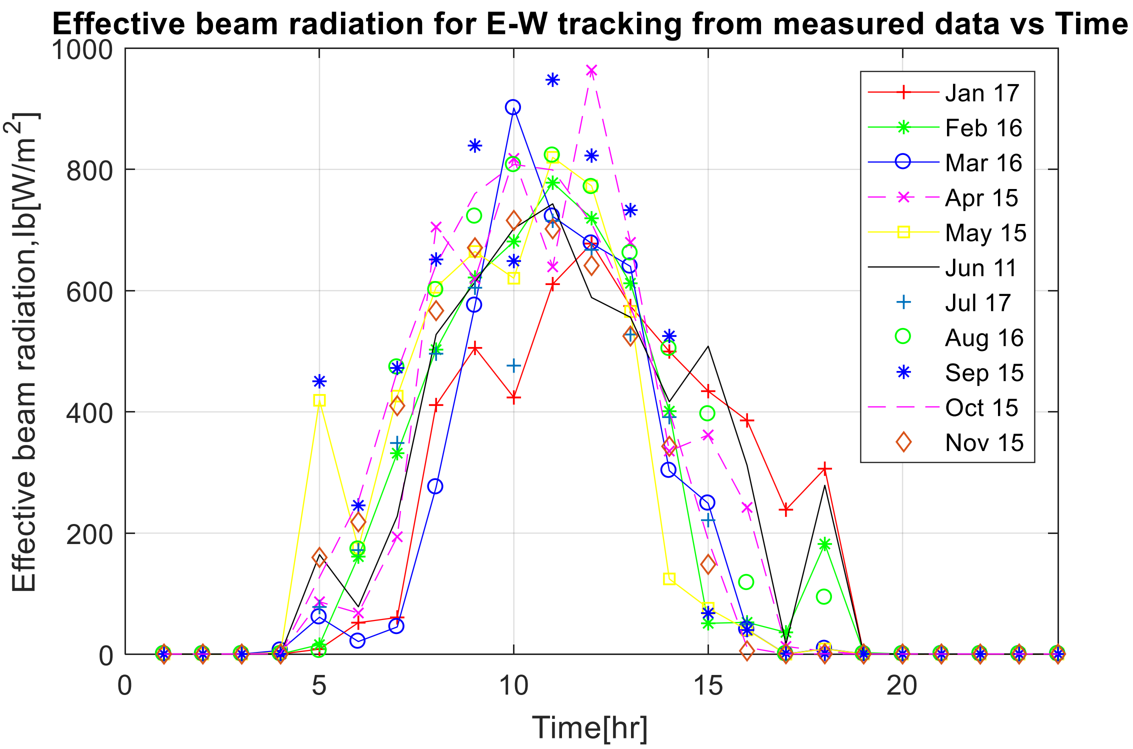

Figure 6- 8: Effective beam radiation for East-West tracking.

Figure 6-5 through 6-8 are indicate that the amount of beam radiation obtained using tracking mechanism. It is observed that East-West tracking is better to obtain a good beam radiation in a short time.

6.2 Result of parabolic trough model

The model is done using MATLAB software. This model is used to determine all overall heat transfer coefficients of shell and tube heat exchangers, mass flow rate of the HTF, optical efficiency and thermal efficiency. The MATLAB model developed is also used to determine the effective area of solar field needed to meet the needed mass flow rate steam.

Wenji pulp and paper factory need 12,902 kg/hr of saturated steam energy for drying the paper. This energy is the net energy demanded from the HTF. The HTF temperature inlet to the heat exchanger is set to $T_{out,\ HTF}$ =300 ^oC. The inlet temperature of the HTF coming from the heat exchangers to the parabolic trough collectors is then set to be equal to $T_{in,\ HTF}$ = 150 ^oC.

Specific heat capacity at constant pressure for the heat transfer fluid (Therminol VP-1) is calculated at average temperature of T_{avg} = 225 ^oC.

For ambient temperature of 19.3 ^oC, the difference between collector outlet temperature and ambient temperature becomes, ΔT_{out} = 280.7 ^oC.

Similarly the difference between collector inlet temperature and ambient temperature becomes, ΔT_{in} = 130.7 ^oC.

- ✓ Maximum efficiency of the collectors is obtained at midday when the incident angle is zero. Thus the incident angle modifier is equal to one. Similarly at midday no collector shades other collector this set row shading factor to be equal to one.
  The end loss factor is also equal to one because theta is set to be equal to zero.

- ✓ Clean reflectivity and cleanness of the solar field (CR and CL) factors are set to be equal to the reference value of 0.94 (Assefa,2011). In the model no broken mirrors are considered and the solar field area is also calculated when it is fully operational.
- ✓ The reference ambient temperature and reference wind velocity variables are used to calculate the design heat losses, and they do not have a significant effect on the solar field sizing calculations. Reasonable values for those two variables are the average annual measured ambient temperature and wind velocity at the project location. Therefore the reference ambient temperature and wind velocity are assumed to be 19.3 ^{o}C and 4 m/s respectively for Adama.

Four factors affect the choice of a reference direct normal radiation value for a given system:

- ✓ Location
- ✓ Thermal energy Storage capacity of the plant
- ✓ Maximum thermal energy storage charge rate (Maximum Power to Storage)
- ✓ Variability of the solar resource over the year, determined by the weather.

Typically, the reference beam radiation (direct normal radiation) value can be set to the actual direct normal radiation value that has a cumulative annual frequency value.

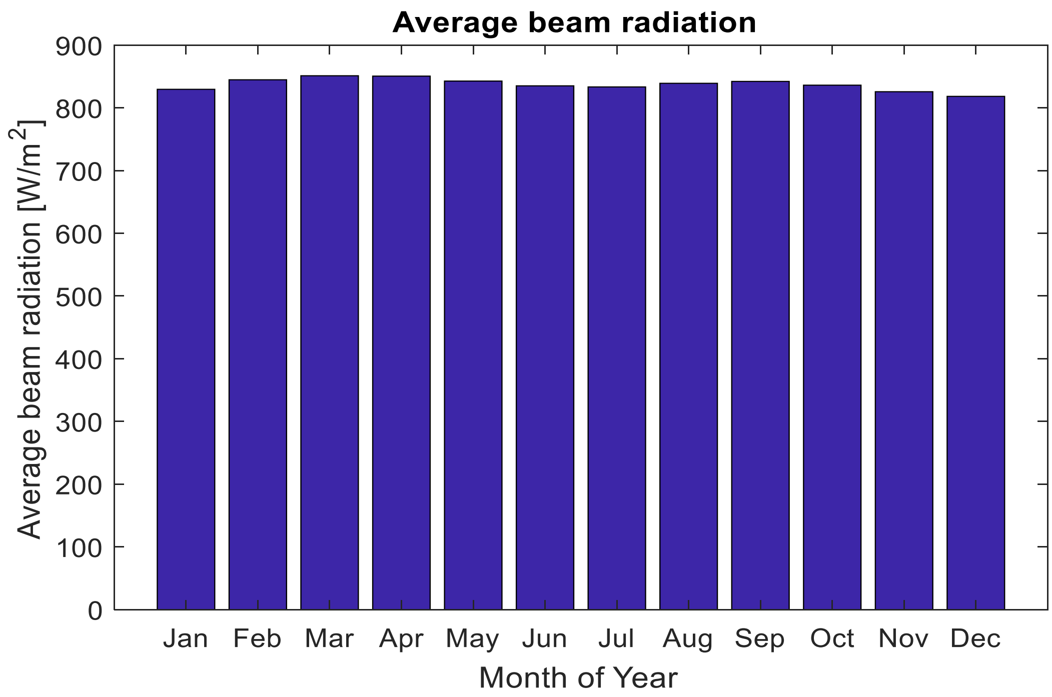

Figure 6- 9: Average beam radiation

Minimum average beam radiation is exist in December 10 which is equal to 818 w/m^2.

Inserting this values in efficiency Equation gives reference efficiency of the solar field η_{SF} = 69%.

This efficiency value is a reference maximum value of the solar field. The actual efficiency of the solar field is less than the above value due to several reasons. First of all the beam radiation is not always found at its maximum value. The incident angle is not also equal to zero. Although one axis tracking system is governed by the collectors, the incident angle depends on solar time and day of the year. Accordingly the end loss and the row shading factors differ from one.

Optical efficiency is calculated from the value given in table 4-2 and its value equal to 75%.

Similarly thermal efficiency is obtained equal to be 68%.

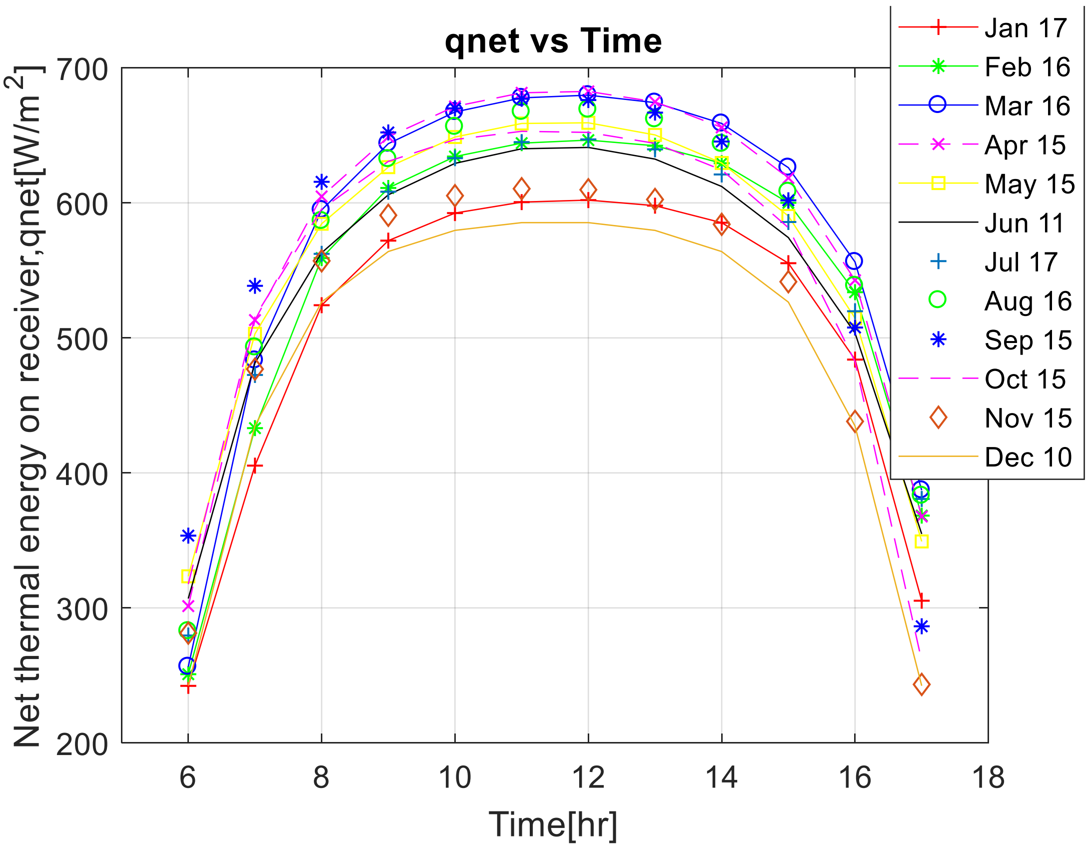

Figure 6- 10: Net thermal energy (q_{net}) available on absorber tube.

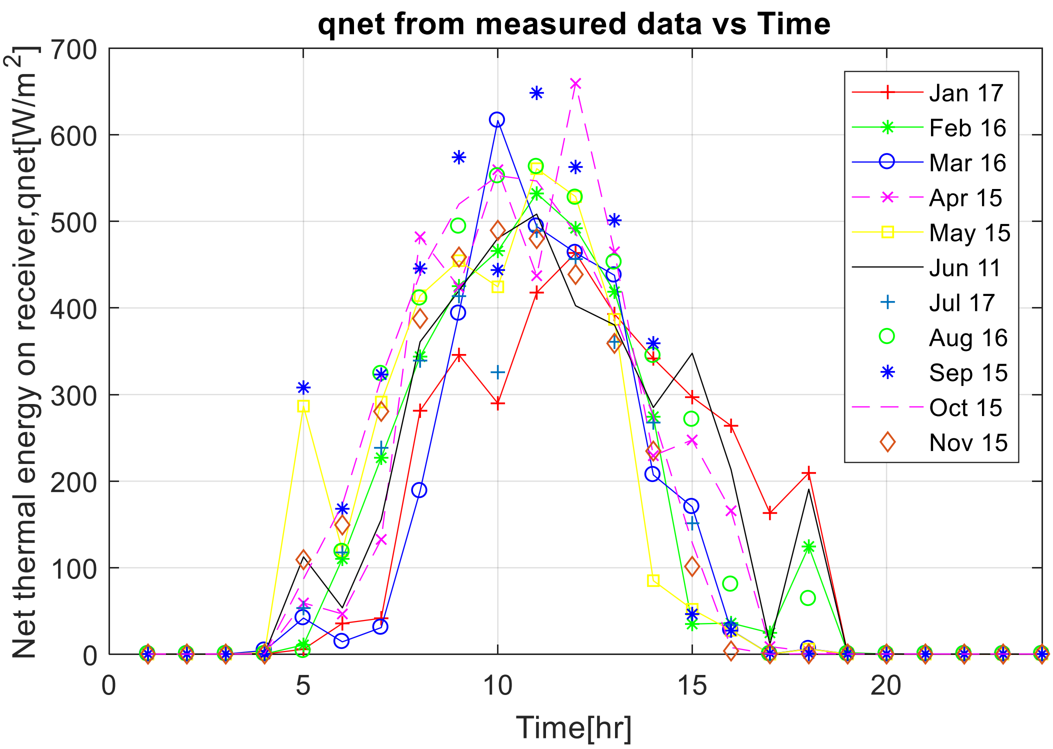

Figure 6- 11:Net thermal energy (q_{net}) available on absorber tube.

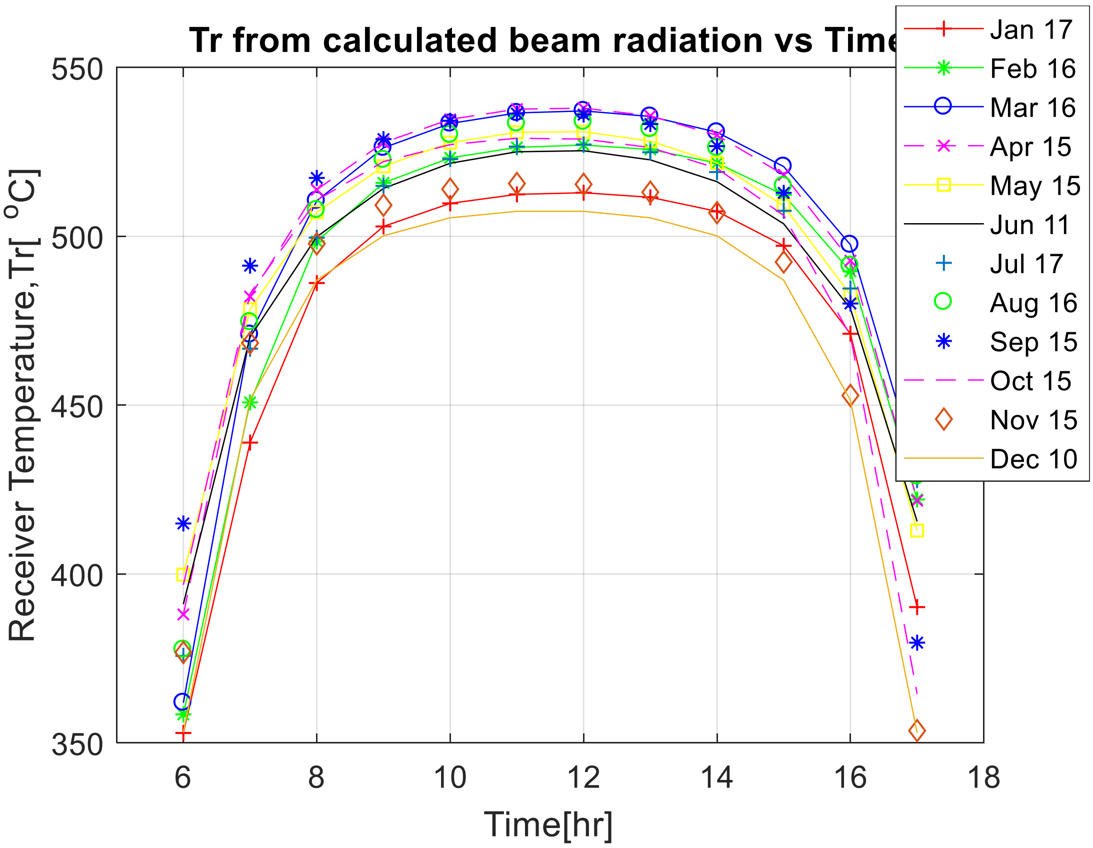

Figure 6- 12: Receiver temperature for clear day.

Receiver temperature for clear day is indicated in figure 6-12. For clear day receiver temperature is attain maximum temperature in April 15, March 16 and September 15 and minimum is obtained in January 17 and December 10.

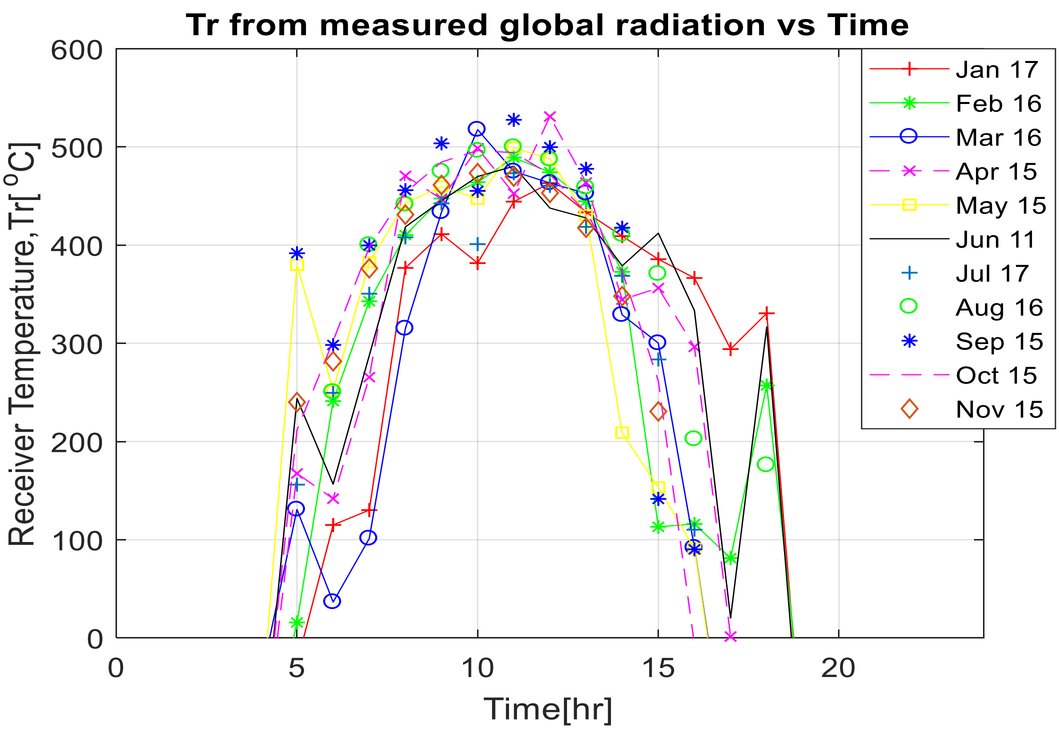

Figure 6- 13: Receiver temperature

The result obtained in the above graph is similar with that obtained for clear in some month like October 15, November 15 and August 16 but in other month like March 16,July 17 and January 17 fluctuation of receiver temperature is obtained. This is due to variation of intensity of solar radiation from time to time.

- Heat transfer fluid

Physical properties of Therminol VP-1 in liquid phase are shown in table (4-4) as a function of temperature (^{o}C) (Benidir et al.,2018).This property is calculated at average temperature of HTF equal to 225(^{o}C).

Density of HTF equal to be $\rho(T_{av}) = \underline{891.54}$ kg/m^3

Specific heat of HTF equal to be $C_p(T_{av})$=$\underline{2.0025}$ kJ/kg K

Thermal conductivity of HTF equal to be $k(T_{av})= \underline{0.1099}\ W/m.K$

Kinematic viscosity of HTF equal to be $v(T_{av}) = \underline{0.3706}$ mm^2/s

- Cross sectional area of absorber is given by:

$A_c = \pi * \frac{D_{ri}^2}{4} = 3.14 * \frac{0.066^2}{4} = \underline{0.0034}\ m^2$

Average mean velocity of HTF is equal to $u_m = \frac{\dot{m}}{\rho A_c} = \frac{0.5}{891.54*0.0034} = \underline{0.165}$ m/s

- **Reynolds number**

The value of Reynolds number is obtained from:

$Re = Re = \rho u_m D_{ri}/\mu = u_m D_{ri}/v = \frac{0.165*0.066}{0.3706*10^{-6}} = \underline{29{,}384.78}$

Because of Re> 2300 ; so the flow in the absorber tube is turbulent.

- Dynamic viscosity is given by:

$\mu = \rho * v(T_{av}) = 891.54*0.3706*10^{-6} = \underline{3.304\times 10^{-4}}$ kg/ms

- Prandtl number is given by:

$Pr = C_p \mu / k(T_{av}) = \frac{2002.5*3.304*10\text{^}-4}{0.1099} = \underline{6.02025}$

- Nusselt number is given by:

$Nu = 0.023(Re)^{0.8}(Pr)^{0.4} = 0.023 * 29{,}384^{0.8} * 6.02025^{0.4} = \underline{177.04}$

- Convective coefficient of HTF is given by:

$h_F = Nu*\frac{k(T_{av})}{D_{ri}} = 177.04*\frac{0.1099}{0.066} = \underline{294.8}\ W/m^2K$

- Mass flow rate in solar field

The mass of HTF in the tank is assumed to be constant and the tank is sized to provide an equivalent mass as the HTF exists in the solar field and expansion vessel. These can be evaluated by using receiver tubes (LS-2 collector) and expansion vessel volumes multiplied by the density of HTF at solar field outlet temperature.

The total mass of the HTF in the solar field can be found by:

$M_{HTF} = \frac{\pi \cdot (D_{HCE})^2}{4} \cdot L_{sca} \cdot N_{sca} \cdot \rho(T_{avg})$

$D_{HCE} = 0.066$ m

$L_{sca} = 47$ m

$N_{sca} = 38$

$M\_HTF = 3.14*\frac{0.066^2}{4}*47*38*891.54 = \underline{5{,}444.8}$ kg

- The volume of the HTF in the solar field can thus approximate as;

$V_{SF} = \frac{M_{SF}}{\rho(T_{avg})} = \frac{5{,}444.8}{891.54} = \underline{6.11}\ m^3$.

- Heat loss coefficient

Heat loss is obtained for representative day of the year using Matlab.

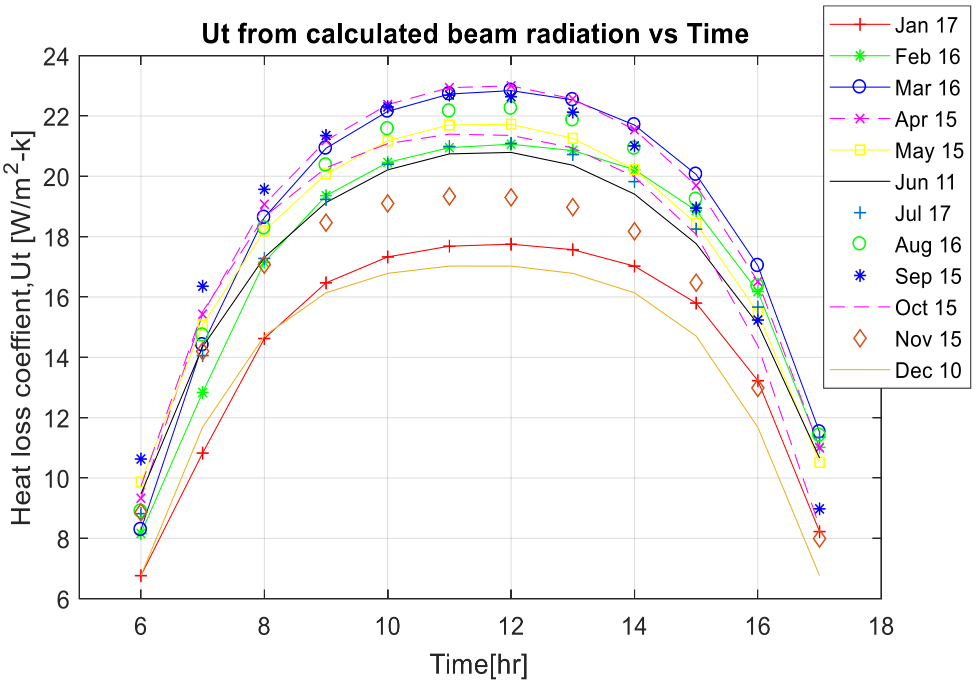

Figure 6- 14: Heat loss coefficient.

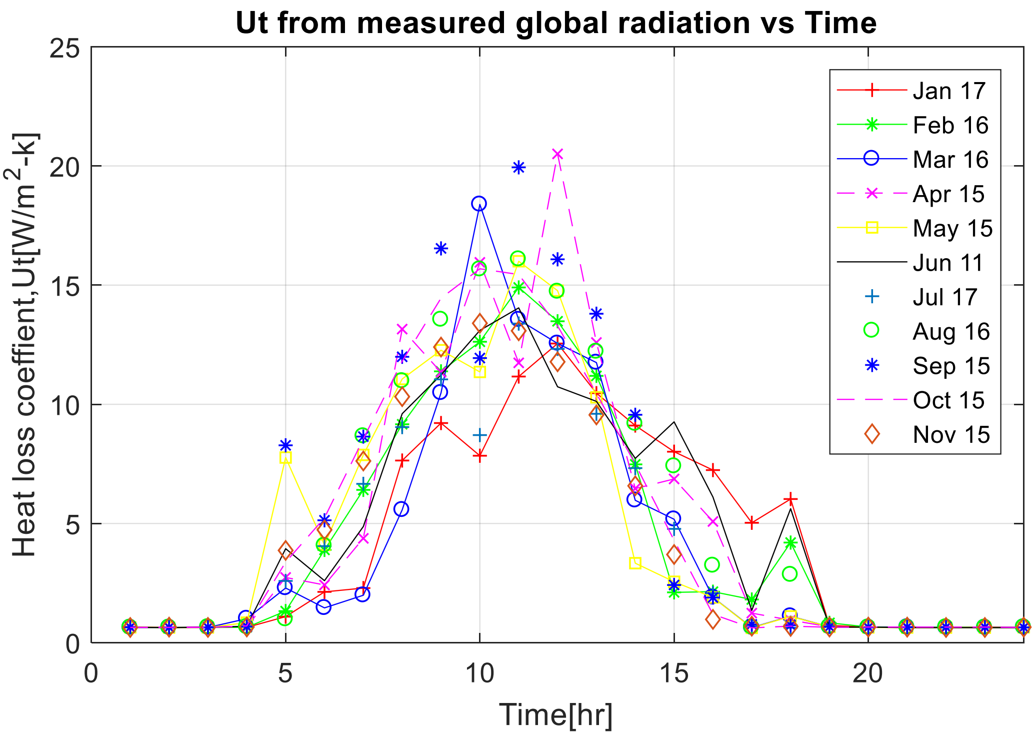

Figure 6- 15: Heat loss coefficient from measured global radiation

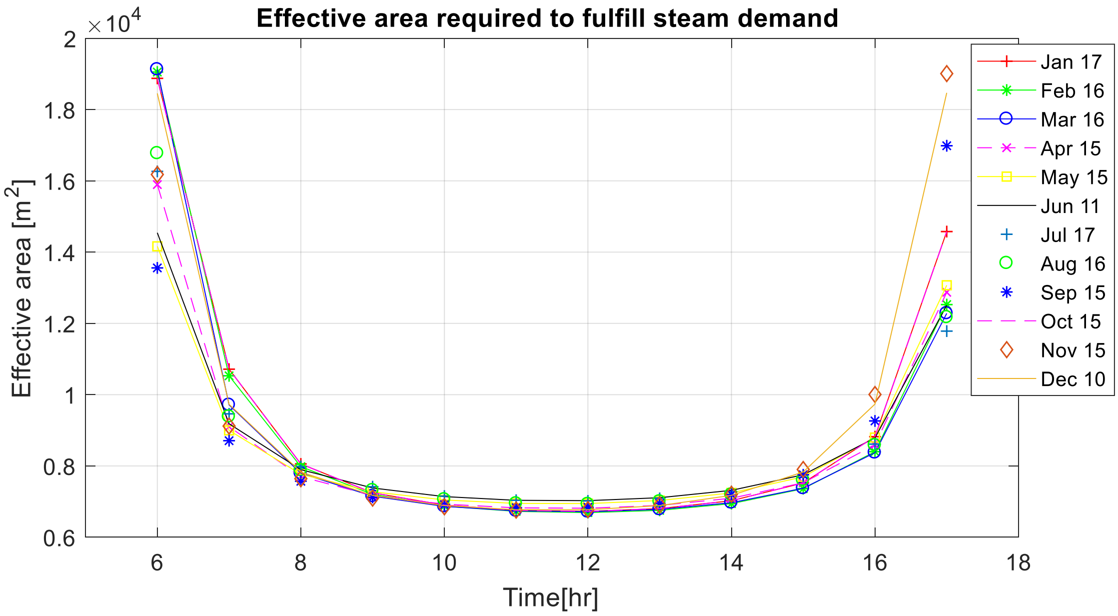

Figure 6- 16: Effective area required to fulfill steam demand.

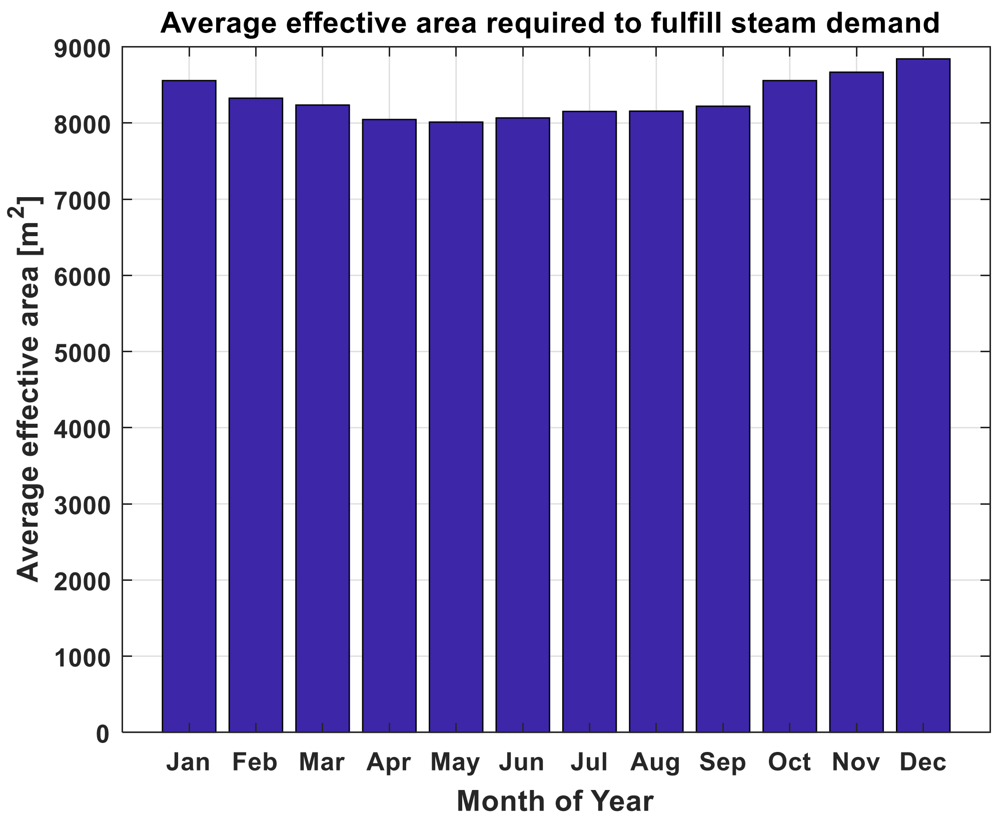

Figure 6- 17: Average effective area required to fulfil steam demand

Table 6- 1: Average effective area, pipe heat loss, heat absorbed by receiver and number of collector

Representative day of the month	Average effective area (m^2)	Average number of collector required
January 17	8557.6	36
February 16	8326.8	35
March 16	8237	35
April 15	8046.5	34
May 15	8013	34
June 11	8067.6	34
July 17	8152.8	35
August 16	8156.9	35
September 15	8221.7	35
October 15	8557.6	36
November 14	8668.3	37
December 10	8843	38

The width of parabolic trough is 5 m. Maximum average effective area is required in December 10 which is equal to 8,843 m^2. Total length of collector is equal to be 1,768.6 m. Length of one row collector is taken to be 47 m (LS-2). The required row number of collector is 38.

Power produced from this aperture area is a function of efficiency of a system and beam radiation.

- ✓ For average reference beam radiation selected in Adama equal to 818 W/m^2 and with zero incident angles the power produced will be:

$P = Ib \times \cos(\theta) \times Ap \times \eta_{SF} = 818 \times \cos(0) \times 8843 \times 0.69 = \underline{4991.2}$ kW

- ✓ For maximum area of PTC which is equal to 17807 m^2 .The power produced from this area when beam radiation is 350 W/m^2 existing will be:

$P = Ib \times \cos(\theta) \times Ap \times \eta_{SF} = 350 \times \cos(0) \times 17807 \times 0.65 = \underline{4051.1}$ kW

- ✓ For minimum area of PTC which is equal to 6253 m^2 .The power produced from this area when maximum beam radiation 1000W/m^2 is exist will be:

$P = Ib \times \cos(\theta) \times Ap \times \eta_{SF} = 1000 \times \cos(0) \times 6253 \times 0.7 = \underline{4377.1}$ kW

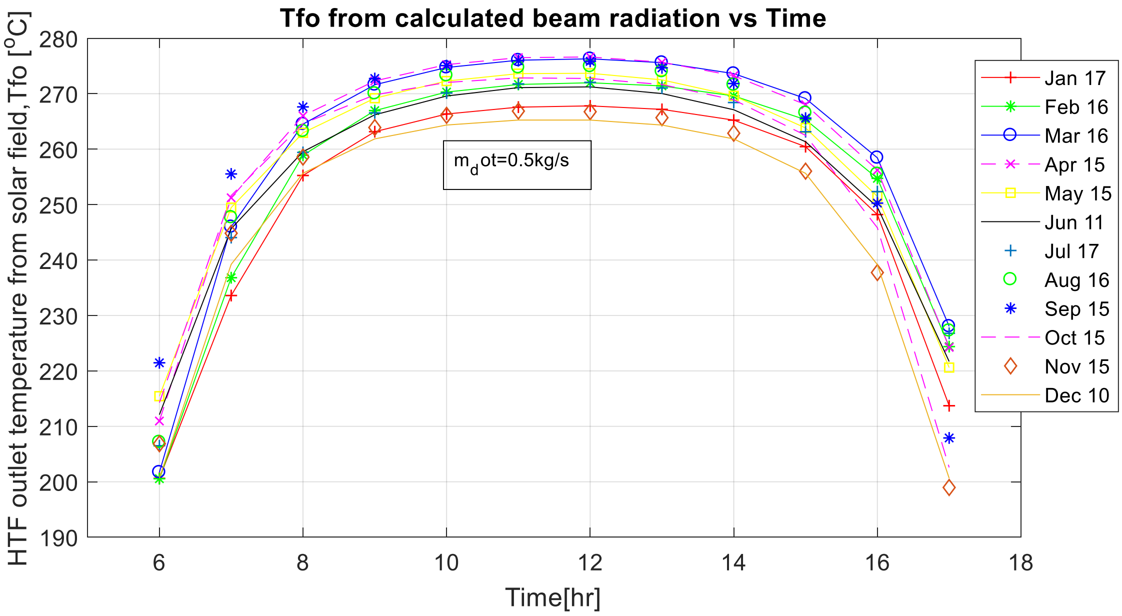

Figure 6- 18: HTF outlet temperature for clear day.

For constant mass flow rate equal to 0.5 kg/s the result of HTF outlet temperature for calculated beam radiation is indicated in figure 6-18 for representative day of the year.

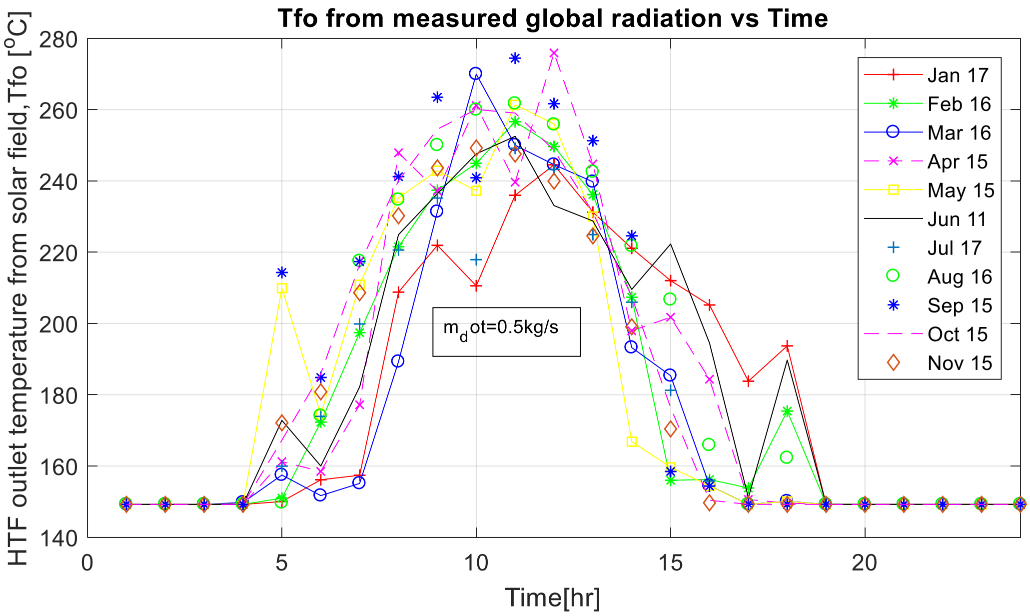

Figure 6- 19: HTF outlet temperature.

For constant mass flow rate equal to 0.5 kg/s the result of HTF outlet temperature for measured global radiation is indicated in figure 6-19 for representative day of the year.

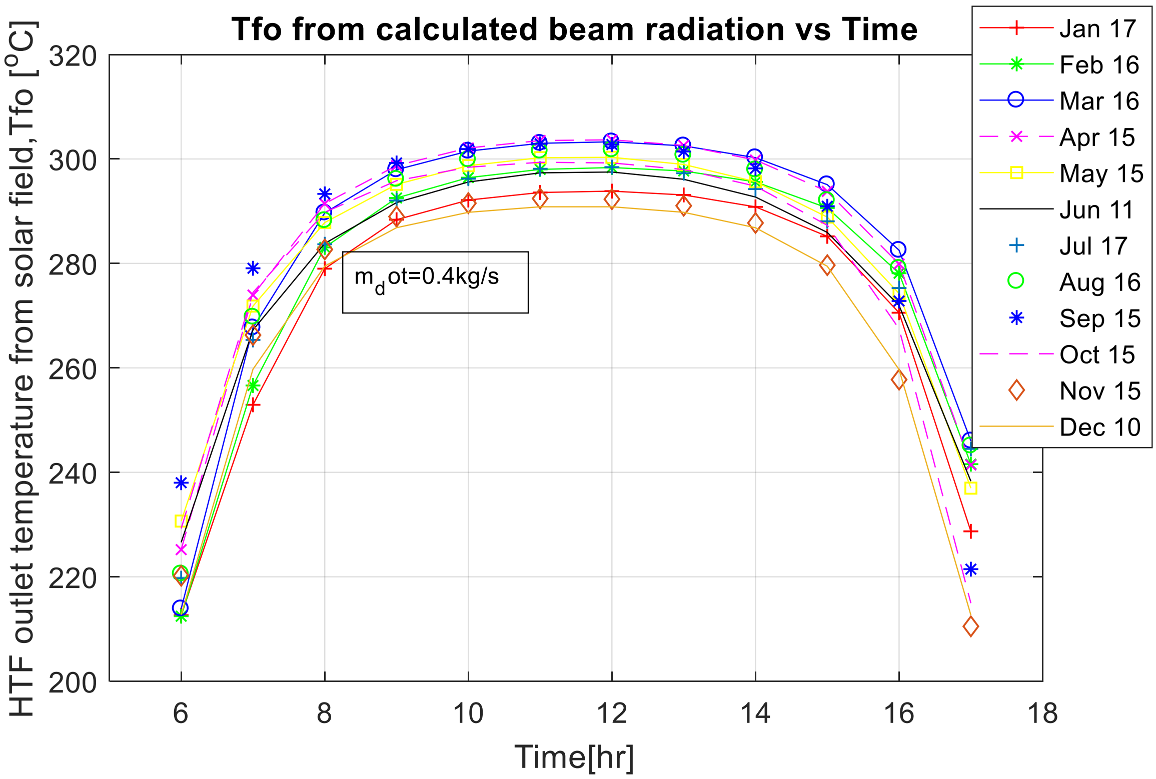

Figure 6- 20:HTF outlet temperature for clear day.

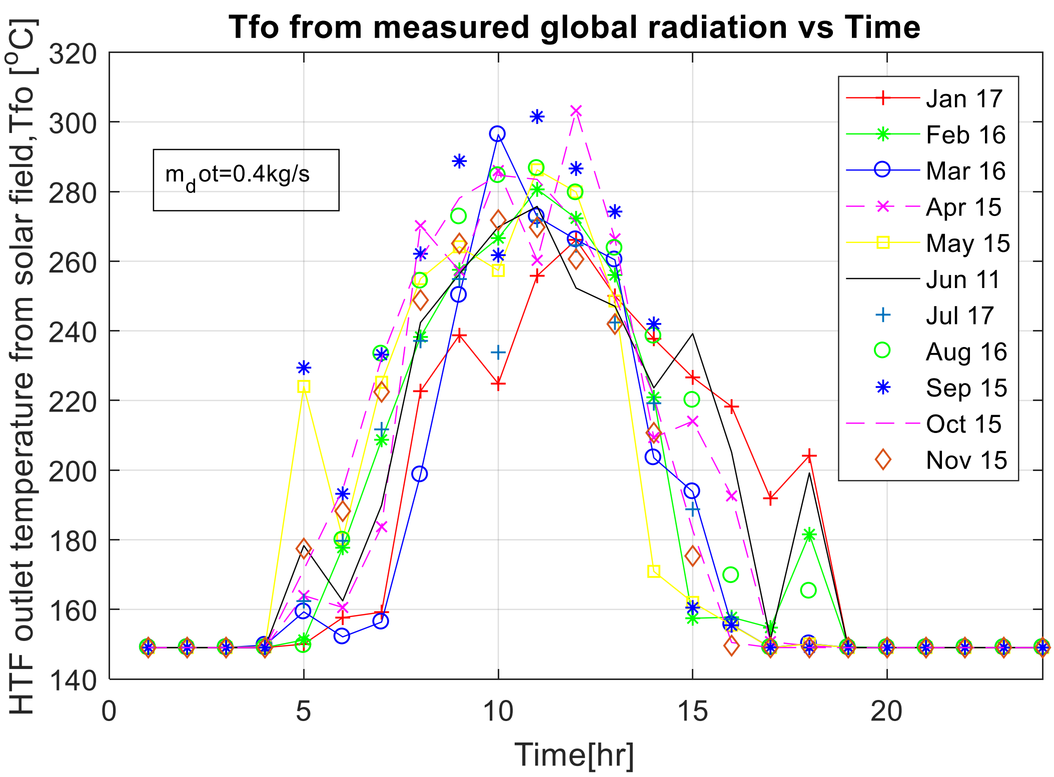

Figure 6- 21: HTF outlet temperature.

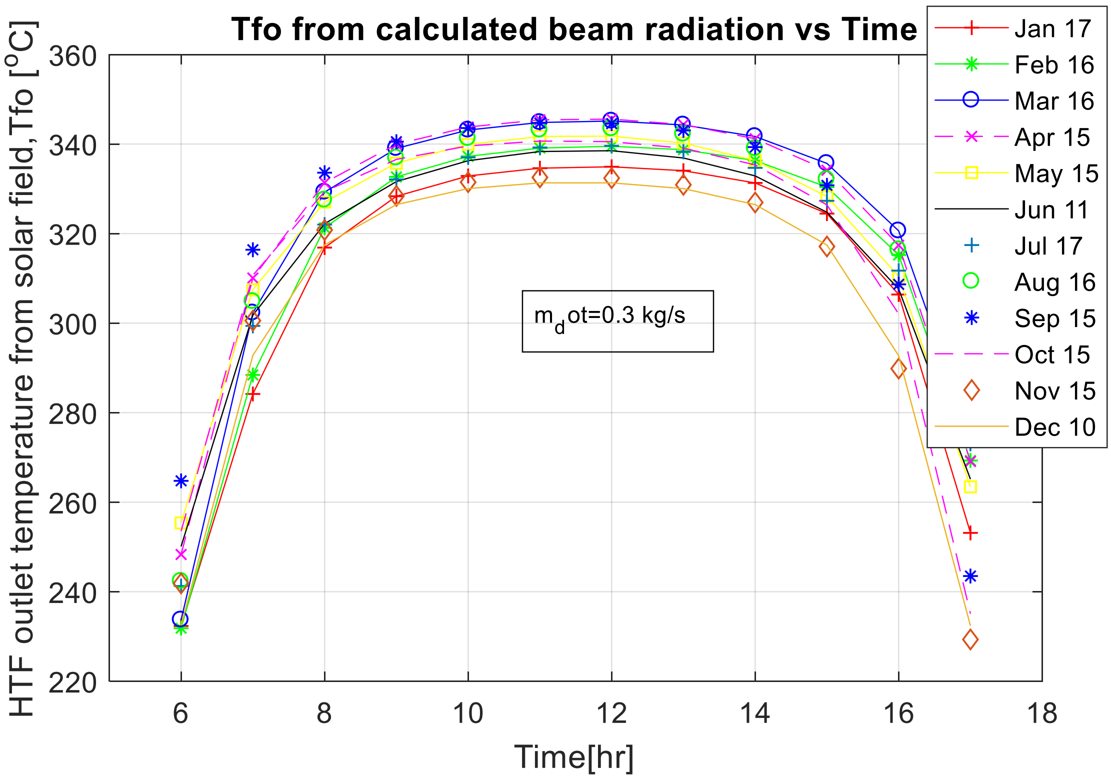

Figure 6- 22: HTF outlet temperature for clear day.

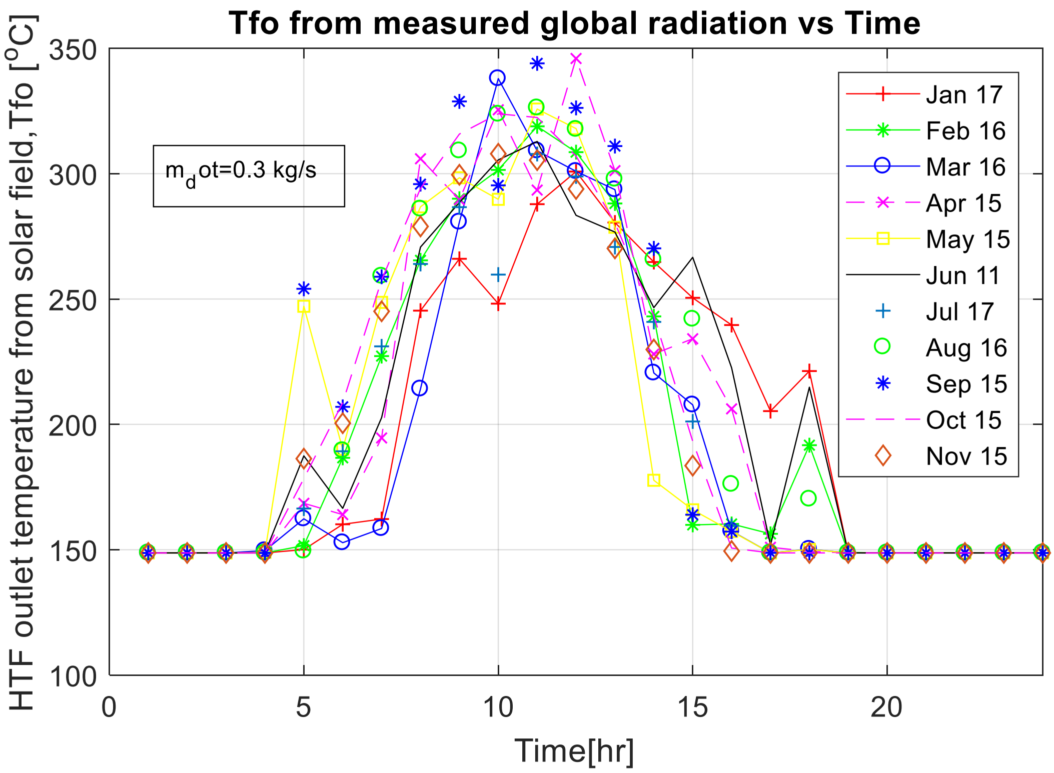

Figure 6- 23: HTF outlet temperature

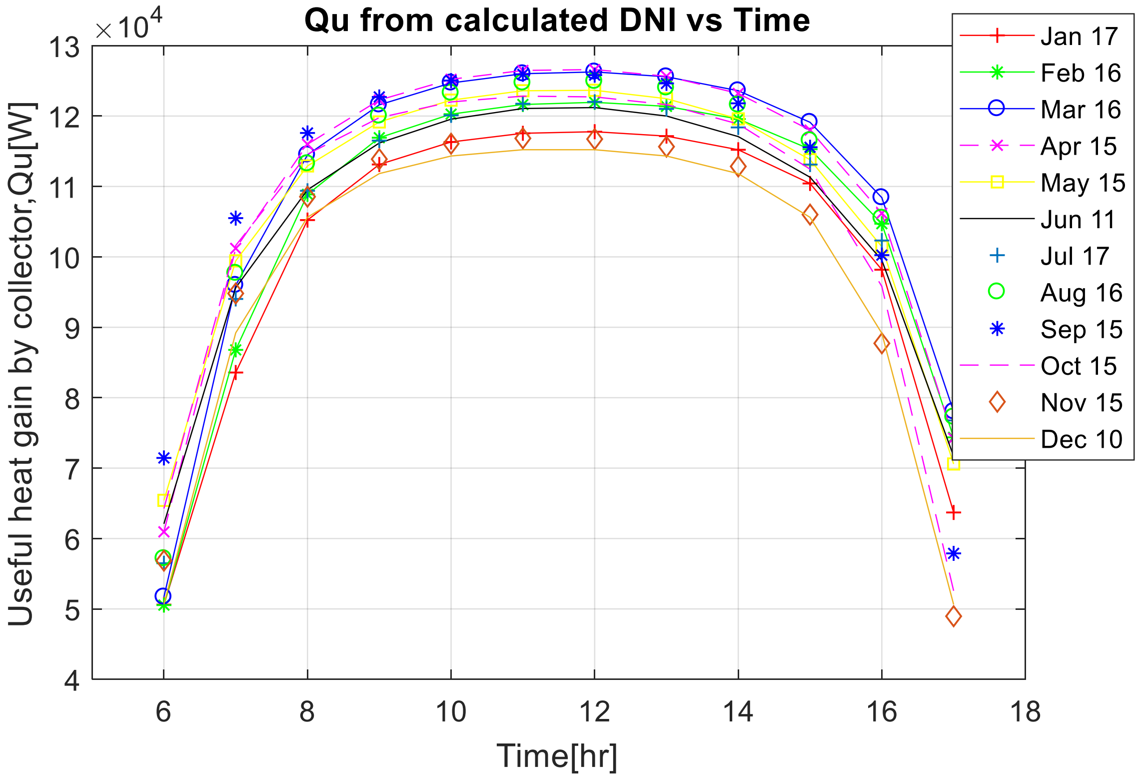

Figure 6- 24: Useful heat gain by collector.

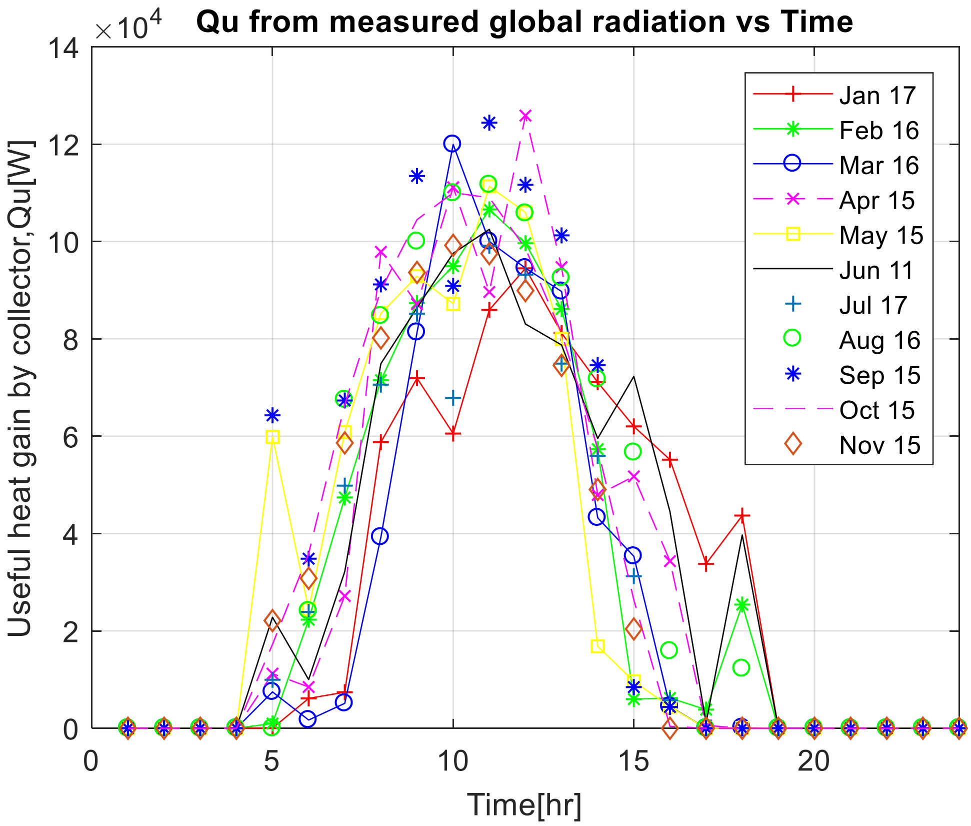

Figure 6- 25: Useful heat gain by collector.

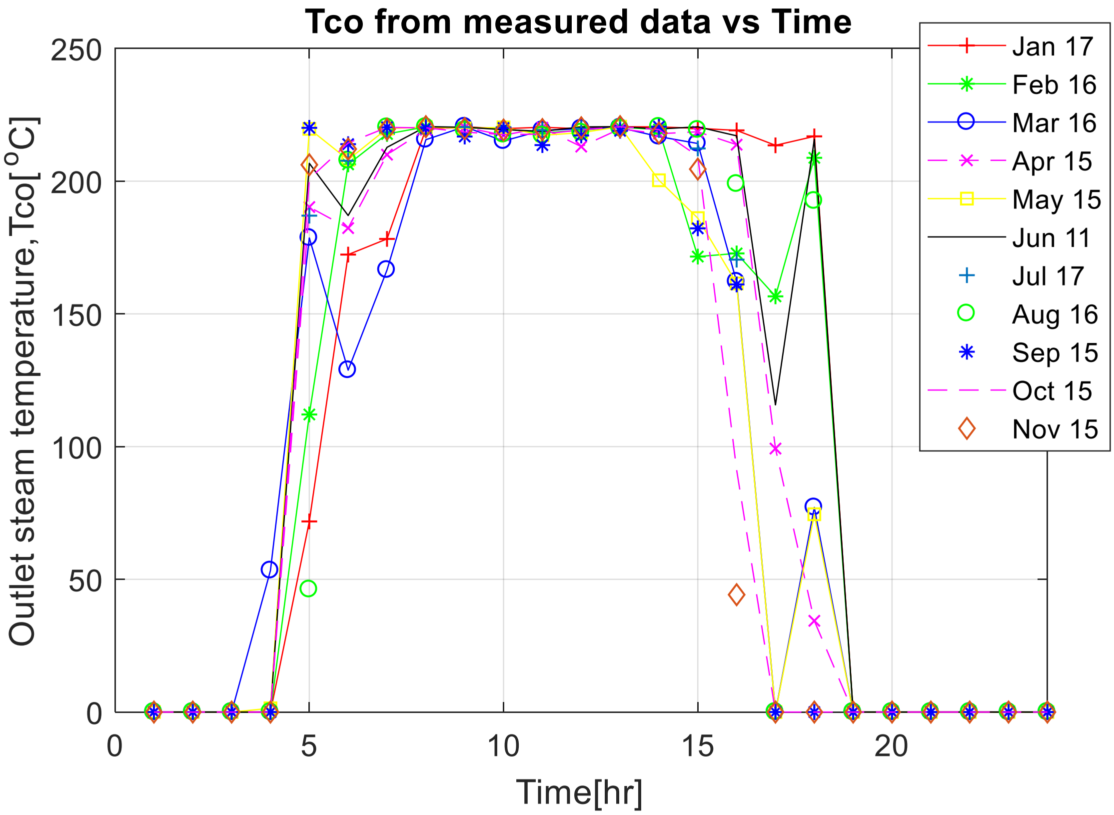

Figure 6- 26: Steam outlet temperature.

Figure 6-26 indicate temperature of steam outlet from heat exchanger. The appropriate mass of HTF inlet to heat exchanger to generate steam is 10 kg/s.

Table 6- 2:Steam outlet temperature (^oC) 2014.

Time(hr)	12am	1am	2am	3am	4am	5am	6pm	7pm	8pm	9pm	10pm	11pm
Jan-17	179.43	201.36	218.8	218.93	218.6	218.08	218.24	218.98	218.19	211.42	165.7	112.2
Feb-16	209.04	217.51	218.9	218.25	217.5	215.58	216.89	218.45	218.7	214.06	175.74	162.8
Mar-16	160.13	139.66	170.67	215.15	218.75	211.8	216.88	215.92	209.9	216.5	190.9	165.46
Apr-16	187.53	210.53	216.86	218.33	214.52	209.56	213.75	215.76	218.89	215.57	152.67	109.72
May-15	209.89	218.74	218.40	217.75	218.37	214.54	215.78	218.82	200.62	187.44	165.12	156.22
Jun-11	191.43	212.98	218.94	218.39	217.19	216.43	218.68	216.37	218.57	183.19	147.68	125.51
Jul-17	210.22	217.82	218.96	218.44	218.91	216.98	217.81	218.96	218.10	211.94	172.82	144.89
Aug-16	209.97	218.95	218.42	216.70	214.8	214.45	215.82	217.86	218.96	218.25	200.08	178.23
Sep-16	214.79	218.95	217.83	213.74	218.04	218.96	215.95	216.22	196.0	175.52	158.70	142.46
Oct-16	215.28	218.94	217.92	215.87	214.77	215.07	217.06	218.75	218.30	209.57	192.69	192.69
Nov-15	213.58	218.64	218.71	217.6	216.89	217.19	218.11	218.95	217.24	205.13	196.31	180.37

Table 6- 3:Steam outlet temperature (^oC) for clear day.

Time(hr)	1am	2am	3am	4am	5am	6pm	7pm	8pm	9pm	10pm	11pm	12pm
Jan-17	224.49	226.63	224.52	222.95	222.15	221.81	221.75	221.9	222.44	223.55	225.52	226.2
Feb-16	216.57	221.49	219.7	217.99	217	216.58	216.47	216.66	217.24	218.39	220.32	221
Mar-16	216.93	221.18	218.58	216.6	215.44	214.89	214.77	215.08	215.88	217.38	219.78	221.27
Apr-16	219.2	220.74	218.23	216.36	215.23	214.68	214.62	215.04	216.02	217.69	220.12	221.01
May-15	219.98	220.9	218.93	217.36	216.36	215.87	215.85	216.29	217.23	218.74	220.71	220.65
Jun-11	219	221.198	219.58	218.18	217.24	216.77	216.7	217	217.9	219.25	220.89	220.76
Jul-17	218.2	221.29	219.6	218.09	217.08	216.5	216.45	216.79	217.59	218.89	220.6	221.19
Aug-16	218.4	221.06	218.87	217.1	216.0	215.44	215.35	215.7	216.6	218.09	220.22	221.22
Sep-15	220.75	220.22	217.8	216.2	215.2	214.9	214.97	215.47	216.5	218.3	220.8	218.56
Oct-15	219.8	220.7	218.56	217.2	216.45	216.16	216.2	216.58	217.45	219.02	221.19	217.19
Nov-14	218.3	221.24	219.75	218.72	218.2	218	218	218.3	218.94	220.14	221.48	216.03
Dec-10	191.85	205.32	210.91	211.8	211.91	211.97	212.25	212.92	214.28	216.98	223.2	221

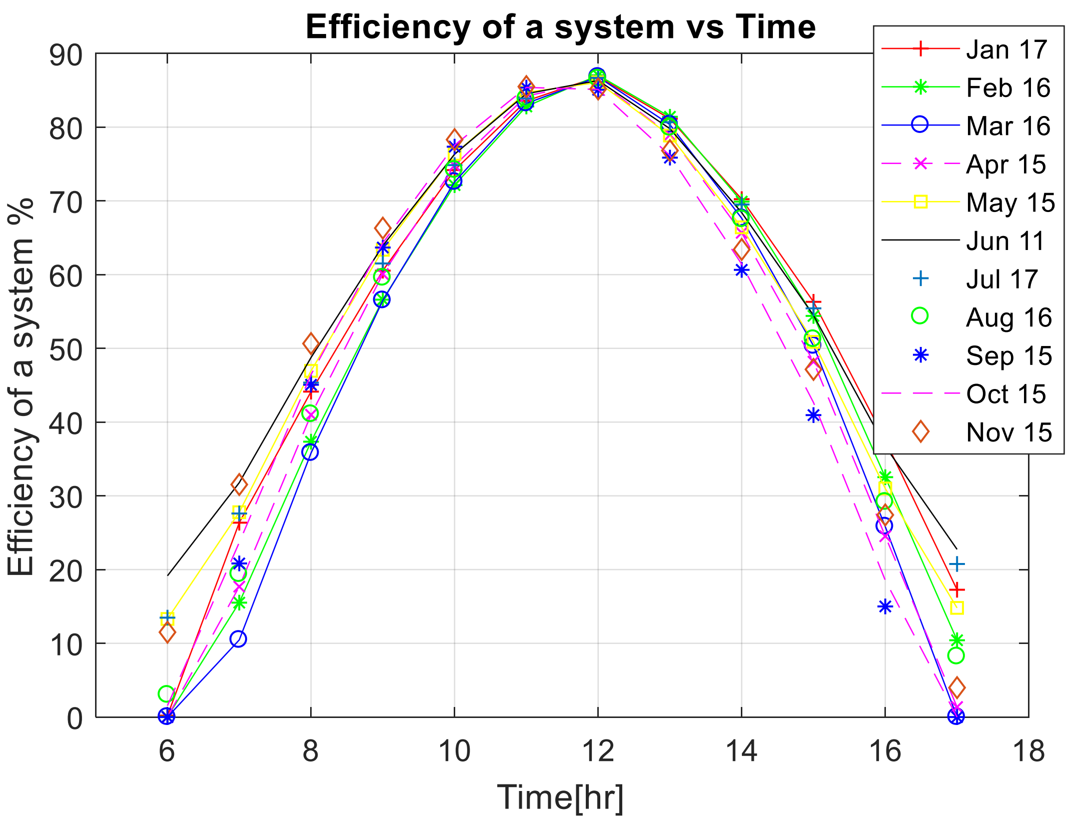

Figure 6- 27: Efficiency of parabolic trough system.

6.3 Model validation

The temperature of HTF computed in the present is compared with the work of Mesfin (2009).

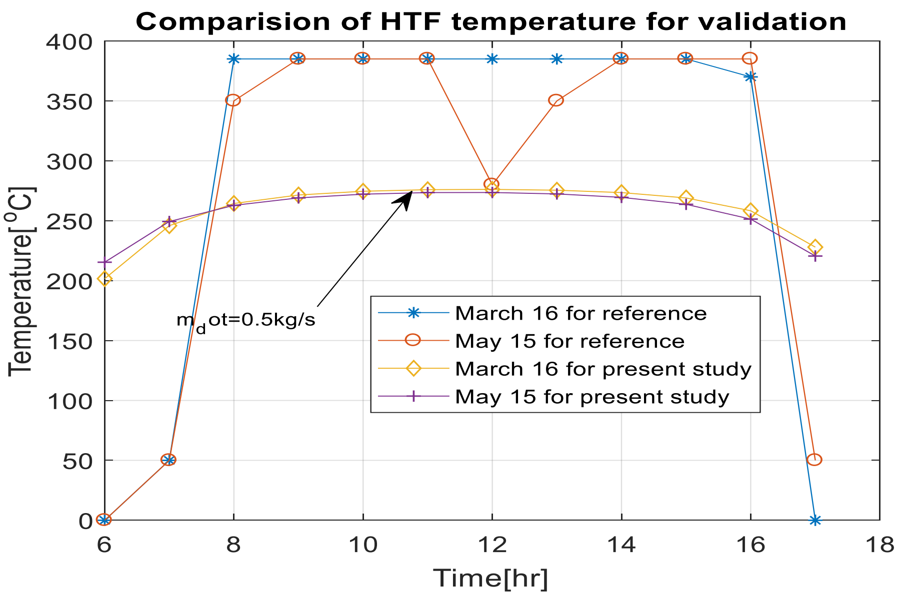

Figure 6- 28: Comparison between presented study and work of mesfin(2009)

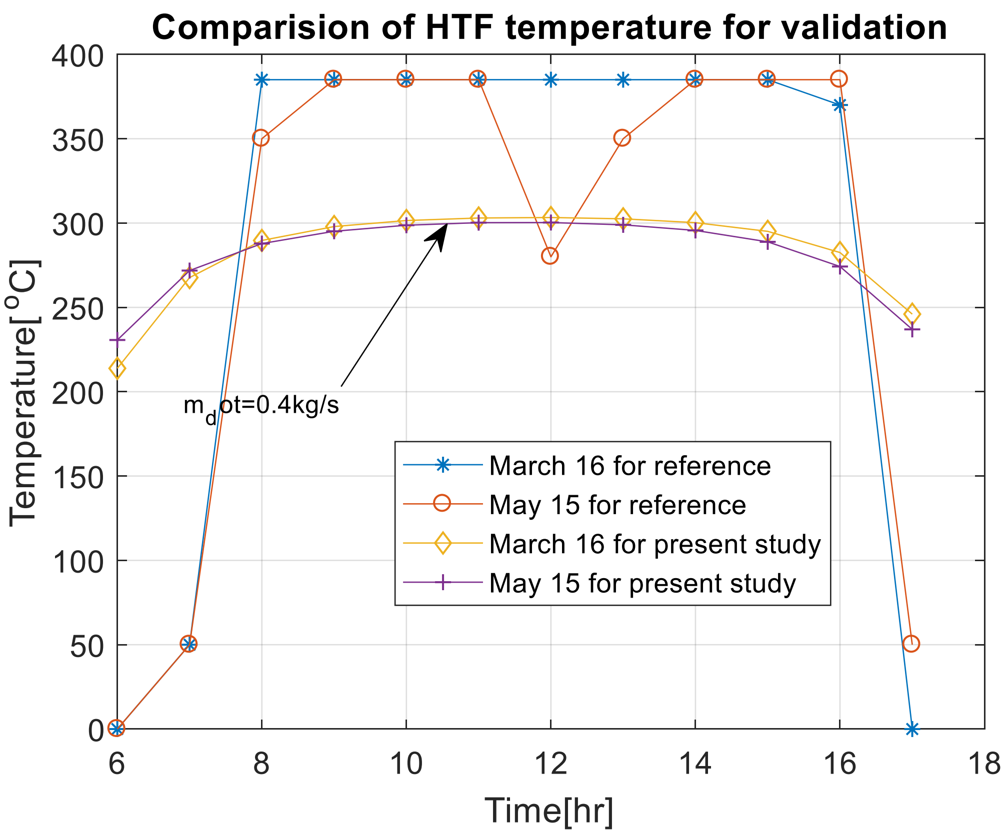

Figure 6- 29: Comparison between presented study and work of mesfin (2009)

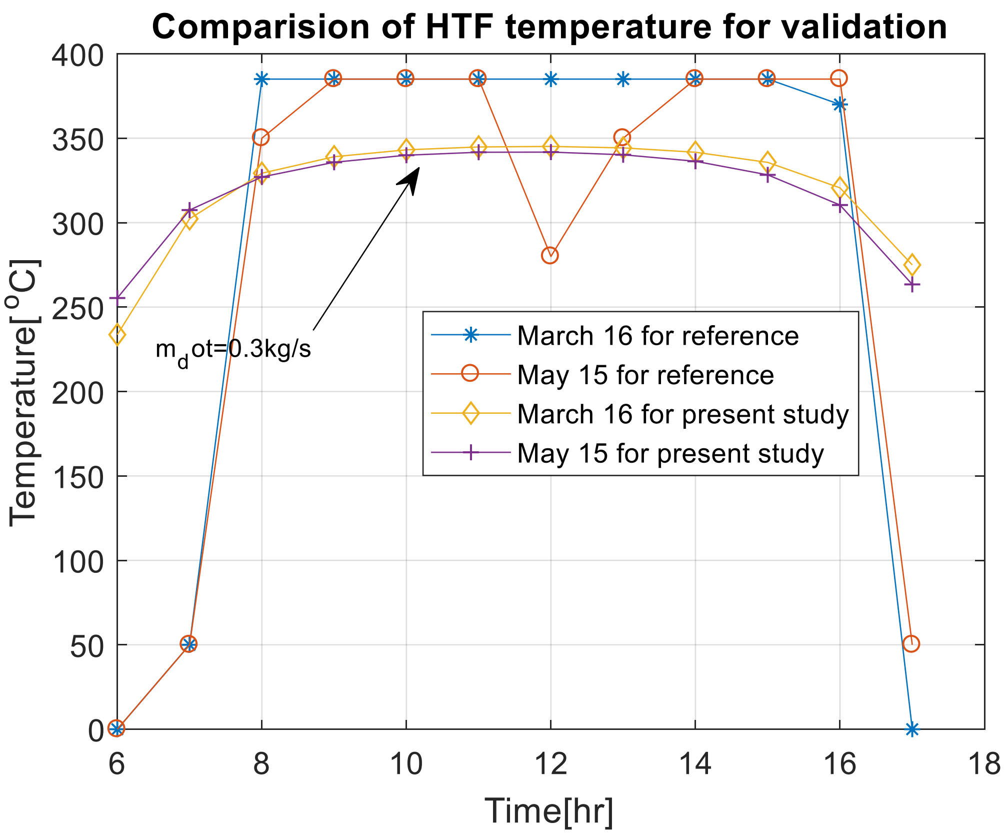

Figure 6- 30: Comparison between presented study and work of mesfin (2009)

In present study three different mass flow rates (0.3kg/s, 0.4kg/s and 0.5kg/s) are taken to test temperature of HTF outlet from solar collector. It's observed that the temperature of HTF is inversely proportional to mass flow rate. So it's possible to increasing or decreasing the temperature of HTF by decreasing or increasing mass flow rate respectively.

In this study the work of mesfin (2009) which is worked on Addis Ababa weather data is taken as reference and compared with the present result obtained.

When mass flow rate of 0.3kg/s is flow through the collectors; the outlet temperature HTF is ranged between 250^{o}C to 340^{o}C.When mass flow rate of 0.4 kg/s is flow through the collectors; the HTF outlet temperature is ranged between 220^{o}C to 300^{o}C.When mass flow rate of 0.5 kg/s is flow through the collectors; the HTF outlet temperature is ranged between 200^{o}C to 275^{o}C. It's observed that with increasing mass flow rate HTF temperature is decreased.

From comparisons of the two graphs it's observed that in present study the HTF outlet temperature is more close to each other throughout the day. The temperature of HTF in reference graph is higher than the temperature of HTF outlet from solar field in present study. The due to large solar field area is used in reference study to generate electricity. In march 15 the temperature of HTF outlet from solar field is decreased in midday is observed by mesfin (2009).

CHAPTER SEVEN

CONCLUSION AND RECOMMENDATIONS

7.1 Conclusion

Throughout a year, Adama have strong solar energy or sunlight. The solar energy is natural, clean and non-polluting energy. The application of solar renewable energy systems such as solar concentration systems in many industrial and domestic areas can solve many problems. These systems can also completely replace electric boiler and fossil fuels.

In this thesis, simulation performance analysis of a parabolic trough steam generator has been done for Wenji Pulp and Paper Factory. The simulation was conducted using MATLAB software. The factory uses resistor electric boiler for the generation of the steam. Currently, the factory needs maximum steam 12,902 kg/hr. The factory utilized an average of electric energy 18,428,492.98 kWh and pays an average of 7,518,825.14 Birr per year.

The simulation result from thermal performance analysis study shows that the parabolic trough steam generator can meet the steam demand of the factory during the day. The parabolic trough aperture area required to fulfil this steam demand by the factory is obtained to be equal to 8,843 m^2. The corresponding efficiency of the system was found to be equal to 69%. The optical efficiency of collector was higher i.e 75 %.The maximum value of thermal efficiency can reach up 68 %.

In present study three different mass flow rates (0.3kg/s, 0.4kg/s and 0.5kg/s) are taken to test temperature of HTF outlet from solar collector. It's observed that the temperature of HTF is inversely proportional to mass flow rate. So it's possible to increasing or decreasing the temperature of HTF by decreasing or increasing mass flow rate respectively.

When mass flow rate of 0.3kg/s is flow through the collectors; the outlet temperature HTF is ranged between 250^oC to 340^oC.When mass flow rate of 0.4 kg/s is flow through the collectors; the HTF outlet temperature is ranged between 220^oC to 300^oC.When mass flow rate of 0.5 kg/s is flow through the collectors; the HTF outlet temperature is ranged between 200^oC to 275^oC. It's observed that with increasing mass flow rate HTF temperature is decreased.

7.2 Recommendations

From the performance analysis of parabolic trough result the following general recommendations are suggested:

1. If concentrated solar steam generation (parabolic through) is implemented, the electric consumption and operational cost of the boiler can be reduced appreciably.
2. It is thus recommended that the government and Wenji pulp and paper factory should consider this outcome for its implementation so as to overcome the high operational cost of the existing boiler by using the parabolic trough steam generation system.
3. Pressure loss in the heat exchangers, pipes and feedwater heater is neglected. This is due to the fact that pressure loss depends on the physical data of the components.
4. If thermal storage used to store molten salt and used for night will be added in this work; the system can produce steam for 24 hour.
5. Parabolic though in this work is done for Wenji Pulp and Paper Factory located in Wenji near Adama town. There are also other places like Afar and Somali regions in Ethiopia where high solar radiation is available for long period over the year. These places are the best locations for concentrated solar steam generation. Hence solar thermal systems can be used for process heat in different activities.
6. The simulation of the performance of the parabolic trough solar steam generator can be repeated by including detail simulation study on the storage tank, the currently available molten salt technology to reduce of the system.

References

1.Abdela ali Benidir1, Fouad Khaldi ,Abdelmoumene Hakim Benmachiche, Fethi Bouras: Numerical Thermal Analysis of Schott 2008 PTR70 solar Receiver Under Hassi RMEL power plant Operation Conditions: Journal of Engineering Science and Technology ,Vol. 13, No. 1 (2018) 122 – 140.

2.Addisu Bekele: Large Scale Application of Solar Water Heating System in Ethiopia;July 2007 Addis Ababa University, Ethiopia.

3. Alem Tafesse: Feasibility Study of Replacement of Electric Steam Boiler by Wood Biomass Boiler and Old Electric Motors in Ethiopian Pulp and Paper Share Company; October, 2016 Addis Ababa, Ethiopia.

4.Canuçkun: Modeling and Simulations of Direct Steam Generation in Solar Power Plants using Parabolic Trough collectors, Msc thesis in Mechanical Engineering Department, Middle East Technical University. March 2013.

5.Dejene Assefa:Techno-Economic Assessment of Parabolic trough Steam Generation for Hospital,Addis Ababe University,2011.

6.Evangelos Bellos and Christos Tzivanidis: Analytical Expression of Parabolic Trough Solar Collector Performance; Accepted: 27 February 2018; Published: 2 March 2018.

7.G.N. Tiwari, Arvind Tiwari and Shyam: Hand book of Solar Energy Theory, Analysis and Applications; More information about this series at http://www.springer.com/series/13509. USA(2016).

8.I. S. Sintali, G. Egbo and H. Dandakouta (2014):Energy Equations for Computation of Parabolic-Trough Collector Efficiency Using Solar Position Coordinates: American Journal of Engineering Research (AJER) Volume-3,www .ajer.org: Issue-10, pp-25-33

9. Irena 2012: Renewable Energy Technologies: Cost Analysis Series volume 1: Power Sector Issue 2/5.

10.John A. Duffie and William A. Beckman :Solar Engineering of Thermal Processes Fourth Edition, Madison, Wisconsin October 2005.

11.Joseph Gosselar and Matthew Johnson: Solar Thermal Energy for Industrial Uses ,December 2011,Environmental and Energy Study Institute. 1112 16th Street, NW, Suite 300 Washington, www.eesi.org.

12.Loh Heng Chew,Wattanapong Rakwichian, Mathanee Sanguansermsri and Suchart Yammen :Design,Fabrication and Monitoring of an Industrial-scale Solar Trough Collector at the Energy Park of Naresuan University, Thailand. International Journal of Renewable Energy, Vol. 1, No. 2, July 2006

13.Matthias Günther ,Michae Joemann and Simon Csambor: Parabolic Trough Technology; Institute for Electrical Engineering, Rational Energy Conversion, University of Kassel,2011.

14.Mekuannint Mesfin:Modelling, Simulation and Performance Evaluation of Parabolic Trough Solar Collector Power Generation System, Department of Mechanical Engineering Addis Ababa University September 2009.

15.Mokhtar Ghodbane and Boussad Boumeddane. A numerical analysis of the energy behaviour of a parabolic trough concentrator, Saad Dahlab University, available at https://www.researchgate.net/publication, 2016 September.

16.Peter Schwarzbözl and Ulrich Eiden : A TRNSYS Model Library for Solar Thermal Electric Components (STEC). German Aerospace Center September 2002.

17.R. Forristall. Heat Transfer Analysis and Modeling of a Parabolic Trough Solar Receiver Implemented in Engineering Equation Solver; National Renewable Energy Laboratory U.S. Department of Energy Laboratory October 2003.

18.Ricardo Vasquez Padilla: "Simplified Methodology for Designing Parabolic Trough Solar Power Plants" (2011). University of South Florida Scholar Commons Graduate Theses and Dissertation. htp://scholarcommons.usf.edu/etd/3390.

19.S. Kalogirou, Solar Energy Engineering: Processes and Systems. Academic Press, 2009.For more information visit: WWW.elsevierdirect.com.

20.Theodore L. Bergman,Adrienne S.Lavine, Frank P. Incropera and David P.Dewitt, Fundamentals of heat and mass transfer, Seventh Edition

APPENDIX

Appendix A: Data of Parabolic Trough Collectors (Vasquez,2011).

Collector	Width	Focal length	Length of module	Lsca
LS-1	2.55	0.94	6.3	50.2
LS-2	5	1.49	8	49.0
LS-3	5.76	1.71	12	99.0
IST	2.3	0.76	6.1	49.0
Euro Trough	5.76	1.71	12	150.0
Sky Trough	6	1.71	13.9	115.0

Appendix B: MATLAB code

```
%%BEAM NORMAL RADIATION,EFFECTIVE BEAM RADIATION,OF ADAMA%

N1=17;            %Jan 17
N2=47;            %Feb 16
N3=75;            %Mar 16
N4=105;           %Apr 15
N5=135;           %May 15
N6=162;           %Jun 11
N7=198;           %Jul 17
N8=228;           %Aug 16
N9=258;           %Sep 15
N10=288;          %Oct 15
N11=318;          %Nov 14
N12=344;          %Dec 10

B1=(N1-1)*(360/365);%%%%Day angle in(radian)
B2=(N2-1)*(360/365);
B3=(N3-1)*(360/365);
B4=(N4-1)*(360/365);
B5=(N5-1)*(360/365);
B6=(N6-1)*(360/365);
B7=(N7-1)*(360/365);
B8=(N8-1)*(360/365);
B9=(N9-1)*(360/365);
B10=(N10-1)*(360/365);
B11=(N11-1)*(360/365);
B12=(N12-1)*(360/365);
%Equation of time in minute
EoT1=229.2*(0.000075+0.001868*cos(B1*pi/180)-0.032077*
sin(B1*pi/180)-0.014615*cos(2*B1*pi/180)-0.04089*sin(2*B1*pi/180));
EoT2=229.2*(0.000075+0.001868*cos(B2*pi/180)-0.032077*
sin(B2*pi/180)-0.014615*cos(2*B2*pi/180)-0.04089*sin(2*B2*pi/180));
EoT3=229.2*(0.000075+0.001868*cos(B3*pi/180)-0.032077*
sin(B3*pi/180)-0.014615*cos(2*B3*pi/180)-0.04089*sin(2*B3*pi/180));
EoT4=229.2*(0.000075+0.001868*cos(B4*pi/180)-0.032077*
sin(B4*pi/180)-0.014615*cos(2*B4*pi/180)-0.04089*sin(2*B4*pi/180));
EoT5=229.2*(0.000075+0.001868*cos(B5*pi/180)-0.032077*
sin(B5*pi/180)-0.014615*cos(2*B5*pi/180)-0.04089*sin(2*B5*pi/180));
EoT6=229.2*(0.000075+0.001868*cos(B6*pi/180)-0.032077*
sin(B6*pi/180)-0.014615*cos(2*B6*pi/180)-0.04089*sin(2*B6*pi/180));
EoT7=229.2*(0.000075+0.001868*cos(B7*pi/180)-0.032077*
sin(B7*pi/180)-0.014615*cos(2*B7*pi/180)-0.04089*sin(2*B7*pi/180));
EoT8=229.2*(0.000075+0.001868*cos(B8*pi/180)-0.032077*
sin(B8*pi/180)-0.014615*cos(2*B8*pi/180)-0.04089*sin(2*B8*pi/180));
EoT9=229.2*(0.000075+0.001868*cos(B9*pi/180)-0.032077*
sin(B9*pi/180)-0.014615*cos(2*B9*pi/180)-0.04089*sin(2*B9*pi/180));
EoT10=229.2*(0.000075+0.001868*cos(B10*pi/180)-0.032077*
sin(B10*pi/180)-0.014615*cos(2*B10*pi/180)-0.04089*sin(2*B10*pi/180));

EoT11=229.2*(0.000075+0.001868*cos(B11*pi/180)-0.032077*
```

```
sin(B11*pi/180)-0.014615*cos(2*B11*pi/180)-0.04089*sin(2*B11*pi/180));
EoT12=229.2*(0.000075+0.001868*cos(B12*pi/180)-0.032077*
sin(B12*pi/180)-0.014615*cos(2*B12*pi/180)-0.04089*sin(2*B12*pi/180));
LT=6:1:17;        %local hour inceased by one hour
Lsite=39.269257; %Longitude of to the east of greenwich of adama
LSTM=45 ;      %Local standard time meridian of Ethiopia
%Local solar time
LST1=LT+(4*(LSTM-Lsite)+EoT1 )/60 ;
LST2=LT+(4*(LSTM-Lsite)+EoT2 )/60 ;
LST3=LT+(4*(LSTM-Lsite)+EoT3 )/60 ;
LST4=LT+(4*(LSTM-Lsite)+EoT4 )/60 ;
LST5=LT+(4*(LSTM-Lsite)+EoT5 )/60 ;
LST6=LT+(4*(LSTM-Lsite)+EoT6 )/60 ;
LST7=LT+(4*(LSTM-Lsite)+EoT7 )/60 ;
LST8=LT+(4*(LSTM-Lsite)+EoT8 )/60 ;
LST9=LT+(4*(LSTM-Lsite)+EoT10 )/60 ;
LST10=LT+(4*(LSTM-Lsite)+EoT10 )/60;
LST11=LT+(4*(LSTM-Lsite)+EoT11)/60 ;
LST12=LT+(4*(LSTM-Lsite)+EoT12 )/60 ;
  %hour angle
omega1=(LST1-12)*15;
omega2=(LST2-12)*15;
omega3=(LST3-12)*15;
omega4=(LST4-12)*15;
omega5=(LST5-12)*15;
omega6=(LST6-12)*15;
omega7=(LST7-12)*15;
omega8=(LST8-12)*15;
omega9=(LST9-12)*15;
omega10=(LST10-12)*15;
omega11=(LST11-12)*15;
omega12=(LST12-12)*15;
 %%%declination angle
de1=23.5*sin((360*(284+N1)/365)*pi/180);
de2=23.5*sin((360*(284+N2)/365)*pi/180);
de3=23.5*sin((360*(284+N3)/365)*pi/180);
de4=23.5*sin((360*(284+N4)/365)*pi/180);
de5=23.5*sin((360*(284+N5)/365)*pi/180);
de6=23.5*sin((360*(284+N6)/365)*pi/180);
de7=23.5*sin((360*(284+N7)/365)*pi/180);
de8=23.5*sin((360*(284+N8)/365)*pi/180);
de9=23.5*sin((360*(284+N9)/365)*pi/180);
de10=23.5*sin((360*(284+N10)/365)*pi/180);
de11=23.5*sin((360*(284+N11)/365)*pi/180);
de12=23.5*sin((360*(284+N12)/365)*pi/180);
phi=8.51447;   %%%%Adama latitude to the north of equator
Gsc=1367;             %[w/m^2] solar constant
Al=1.869;             %[Km] altitude
%%%%%%%%%FOR  TROPIC  CLIMATE  CONDITION  THE  CORELATION  r  has  the  foloowing
value%%%%%%
r_o=0.95;
r_1=0.98;
r_k=1.02;
a_o=r_o*(0.4237-0.00821*(6-Al)^2);
a_1=r_1*(0.5055+0.00595*(6.5-Al)^2);
k=r_k*(0.2711+0.01858*(2.5-Al)^2);
%%%%%%ZENITH ANGLE FOR EACH REPRASANTATIVE WILL BE AS FOLLOW%
zenith1=acos(cos(phi*pi/180).*cos(de1*pi/180).*cos(omega1*pi/180)+
sin(phi*pi/180).*sin(de1*pi/180))*180/pi;
zenith2=acos(cos(phi*pi/180).*cos(de2*pi/180).*cos(omega2*pi/180)+
sin(phi*pi/180).*sin(de2*pi/180))*180/pi;
zenith3=acos(cos(phi*pi/180).*cos(de3*pi/180).*cos(omega3*pi/180)+
sin(phi*pi/180).*sin(de3*pi/180))*180/pi;
zenith4=acos(cos(phi*pi/180).*cos(de4*pi/180).*cos(omega4*pi/180)+
sin(phi*pi/180).*sin(de4*pi/180))*180/pi;
zenith5=acos(cos(phi*pi/180).*cos(de5*pi/180).*cos(omega5*pi/180)+
sin(phi*pi/180).*sin(de5*pi/180))*180/pi;
zenith6=acos(cos(phi*pi/180).*cos(de6*pi/180).*cos(omega6*pi/180)+
```

```
sin(phi*pi/180).*sin(de6*pi/180))*180/pi;
zenith7=acos(cos(phi*pi/180).*cos(de7*pi/180).*cos(omega7*pi/180)+
sin(phi*pi/180).*sin(de7*pi/180))*180/pi;
zenith8=acos(cos(phi*pi/180).*cos(de8*pi/180).*cos(omega8*pi/180)+
sin(phi*pi/180).*sin(de8*pi/180))*180/pi;
zenith9=acos(cos(phi*pi/180).*cos(de9*pi/180).*cos(omega9*pi/180)+
sin(phi*pi/180).*sin(de9*pi/180))*180/pi;
zenith10=acos(cos(phi*pi/180).*cos(de10*pi/180).*cos(omega10*pi/180)+
sin(phi*pi/180).*sin(de10*pi/180))*180/pi;
zenith11=acos(cos(phi*pi/180).*cos(de11*pi/180).*cos(omega11*pi/180)+
sin(phi*pi/180).*sin(de11*pi/180))*180/pi;
zenith12=acos(cos(phi*pi/180).*cos(de12*pi/180).*cos(omega12*pi/180)+
sin(phi*pi/180).*sin(de12*pi/180))*180/pi;
% ATMOSPHERE TRANSMITTANCE FOR BEAM RADIATION WILL BE %%%%
Btrans1=a_o+a_1*exp(-k./cos(zenith1*pi/180));
Btrans2=a_o+a_1*exp(-k./cos(zenith2*pi/180));
Btrans3=a_o+a_1*exp(-k./cos(zenith3*pi/180));
Btrans4=a_o+a_1*exp(-k./cos(zenith4*pi/180));
Btrans5=a_o+a_1*exp(-k./cos(zenith5*pi/180));
Btrans6=a_o+a_1*exp(-k./cos(zenith6*pi/180));
Btrans7=a_o+a_1*exp(-k./cos(zenith7*pi/180));
Btrans8=a_o+a_1*exp(-k./cos(zenith8*pi/180));
Btrans9=a_o+a_1*exp(-k./cos(zenith9*pi/180));
Btrans10=a_o+a_1*exp(-k./cos(zenith10*pi/180));
Btrans11=a_o+a_1*exp(-k./cos(zenith11*pi/180));
Btrans12=a_o+a_1*exp(-k./cos(zenith12*pi/180));
plot(LT,Btrans1,'+-r',LT,Btrans2,'o-g',LT,Btrans3,'*-b',LT,Btrans4,'o--
m',LT,Btrans5,'s-y',LT,Btrans6,'d-k')
legend('Jan 17','Feb 16','Mar 16','Apr 15','May 15','Jun 11')
plot(LT,Btrans7,'+-r',LT,Btrans8,'o-g',LT,Btrans9,'*-b',LT,Btrans10,'o--
m',LT,Btrans11,'s-y',LT,Btrans12,'d-k')
legend('Jul 17','Aug 16','Sep 15','Oct 15','Nov 15','Dec 10')
grid on
xlabel('Time(hr)')
ylabel('Atmospheric beam transmittance')
title(' vs Time')
Io1=Gsc*(1+0.033*cos((360*N1/365)*pi/180));%[W/m2]    extraterrestrial    radiation
incident on the plane normal to the radiation on the nth day of the year
Io2=Gsc*(1+0.033*cos((360*N2/365)*pi/180));
Io3=Gsc*(1+0.033*cos((360*N3/365)*pi/180));
Io4=Gsc*(1+0.033*cos((360*N4/365)*pi/180));
Io5=Gsc*(1+0.033*cos((360*N5/365)*pi/180));
Io6=Gsc*(1+0.033*cos((360*N6/365)*pi/180));
Io7=Gsc*(1+0.033*cos((360*N7/365)*pi/180));
Io8=Gsc*(1+0.033*cos((360*N8/365)*pi/180));
Io9=Gsc*(1+0.033*cos((360*N9/365)*pi/180));
Io10=Gsc*(1+0.033*cos((360*N10/365)*pi/180));
Io11=Gsc*(1+0.033*cos((360*N11/365)*pi/180));
Io12=Gsc*(1+0.033*cos((360*N12/365)*pi/180));
%clear sky beam normal radiation(beam radiation under clear sky conditions) [W/m2]
Inb1=Io1.*Btrans1;
Inb2=Io2.*Btrans2;
Inb3=Io3.*Btrans3;
Inb4=Io4.*Btrans4;
Inb5=Io5.*Btrans5;
Inb6=Io6.*Btrans6;
Inb7=Io7.*Btrans7;
Inb8=Io8.*Btrans8;
Inb9=Io9.*Btrans9;
Inb10=Io10.*Btrans10;
Inb11=Io11.*Btrans11;
Inb12=Io12.*Btrans12;
plot(LT,Inb1,'+-r',LT,Inb2,'o-g',LT,Inb3,'*-b',LT,Inb4,'o--m',LT,Inb5,'s-
y',LT,Inb6,'d-k')
legend('Jan 17','Feb 16','Mar 16','Apr 15','May 15','Jun 11')
plot(LT,Inb7,'+-r',LT,Inb8,'o-g',LT,Inb9,'*-b',LT,Inb10,'o--m',LT,Inb11,'s-
y',LT,Inb12,'d-k')
legend('Jul 17','Aug 16','Sep 15','Oct 15','Nov 14','Dec 10')
```

```
legend('Dec10')
grid on
xlabel('Time(hr)')
ylabel('Direct normal insolation for clear day(W/m^2)')
title('Calculated DNI vs Time')
%Clear-sky horizontal  beam radiation for january 17
Icb1=Inb1.*cos(zenith1*pi/180);
Icb2=Inb2.*cos(zenith2*pi/180);
 Icb3=Inb3.*cos(zenith3*pi/180);
 Icb4=Inb4.*cos(zenith4*pi/180);
 Icb5=Inb5.*cos(zenith5*pi/180);
 Icb6=Inb6.*cos(zenith6*pi/180);
 Icb7=Inb7.*cos(zenith7*pi/180);
 Icb8=Inb8.*cos(zenith8*pi/180);
 Icb9=Inb9.*cos(zenith9*pi/180);
 Icb10=Inb10.*cos(zenith10*pi/180);
 Icb11=Inb11.*cos(zenith11*pi/180);
 Icb12=Inb12.*cos(zenith12*pi/180);
Icb1=max(0,Inb1.*cos(zenith1*pi/180));
Icb2=max(0,Inb2.*cos(zenith2*pi/180));
Icb3=max(0,Inb3.*cos(zenith3*pi/180));
Icb4=max(0,Inb4.*cos(zenith4*pi/180));
Icb5=max(0,Inb5.*cos(zenith5*pi/180));
Icb6=max(0,Inb6.*cos(zenith6*pi/180));
plot(LT,Icb1,LT,Icb2,LT,Icb3,LT,Icb4,LT,Icb5,LT,Icb6)
plot(LT,Icb1,'+-r',LT,Icb2,'o-g',LT,Icb3,'*-b',LT,Icb4,'o--m',LT,Icb5,'s-
y',LT,Icb6,'d-k')
legend('Jan 17','Feb 16','Mar 16','Apr 15','May 15','Jun 11')
legend('June11')
Icb7=max(0,Inb7.*cos(zenith7*pi/180));
Icb8=max(0,Inb8.*cos(zenith8*pi/180));
Icb9=max(0,Inb9.*cos(zenith9*pi/180));
Icb10=max(0,Inb10.*cos(zenith10*pi/180));
Icb11=max(0,Inb11.*cos(zenith11*pi/180));
Icb12=max(0,Inb12.*cos(zenith12*pi/180));
plot(LT,Icb7,'+-r',LT,Icb8,'o-g',LT,Icb9,'*-b',LT,Icb10,'o--m',LT,Icb11,'s-
y',LT,Icb12,'d-k')
legend('Jul 17','Aug 16','Sep 15','Oct 15','Nov 14','Dec 10')
grid on
xlabel('Time(hr)')
ylabel('Clear-sky horizontal beam radiation (Icb)(W/m2)')
title('Icb vs Time')
%Incident angle for north-south tracking
theta1=acos(sqrt(1-cos(de1*pi/180)^2*sin(omega1*pi/180).^2))*180/pi;
theta2=acos(sqrt(1-cos(de2*pi/180)^2*sin(omega2*pi/180).^2))*180/pi;
theta3=acos(sqrt(1-cos(de3*pi/180)^2*sin(omega3*pi/180).^2))*180/pi;
theta4=acos(sqrt(1-cos(de4*pi/180)^2*sin(omega4*pi/180).^2))*180/pi;
theta5=acos(sqrt(1-cos(de5*pi/180)^2*sin(omega5*pi/180).^2))*180/pi;
theta6=acos(sqrt(1-cos(de6*pi/180)^2*sin(omega6*pi/180).^2))*180/pi;
theta7=acos(sqrt(1-cos(de7*pi/180)^2*sin(omega7*pi/180).^2))*180/pi;
theta8=acos(sqrt(1-cos(de8*pi/180)^2*sin(omega8*pi/180).^2))*180/pi;
theta9=acos(sqrt(1-cos(de9*pi/180)^2*sin(omega9*pi/180).^2))*180/pi;
theta10=acos(sqrt(1-cos(de10*pi/180)^2*sin(omega10*pi/180).^2))*180/pi;
theta11=acos(sqrt(1-cos(de11*pi/180)^2*sin(omega11*pi/180).^2))*180/pi;
theta12=acos(sqrt(1-cos(de12*pi/180)^2*sin(omega12*pi/180).^2))*180/pi;
% Effective Beam Radiation For East-West Axis Of rotation(N-S Tracking)
Ib1=Inb1.*cos(theta1*pi/180);
Ib2=Inb2.*cos(theta2*pi/180);
Ib3=Inb3.*cos(theta3*pi/180);
Ib4=Inb4.*cos(theta4*pi/180);
Ib5=Inb5.*cos(theta5*pi/180);
Ib6=Inb6.*cos(theta6*pi/180);
Ib7=Inb7.*cos(theta7*pi/180);
Ib8=Inb8.*cos(theta8*pi/180);
Ib9=Inb9.*cos(theta9*pi/180);
Ib10=Inb10.*cos(theta10*pi/180);
Ib11=Inb11.*cos(theta11*pi/180);
Ib12=Inb12.*cos(theta12*pi/180);
```

```
plot(LT,Ib1,'+-r',LT,Ib2,'o-g',LT,Ib3,'*-b',LT,Ib4,'o--m',LT,Ib5,'s-y',LT,Ib6,'d-
k')
legend('Jan 17','Feb 16','Mar 16','Apr 15','May 15','Jun 11')
plot(LT,Ib7,'+-r',LT,Ib8,'o-g',LT,Ib9,'*-b',LT,Ib10,'o--m',LT,Ib11,'s-
y',LT,Ib12,'d-k')
legend('Jul 17','Aug 16','Sep 15','Oct 15','Nov 14','Dec 10')
grid on
xlabel('Time(hr)')
ylabel('Effective beam radiation(Ib)(W/m^2)')
title('Ib for North-South tracking vs Time')
%incident angle for North-South axis(East-West Tracking)
theta01=acos(sqrt(cos(zenith1*pi/180).^2+cos(de1*pi/180)^2*
sin(omega1*pi/180).^2))*180/pi;
theta02=acos(sqrt(cos(zenith2*pi/180).^2+cos(de2*pi/180)^2*
sin(omega2*pi/180).^2))*180/pi;
theta03=acos(sqrt(cos(zenith3*pi/180).^2+cos(de3*pi/180)^2*
sin(omega3*pi/180).^2))*180/pi;
theta04=acos(sqrt(cos(zenith4*pi/180).^2+cos(de4*pi/180)^2*
sin(omega4*pi/180).^2))*180/pi;
theta05=acos(sqrt(cos(zenith5*pi/180).^2+cos(de5*pi/180)^2*
sin(omega5*pi/180).^2))*180/pi;
theta06=acos(sqrt(cos(zenith6*pi/180).^2+cos(de6*pi/180)^2*
sin(omega6*pi/180).^2))*180/pi;
theta07=acos(sqrt(cos(zenith7*pi/180).^2+cos(de7*pi/180)^2*
sin(omega7*pi/180).^2))*180/pi;
theta08=acos(sqrt(cos(zenith8*pi/180).^2+cos(de8*pi/180)^2*
sin(omega8*pi/180).^2))*180/pi;
theta09=acos(sqrt(cos(zenith9*pi/180).^2+cos(de9*pi/180)^2*
sin(omega9*pi/180).^2))*180/pi;
theta010=acos(sqrt(cos(zenith10*pi/180).^2+cos(de10*pi/180)^2*
sin(omega10*pi/180).^2))*180/pi;
theta011=acos(sqrt(cos(zenith11*pi/180).^2+cos(de11*pi/180)^2*
sin(omega11*pi/180).^2))*180/pi;
theta012=acos(sqrt(cos(zenith12*pi/180).^2+cos(de12*pi/180)^2*
sin(omega12*pi/180).^2))*180/pi;
% Effective Beam Radiation For East-West tracking
Ib01=Inb1.*cos(theta01*pi/180);
Ib02=Inb2.*cos(theta02*pi/180);
Ib03=Inb3.*cos(theta03*pi/180);
Ib04=Inb4.*cos(theta04*pi/180);
Ib05=Inb5.*cos(theta05*pi/180);
Ib06=Inb6.*cos(theta06*pi/180);
Ib07=Inb7.*cos(theta07*pi/180);
Ib08=Inb8.*cos(theta08*pi/180);
Ib09=Inb9.*cos(theta09*pi/180);
Ib010=Inb10.*cos(theta010*pi/180);
Ib011=Inb11.*cos(theta011*pi/180);
Ib012=Inb12.*cos(theta012*pi/180);
plot(LT,Ib01,'+-r',LT,Ib02,'o-g',LT,Ib03,'*-b',LT,Ib04,'o--m',LT,Ib05,'s-
y',LT,Ib06,'d-k')
legend('Jan 17','Feb 16','Mar 16','Apr 15','May 15','Jun 11')
plot(LT,Ib07,'+-r',LT,Ib08,'o-g',LT,Ib09,'*-b',LT,Ib010,'o--m',LT,Ib011,'s-
y',LT,Ib012,'d-k')
legend('Jul 17','Aug 16','Sep 15','Oct 15','Nov 14','Dec 10')
grid on
xlabel('Time(hr)')
ylabel('Effective beam radiation(Ib)(W/m^2)')
title('Ib for East-West tracking vs Time')
Ap=5;               %[m] width of collector
eta_op=0.75;        %optical efficiency
rabso=0.96;         %Receiver absorptance [LS-2]
Gtrans=0.95;        %Glass cover transmittance
mreflect=0.83;      %Mirror reflectance [LS-2]
%Net thermal energy available at the absorber per receiver per area
qu_net1=rabso*Gtrans*eta_op*Ib01;
qu_net2=rabso*Gtrans*eta_op*Ib02;
qu_net3=rabso*Gtrans*eta_op*Ib03;
qu_net4=rabso*Gtrans*eta_op*Ib04;
```

```
qu_net5=rabso*Gtrans*eta_op*Ib05;
qu_net6=rabso*Gtrans*eta_op*Ib06;
qu_net7=rabso*Gtrans*eta_op*Ib07;
qu_net8=rabso*Gtrans*eta_op*Ib08;
qu_net9=rabso*Gtrans*eta_op*Ib09;
qu_net10=rabso*Gtrans*eta_op*Ib010;
qu_net11=rabso*Gtrans*eta_op*Ib011;
qu_net12=rabso*Gtrans*eta_op*Ib012;
plot(LT,qu_net1,'+-r',LT,qu_net2,'o-g',LT,qu_net3,'*-b',LT,qu_net4,'o--
m',LT,qu_net5,'s-y',LT,qu_net6,'d-k')
legend('Jan 17','Feb 16','Mar 16','Apr 15','May 15','Jun 11')
plot(LT,qu_net7,'+-r',LT,qu_net8,'o-g',LT,qu_net9,'*-b',LT,qu_net10,'o--
m',LT,qu_net11,'s-y',LT,qu_net12,'d-k')
legend('Jul 17','Aug 16','Sep 15','Oct 15','Nov 14','Dec 10')
grid on
xlabel('Time(hr)')
ylabel('Net thermal energy on receiver,qnet(W/m^2)')
title('qnet vs Time')
C=22.74;%Concentration ratio
eta_opt=0.75 ;%Optical efficiency
eta_the=qu_net1/Ib01; %Thermal efficiency
E_r=0.2;%Receiver emittance
sigma=5.67*10^-8;%[W/m2-K^4] Stefan-Boltzmann constant
  %Receiver temperature
T_r1=((1-eta_the).*(1/(E_r*sigma))*rabso*Gtrans*eta_opt*C.*Ib01).^0.25;
T_r2=((1-eta_the)*(1/(E_r*sigma))*rabso*Gtrans*eta_opt*C*Ib02).^0.25;
T_r3=((1-eta_the)*(1/(E_r*sigma))*rabso*Gtrans*eta_opt*C*Ib03).^0.25;
T_r4=((1-eta_the)*(1/(E_r*sigma))*rabso*Gtrans*eta_opt*C*Ib04).^0.25;
T_r5=((1-eta_the)*(1/(E_r*sigma))*rabso*Gtrans*eta_opt*C*Ib05).^0.25;
T_r6=((1-eta_the)*(1/(E_r*sigma))*rabso*Gtrans*eta_opt*C*Ib06).^0.25;
T_r7=((1-eta_the)*(1/(E_r*sigma))*rabso*Gtrans*eta_opt*C*Ib07).^0.25;
T_r8=((1-eta_the)*(1/(E_r*sigma))*rabso*Gtrans*eta_opt*C*Ib08).^0.25;
T_r9=((1-eta_the)*(1/(E_r*sigma))*rabso*Gtrans*eta_opt*C*Ib09).^0.25;
T_r10=((1-eta_the)*(1/(E_r*sigma))*rabso*Gtrans*eta_opt*C*Ib010).^0.25;
T_r11=((1-eta_the)*(1/(E_r*sigma))*rabso*Gtrans*eta_opt*C*Ib011).^0.25;
T_r12=((1-eta_the)*(1/(E_r*sigma))*rabso*Gtrans*eta_opt*C*Ib012).^0.25;
plot(LT,T_r1-273,'+-r',LT,T_r2-273,'o-g',LT,T_r3-273,'*-b',LT,T_r4-273,'o--
m',LT,T_r5-273,'s-y',LT,T_r6-273,'d-k')
legend('Jan 17','Feb 16','Mar 16','Apr 15','May 15','Jun 11')
plot(LT,T_r7-273,'+-r',LT,T_r8-273,'o-g',LT,T_r9-273,'*-b',LT,T_r10-273,'o--
m',LT,T_r11-273,'s-y',LT,T_r12-273,'d-k')
legend('Jul 17','Aug 16','Sep 15','Oct 15','Nov 14','Dec 10')
grid on
xlabel('Time(hr)')
ylabel('Receiver Temperature,Tr(oC)')
title('Tr from calculated DNI vs Time')
T_in=150; %[℃]HTF outlet temperature assumed
T_out=300; [℃] HTF inlet temperature assumed
Tavg_sf=(T_out+T_in)/2; %average Temp
A_sca=235;           %[m^2]area of solar collector assembly
A_co=2.818;         %[m^2] Outer surface of the cover
A_ci=2.671;         %[m^2]Cover inner surface
A_ri=1.617;         %[m^2]receiver inner surface
A_ro=1.715;         %[m2]Receiver outer surface
E_c=0.9;            %Emissivity of glass cover
Tam=19.3;           %[oC]average ambient temperature
Lsca=47;            %[LS-2]Length of collector assembly
D_ri=0.066;         %[m]Diameter of inner absorber
D_ro=0.07;          %[m]Diameter of outer absorber
D_gi=0.109;         %[m]Diameter of inner glass cover
D_go=0.115;         %[m]Diameter of outer glass cover
Qv=5.6*10^-4;      %[m^3/s]volumetric flow rate
Rho=-0.90797*Tavg_sf+0.00078116*Tavg_sf^2-2.367*10^-6*Tavg_sf^3+1083.25;    %Density
of HTF
m=Rho*Qv;
cp_HTF=(0.002414*Tavg_sf  +  5.9591*10^-6*  Tavg_sf^2-2.9879*10^-8*  Tavg_sf^3    +
1.498)*1000;     %[J/kg-K] specific heat of HTF
```

```
h=(0.002414*Tavg_sf  +  5.9591*10^-6*  Tavg_sf^2-2.9879*10^-8*  Tavg_sf^3+4.4171*10^-
11*Tavg_sf^4+1498);   %[W/m2*K]Convective coefficient of HTF
m_HTF=Rho*u_m*A_c      %[kg/s]HTF mass flow rate
k_v=exp((544.149/(Tavg_sf+114.43))-2.59578)*10^-6;   %[mm2/s]Kinematic viscosity of
HTF
R_e=u_m*D_ri/k_v;         %Reynolds number
K_HTF=-8.19477*10^-5*Tavg_sf-1.92257*10^-7*Tavg_sf^2+2.5034*10^-11*Tavg_sf^3+
0.137743;    %[W/m*k]Thermal coductivity of HTF
mu=Rho*k_v;                %Dynamic viscosity
P_r=cp_HTF*mu/K_HTF;       %Prandtl number
Nu=0.023*R_e^0.8*P_r^0.4;  %Number of Nusselt
h_HTF=Nu*K_HTF/D_ri;       %[W/m2*K]Convective coefficient of HTF
Tf=423;             %[K]Temperature of inlet HTF to collector
m_steam=3.6;               %Rate steam required in the factory
cp_w=4180;                 %Specific heat of water
Tin=343;                   %[k]Temperature of feed water
v_w=4;                     %[m/s]wind speed
h_v=2.8+3*v_w;             %convection coefficient of the wind
a=D_ro^0.6-D_ri^0.6;
b=(1/a)^1.25;
C_1=(1.45+0.96*(E_r-0.5)^2)/(D_ri*b);
f1=D_ri^-0.4*(1.61+1.3*E_c)*h_v^-0.9*exp(0.00325*(T_r1-273));
f2=D_ri^-0.4*(1.61+1.3*E_c)*h_v^-0.9*exp(0.00325*(T_r2-273));
f3=D_ri^-0.4*(1.61+1.3*E_c)*h_v^-0.9*exp(0.00325*(T_r3-273));
f4=D_ri^-0.4*(1.61+1.3*E_c)*h_v^-0.9*exp(0.00325*(T_r4-273));
f5=D_ri^-0.4*(1.61+1.3*E_c)*h_v^-0.9*exp(0.00325*(T_r5-273));
f6=D_ri^-0.4*(1.61+1.3*E_c)*h_v^-0.9*exp(0.00325*(T_r6-273));
f7=D_ri^-0.4*(1.61+1.3*E_c)*h_v^-0.9*exp(0.00325*(T_r7-273));
f8=D_ri^-0.4*(1.61+1.3*E_c)*h_v^-0.9*exp(0.00325*(T_r8-273));
f9=D_ri^-0.4*(1.61+1.3*E_c)*h_v^-0.9*exp(0.00325*(T_r9-273));
f10=D_ri^-0.4*(1.61+1.3*E_c)*h_v^-0.9*exp(0.00325*(T_r10-273));
f11=D_ri^-0.4*(1.61+1.3*E_c)*h_v^-0.9*exp(0.00325*(T_r11-273));
f12=D_ri^-0.4*(1.61+1.3*E_c)*h_v^-0.9*exp(0.00325*(T_r12-273));
Tam=292.3;
x1=(sigma*(T_r1.^2+Tam^2).*(T_r1+Tam));
x2=(sigma*(T_r2.^2+Tam^2).*(T_r2+Tam));
x3=(sigma*(T_r3.^2+Tam^2).*(T_r3+Tam));
x4=(sigma*(T_r4.^2+Tam^2).*(T_r4+Tam));
x5=(sigma*(T_r5.^2+Tam^2).*(T_r5+Tam));
x6=(sigma*(T_r6.^2+Tam^2).*(T_r6+Tam));
x7=(sigma*(T_r7.^2+Tam^2).*(T_r7+Tam));
x8=(sigma*(T_r8.^2+Tam^2).*(T_r8+Tam));
x9=(sigma*(T_r9.^2+Tam^2).*(T_r9+Tam));
x10=(sigma*(T_r10.^2+Tam^2).*(T_r10+Tam));
x11=(sigma*(T_r11.^2+Tam^2).*(T_r11+Tam));
x12=(sigma*(T_r12.^2+Tam^2).*(T_r12+Tam));
y1=(E_r-0.04*(1-E_r)*(T_r1/450)).^-1;
y2=(E_r-0.04*(1-E_r)*(T_r2/450)).^-1;
y3=(E_r-0.04*(1-E_r)*(T_r3/450)).^-1;
y4=(E_r-0.04*(1-E_r)*(T_r4/450)).^-1;
y5=(E_r-0.04*(1-E_r)*(T_r5/450)).^-1;
y6=(E_r-0.04*(1-E_r)*(T_r6/450)).^-1;
y7=(E_r-0.04*(1-E_r)*(T_r7/450)).^-1;
y8=(E_r-0.04*(1-E_r)*(T_r8/450)).^-1;
y9=(E_r-0.04*(1-E_r)*(T_r9/450)).^-1;
y10=(E_r-0.04*(1-E_r)*(T_r10/450)).^-1;
y11=(E_r-0.04*(1-E_r)*(T_r11/450)).^-1;
y12=(E_r-0.04*(1-E_r)*(T_r12/450)).^-1;
z1=(D_ri/D_ro)*(1/E_c)*(f1/E_c);
z2=(D_ri/D_ro)*(1/E_c)*(f2/E_c);
z3=(D_ri/D_ro)*(1/E_c)*(f3/E_c);
z4=(D_ri/D_ro)*(1/E_c)*(f4/E_c);
z5=(D_ri/D_ro)*(1/E_c)*(f5/E_c);
z6=(D_ri/D_ro)*(1/E_c)*(f6/E_c);
z7=(D_ri/D_ro)*(1/E_c)*(f7/E_c);
z8=(D_ri/D_ro)*(1/E_c)*(f8/E_c);
z9=(D_ri/D_ro)*(1/E_c)*(f9/E_c);
z10=(D_ri/D_ro)*(1/E_c)*(f10/E_c);
```

```
z11=(D_ri/D_ro)*(1/E_c)*(f11/E_c);
z12=(D_ri/D_ro)*(1/E_c)*(f12/E_c);
%[W/m^2K]heat loss coefficient of collector
UL_1=1/[1/(C_1*((T_r1-Tam)/(1+f1))^0.25)+D_ri/(D_ro*h_v)]+x1./(y1-z1);
UL_2=[1/(C_1*(T_r2-Tam)/(1+f2))^0.25+D_ri/(D_ro*h_v)]^-1+x2./(y2-z2);
UL_3=[1/(C_1*(T_r3-Tam)/(1+f3))^0.25+D_ri/(D_ro*h_v)]^-1+x3./(y3-z3);
UL_4=[1/(C_1*(T_r4-Tam)/(1+f4))^0.25+D_ri/(D_ro*h_v)]^-1+x4./(y4-z4);
UL_5=[1/(C_1*(T_r5-Tam)/(1+f5))^0.25+D_ri/(D_ro*h_v)]^-1+x5./(y5-z5);
UL_6=[1/(C_1*(T_r6-Tam)/(1+f6))^0.25+D_ri/(D_ro*h_v)]^-1+x6./(y6-z6);
UL_7=[1/(C_1*(T_r7-Tam)/(1+f7))^0.25+D_ri/(D_ro*h_v)]^-1+x7./(y7-z7);
UL_8=[1/(C_1*(T_r8-Tam)/(1+f8))^0.25+D_ri/(D_ro*h_v)]^-1+x8./(y8-z8);
UL_9=[1/(C_1*(T_r9-Tam)/(1+f9))^0.25+D_ri/(D_ro*h_v)]^-1+x9./(y9-z9);
UL_10=[1/(C_1*(T_r10-Tam)/(1+f10))^0.25+D_ri/(D_ro*h_v)]^-1+x10./(y10-z10);
UL_11=[1/(C_1*(T_r11-Tam)/(1+f11))^0.25+D_ri/(D_ro*h_v)]^-1+x11./(y11-z11);
UL_12=[1/(C_1*((T_r12-Tam)/(1+f12))^0.25)+D_ri/(D_ro*h_v)]^-1+x12./(y12-z12);
plot(LT,UL_1,'+-r',LT,UL_2,'o-g',LT,UL_3,'*-b',LT,UL_4,'o--m',LT,UL_5,'s-
y',LT,UL_6,'d-k')
legend('Jan 17','Feb 16','Mar 16','Apr 15','May 15','Jun 11')
plot(LT,UL_7,'+-r',LT,UL_8,'o-g',LT,UL_9,'*-b',LT,UL_10,'o--m',LT,UL_11,'s-
y',LT,UL_12,'d-k')
legend('Jul 17','Aug 16','Sep 15','Oct 14','Nov 14','Dec 10')
grid on
xlabel('Time(hr)')
ylabel('Heat loss coeffient,Ut (W/m^2-k)')
title('Ut from calculated DNI vs Time ')
K=54;          %[W/mK]thermal conductivity absorber
hfi=Nu*K/D_ri;  %[W/m^2K]convective heat transfer coefficient
Uo_1=[1./UL_1+D_ro/(hfi*D_ri)+D_ro*log(D_ro/D_ri)/(2*K)].^-1;
Uo_2=[1./UL_2+D_ro/(hfi*D_ri)+D_ro*log(D_ro/D_ri)/(2*K)].^-1;
Uo_3=[1./UL_3+D_ro/(hfi*D_ri)+D_ro*log(D_ro/D_ri)/(2*K)].^-1;
Uo_4=[1./UL_4+D_ro/(hfi*D_ri)+D_ro*log(D_ro/D_ri)/(2*K)].^-1;
Uo_5=[1./UL_5+D_ro/(hfi*D_ri)+D_ro*log(D_ro/D_ri)/(2*K)].^-1;
Uo_6=[1./UL_6+D_ro/(hfi*D_ri)+D_ro*log(D_ro/D_ri)/(2*K)].^-1;
Uo_7=[1./UL_7+D_ro/(hfi*D_ri)+D_ro*log(D_ro/D_ri)/(2*K)].^-1;
Uo_8=[1./UL_8+D_ro/(hfi*D_ri)+D_ro*log(D_ro/D_ri)/(2*K)].^-1;
Uo_9=[1./UL_9+D_ro/(hfi*D_ri)+D_ro*log(D_ro/D_ri)/(2*K)].^-1;
Uo_10=[1./UL_10+D_ro/(hfi*D_ri)+D_ro*log(D_ro/D_ri)/(2*K)].^-1;
Uo_11=[1./UL_11+D_ro/(hfi*D_ri)+D_ro*log(D_ro/D_ri)/(2*K)].^-1;
Uo_12=[1./UL_12+D_ro/(hfi*D_ri)+D_ro*log(D_ro/D_ri)/(2*K)].^-1;
F1=(1./UL_1)./(1./Uo_1);
F2=(1./UL_2)./(1./Uo_2);
F3=(1./UL_3)./(1./Uo_3);
F4=(1./UL_4)./(1./Uo_4);
F5=(1./UL_5)./(1./Uo_5);
F6=(1./UL_6)./(1./Uo_6);
F7=(1./UL_7)./(1./Uo_7);
F8=(1./UL_8)./(1./Uo_8);
F9=(1./UL_9)./(1./Uo_9);
F10=(1./UL_10)./(1./Uo_10);
F11=(1./UL_11)./(1./Uo_11);
F12=(1./UL_12)./(1./Uo_12);
Tam=292.3;
Tfi=423;%[K]Heat transfer inlet temperature
S1=rabso*Gtrans*mreflect*Ib01;
S2=rabso*Gtrans*mreflect*Ib02;
S3=rabso*Gtrans*mreflect*Ib03;
S4=rabso*Gtrans*mreflect*Ib04;
S5=rabso*Gtrans*mreflect*Ib05;
S6=rabso*Gtrans*mreflect*Ib06;
S7=rabso*Gtrans*mreflect*Ib07;
S8=rabso*Gtrans*mreflect*Ib08;
S9=rabso*Gtrans*mreflect*Ib09;
S10=rabso*Gtrans*mreflect*Ib010;
S11=rabso*Gtrans*mreflect*Ib011;
S12=rabso*Gtrans*mreflect*Ib012;
n=38;     %number of collector in the loop
%[K]HTF outlet  temperature for representative days
Tfo_1=((Aa.*S1)./(Aro.*UL_1)+Tam).*(1-exp((-n*F1.*Aro.*UL_1)/(m.*cp_HTF)))+
```

```
Tfi.*exp((-n*F1.*Aro.*UL_1)./(m*cp_HTF));
Tfo_2=((Aa.*S2)./(Aro.*UL_2)+Tam).*(1-exp((-n*F2.*Aro.*UL_2)/(m.*cp_HTF)))+
Tfi.*exp((-n*F2.*Aro.*UL_2)./(m*cp_HTF));
Tfo_3=((Aa.*S3)./(Aro.*UL_3)+Tam).*(1-exp((-n*F3.*Aro.*UL_3)/(m.*cp_HTF)))+
Tfi.*exp((-n*F3.*Aro.*UL_3)./(m*cp_HTF));
Tfo_4=((Aa.*S4)./(Aro.*UL_4)+Tam).*(1-exp((-n*F4.*Aro.*UL_4)/(m.*cp_HTF)))+
Tfi.*exp((-n*F4.*Aro.*UL_4)./(m*cp_HTF));
Tfo_5=((Aa.*S5)./(Aro.*UL_5)+Tam).*(1-exp((-n*F5.*Aro.*UL_5)/(m.*cp_HTF)))+
Tfi.*exp((-n*F5.*Aro.*UL_5)./(m*cp_HTF));
Tfo_6=((Aa.*S6)./(Aro.*UL_6)+Tam).*(1-exp((-n*F6.*Aro.*UL_6)/(m.*cp_HTF)))+
Tfi.*exp((-n*F6.*Aro.*UL_6)./(m*cp_HTF));
Tfo_7=((Aa.*S7)./(Aro.*UL_7)+Tam).*(1-exp((-n*F7.*Aro.*UL_7)/(m.*cp_HTF)))+
Tfi.*exp((-n*F7.*Aro.*UL_7)./(m*cp_HTF));
Tfo_8=((Aa.*S8)./(Aro.*UL_8)+Tam).*(1-exp((-n*F8.*Aro.*UL_8)/(m.*cp_HTF)))+
Tfi.*exp((-n*F8.*Aro.*UL_8)./(m*cp_HTF));
Tfo_9=((Aa.*S9)./(Aro.*UL_9)+Tam).*(1-exp((-n*F9.*Aro.*UL_9)/(m.*cp_HTF)))+
Tfi.*exp((-n*F9.*Aro.*UL_9)./(m*cp_HTF));
Tfo_10=((Aa.*S10)./(Aro.*UL_10)+Tam).*(1-exp((-
n*F10.*Aro.*UL_10)/(m.*cp_HTF)))+Tfi.*exp((-n*F10.*Aro.*UL_10)./(m*cp_HTF));
Tfo_11=((Aa.*S11)./(Aro.*UL_11)+Tam).*(1-exp((-
n*F11.*Aro.*UL_11)/(m.*cp_HTF)))+Tfi.*exp((-n*F11.*Aro.*UL_11)./(m*cp_HTF));
Tfo_12=((Aa.*S12)./(Aro.*UL_12)+Tam).*(1-exp((-
n*F12.*Aro.*UL_12)/(m.*cp_HTF)))+Tfi.*exp((-n*F12.*Aro.*UL_12)./(m*cp_HTF));
plot(LT,Tfo_1-273,'+-r',LT,Tfo_2-273,'o-g',LT,Tfo_3-273,'*-b',LT,Tfo_4-273,'o--
m',LT,Tfo_5-273,'s-y',LT,Tfo_6-273,'d-k')
legend('Jan 17','Feb 16','Mar 16','Apr 15','May 15','Jun 11')
plot(LT,Tfo_7-273,'+-r',LT,Tfo_8-273,'o-g',LT,Tfo_9-273,'*-b',LT,Tfo_10-273,'o--
m',LT,Tfo_11-273,'s-y',LT,Tfo_12-273,'d-k')
legend('Jul 17','Aug 16','Sep 15','Oct 15','Nov 14','Dec 10')
xlabel('Time(hr)')
ylabel('HTF outlet temperature from solar field,Tfo (oC)')
title('Tfo from calculated DNI vs Time')
grid on
%[W]Useful heat gain by collector
Qu_1=m*cp_HTF*(Tfo_1-Tfi);
Qu_2=m*cp_HTF*(Tfo_2-Tfi);
Qu_3=m*cp_HTF*(Tfo_3-Tfi);
Qu_4=m*cp_HTF*(Tfo_4-Tfi);
Qu_5=m*cp_HTF*(Tfo_5-Tfi);
Qu_6=m*cp_HTF*(Tfo_6-Tfi);
Qu_7=m*cp_HTF*(Tfo_7-Tfi);
Qu_8=m*cp_HTF*(Tfo_8-Tfi);
Qu_9=m*cp_HTF*(Tfo_9-Tfi);
Qu_10=m*cp_HTF*(Tfo_10-Tfi);
Qu_11=m*cp_HTF*(Tfo_11-Tfi);
Qu_12=m*cp_HTF*(Tfo_12-Tfi);
Qu_1=max(0,m.*cp_HTF.*(Tfo_1-Tfi));
Qu_2=max(0,m*cp_HTF*(Tfo_2-Tfi));
Qu_3=max(0,m*cp_HTF*(Tfo_3-Tfi));
Qu_4=max(0,m*cp_HTF*(Tfo_4-Tfi));
Qu_5=max(0,m*cp_HTF*(Tfo_5-Tfi));
Qu_6=max(0,m*cp_HTF*(Tfo_6-Tfi));
Qu_7=max(0,m*cp_HTF*(Tfo_7-Tfi));
Qu_8=max(0,m*cp_HTF*(Tfo_8-Tfi));
Qu_9=max(0,m*cp_HTF*(Tfo_9-Tfi));
Qu_10=max(0,m*cp_HTF*(Tfo_10-Tfi));
Qu_11=max(0,m*cp_HTF*(Tfo_11-Tfi));
Qu_12=max(0,m*cp_HTF*(Tfo_12-Tfi));
plot(LT,Qu_1,'+-r',LT,Qu_2,'o-g',LT,Qu_3,'*-b',LT,Qu_4,'o--m',LT,Qu_5,'s-
y',LT,Qu_6,'d-k')
legend('Jan 17','Feb 16','Mar 16','Apr 15','May 15','Jun 11')
plot(LT,Qu_7,'+-r',LT,Qu_8,'o-g',LT,Qu_9,'*-b',LT,Qu_10,'o--m',LT,Qu_11,'s-
y',LT,Qu_12,'d-k')
legend('Jul 17','Aug 16','Sep 15','Oct 15','Nov 14','Dec 10')
grid on
xlabel('Time(hr)')
ylabel('Useful heat gain by collector,Qu(W)')
title('Qu from calculated DNI vs Time')
```

```
x1=(-n.*F1.*Ari.*UL_1)/cp_HTF;
x2=(-n.*F2.*Ari.*UL_2)/cp_HTF;
x3=(-n.*F3.*Ari.*UL_3)/cp_HTF;
x4=(-n.*F4.*Ari.*UL_4)/cp_HTF;
x5=(-n.*F5.*Ari.*UL_5)/cp_HTF;
x6=(-n.*F6.*Ari.*UL_6)/cp_HTF;
x7=(-n.*F7.*Ari.*UL_7)/cp_HTF;
x8=(-n.*F8.*Ari.*UL_8)/cp_HTF;
x9=(-n.*F9.*Ari.*UL_9)/cp_HTF;
x10=(-n.*F10.*Ari.*UL_10)/cp_HTF;
x11=(-n.*F11.*Ari.*UL_11)/cp_HTF;
x12=(-n.*F12.*Ari.*UL_12)/cp_HTF;
y1=To-((Aa/Aro).*(S1./UL_1)+Tam);
y2=To-((Aa/Aro).*(S2./UL_2)+Tam);
y3=To-((Aa/Aro).*(S3./UL_3)+Tam);
y4=To-((Aa/Aro).*(S4./UL_4)+Tam);
y5=To-((Aa/Aro).*(S5./UL_5)+Tam);
y6=To-((Aa/Aro).*(S6./UL_6)+Tam);
y7=To-((Aa/Aro).*(S7./UL_7)+Tam);
y8=To-((Aa/Aro).*(S8./UL_8)+Tam);
y9=To-((Aa/Aro).*(S9./UL_9)+Tam);
y10=To-((Aa/Aro).*(S10./UL_10)+Tam);
y11=To-((Aa/Aro).*(S11./UL_11)+Tam);
y12=To-((Aa/Aro).*(S12./UL_12)+Tam);
z1=Tf_in-((Aa/Aro).*(S1./UL_1)+Tam);
z2=Tf_in-((Aa/Aro).*(S2./UL_2)+Tam);
z3=Tf_in-((Aa/Aro).*(S3./UL_3)+Tam);
z4=Tf_in-((Aa/Aro).*(S4./UL_4)+Tam);
z5=Tf_in-((Aa/Aro).*(S5./UL_5)+Tam);
z6=Tf_in-((Aa/Aro).*(S6./UL_6)+Tam);
z7=Tf_in-((Aa/Aro).*(S7./UL_7)+Tam);
z8=Tf_in-((Aa/Aro).*(S8./UL_8)+Tam);
z9=Tf_in-((Aa/Aro).*(S9./UL_9)+Tam);
z10=Tf_in-((Aa/Aro).*(S10./UL_10)+Tam);
z11=Tf_in-((Aa/Aro).*(S11./UL_11)+Tam);
z12=Tf_in-((Aa/Aro).*(S12./UL_12)+Tam);
zz1=log(y1./z1);
zz2=log(y2./z2);
zz3=log(y3./z3);
zz4=log(y4./z4);
zz5=log(y5./z5);
zz6=log(y6./z6);
zz7=log(y7./z7);
zz8=log(y8./z8);
zz9=log(y9./z9);
zz10=(log(y10./z10));
zz11=log(y11./z11);
zz12=log(y12./z12);
%mass of HTF flow in solar collector
mf1=x1./zz1;
mf2=x2./zz2;
mf3=x3./zz3;
mf4=x4./zz4;
mf5=x5./zz5;
mf6=x6./zz6;
mf7=x7./zz7;
mf8=x8./zz8;
mf9=x9./zz9;
mf10=x10./zz10;
mf11=x11./zz11;
mf12=x12./zz12;
plot(LT,mf1,'+-r',LT,mf2,'o-g',LT,mf3,'*-b',LT,mf4,'o--m',LT,mf5,'s-y',LT,mf6,'d-
k')
legend('Jan 17','Feb 16','Mar 16','Apr 15','May 15','Jun 11')
plot(LT,mf7,'+-r',LT,mf8,'o-g',LT,mf9,'*-b',LT,mf10,'o--m',LT,mf11,'s-y')
legend('Jul 17','Aug 16','Sep 15','Oct 15','Nov 14',’Dec 10’,’d-k’)
grid on
```

```
xlabel('Time(hr)')
ylabel('Mass flow rate,m(kg/s)')
title('m from calculated DNI vs Time')
Tfo1=((Aa.*S1)./(Aro.*UL_1)+Tam).*
(1-exp((n*F1.*Aro.*UL_1)./(mf1.*cp_HTF)))+
Tfi.*exp((-n*F1.*Aro.*UL_1)./(mf1*cp_HTF)); %HTF outlet temp on Jan 17
Tfo2=((Aa.*S2)./(Aro.*UL_2)+Tam).*
(1-exp((-n*F2.*Aro.*UL_2)./(mf2.*cp_HTF)))+
Tfi.*exp((-n*F2.*Aro.*UL_2)./(mf2*cp_HTF));  %HTF outlet temp on Feb 17
Tfo3=((Aa.*S3)./(Aro.*UL_3)+Tam).
*(1-exp((-n*F3.*Aro.*UL_3)./(mf3.*cp_HTF)))+
Tfi.*exp((-n*F3.*Aro.*UL_3)./(mf3*cp_HTF));    %HTF outlet temp on Mar 16
Tfo4=((Aa.*S4)./(Aro.*UL_4)+Tam).*
(1-exp((-n*F4.*Aro.*UL_4)./(mf4.*cp_HTF)))+
Tfi.*exp((-n*F4.*Aro.*UL_4)./(mf4*cp_HTF));   %HTF outlet temp on Apr 15
Tfo5=((Aa.*S5)./(Aro.*UL_5)+Tam).*
(1-exp((-n*F5.*Aro.*UL_5)./(mf5.*cp_HTF)))+
Tfi.*exp((-n*F5.*Aro.*UL_5)./(mf5*cp_HTF));  %HTF outlet temp on May 15
Tfo6=((Aa.*S6)./(Aro.*UL_6)+Tam).*
(1-exp((-n*F6.*Aro.*UL_6)./(mf6.*cp_HTF)))+
Tfi.*exp((-n*F6.*Aro.*UL_6)./(mf6*cp_HTF));   %HTF outlet temp on June 11
Tfo7=((Aa.*S7)./(Aro.*UL_7)+Tam).*
(1-exp((-n*F7.*Aro.*UL_7)./(mf7.*cp_HTF)))+
Tfi.*exp((-n*F7.*Aro.*UL_7)./(mf7*cp_HTF));   %HTF outlet temp on july 17
Tfo8=((Aa.*S8)./(Aro.*UL_8)+Tam).*
(1-exp((-n*F8.*Aro.*UL_8)./(mf8.*cp_HTF)))+
Tfi.*exp((-n*F8.*Aro.*UL_8)./(mf8*cp_HTF));  %HTF outlet temp on Aug 16
Tfo9=((Aa.*S9)./(Aro.*UL_9)+Tam).*
(1-exp((-n*F9.*Aro.*UL_9)./(mf9.*cp_HTF)))+
Tfi.*exp((-n*F9.*Aro.*UL_9)./(mf9*cp_HTF));   %HTF outlet temp on Sep 17
Tfo10=((Aa.*S10)./(Aro.*UL_10)+Tam).*
(1-exp((-n*F10.*Aro.*UL_10)./(mf10.*cp_HTF)))+
Tfi.*exp((-n*F10.*Aro.*UL_10)./(mf10*cp_HTF)); %HTF outlet temp on Oct 15
Tfo11=((Aa.*S11)./(Aro.*UL_11)+Tam).*(1-exp((-
n*F11.*Aro.*UL_11)./(mf11.*cp_HTF)))+Tfi.*exp((-n*F11.*Aro.*UL_11)./(mf11*cp_HTF));
%HTF outlet temp on Nov 14
Tfo12=((Aa.*S12)./(Aro.*UL_12)+Tam).*
(1-exp((-n*F12.*Aro.*UL_12)./(mf11.*cp_HTF)))+
Tfi.*exp((-n*F12.*Aro.*UL_12)./(mf12*cp_HTF)); %HTF outlet temp on Dec 10
plot(LT,Tfo1-273,'+-r',LT,Tfo_1-273,'+-b',LT,Tfo2-273,'*-g',LT,Tfo_2-273,'o-
g',LT,Tfo3-273,'*-b',LT,Tfo_3-273,'.-',LT,Tfo4-273,'o-m',LT,Tfo_4-273,'o--
m',LT,Tfo5-273,'s--g',LT,Tfo_5-273,'s-y',LT,Tfo6-273,'d--k',LT,Tfo_6-273,'d-k')
legend('Jan 17','Jan 17','Feb 16','Feb 16','Mar 16','Mar 16','Apr 15','Apr 15','May
15','May 15','Jun 11','Jun 11')
plot(LT,Tfo7-273,'+-r',LT,Tfo_7-273,'+-b',LT,Tfo8-273,'*-g',LT,Tfo_8-273,'o-
g',LT,Tfo9-273,'*-b',LT,Tfo_9-273,'.-',LT,Tfo10-273,'o-m',LT,Tfo_10-273,'o--
m',LT,Tfo11-273,'s--g',LT,Tfo_11-273,'s-y',LT,Tfo12-273,'d--k',LT,Tfo_12-273,'d-k')
legend('Jul 17','Jul 17','Aug 16','Aug 16','Sep 15','Sep 15','Oct 15','Oct 15','Nov
14','Nov 14','Dec 10','Dec 10')
xlabel('Time(hr)')
ylabel('HTF outlet temperature from solar field,Tfo (oC)')
title('Tfo from calculated DNI vs Time')
grid on
R=38;%Proper Number of row
M_1=R*mf1;  %[kg/s]Total mass of HTF flow in solar collector on january 17
M_2=R*mf2;
M_3=R*mf3;
M_4=R*mf4;
M_5=R*mf5;
M_6=R*mf6;
M_7=R*mf7;
M_8=R*mf8;
M_9=R*mf9;
M_10=R*mf10;
M_11=R*mf11;
M_12=R*mf12;
plot(LT,M_1,'+-r',LT,M_2,'o-g',LT,M_3,'*-b',LT,M_4,'o--m',LT,M_5,'s-y',LT,M_6,'d-
k')
```

```
legend('Jan 17','Feb 16','Mar 16','Apr 15','May 15','Jun 11')
plot(LT,M_7,'+-r',LT,M_8,'o-g',LT,M_9,'*-b',LT,M_10,'o--m',LT,M_11,'s-y')
legend('Jul 17','Aug 16','Sep 15','Oct 15','Nov 14')
grid on
xlabel('Time(hr)')
ylabel('Mass flow rate inter to heat exchanger,M(kg/s)')
title('M from measured DNI vs Time')
M=10;         %[kg/s] mass flow rate of HTF inlet to HX should be 9.5 kg/s.this is
obtain by try and error.
T_in=343;      %[K]water inlet temperature to HX
T_so=423;      %[K]HTF outlet temperature from HX
Qmax=M.*cp_HTF.*(Tfo_1-T_in);
plot(LT,Qmax)
m_w=3.6;     %[Kg/s]Feed water mass flow rate
cp_w=4180;   %[J/kgK]Specific heat water
%[oC]Steam temperature outlet from HX on january 17
Tco_1=(M.*cp_HTF.*(Tfo1-T_so)./(m_w*cp_w)+T_in);
Tco_2=(M.*cp_HTF.*(Tfo2-T_so)./(m_w*cp_w)+T_in);
Tco_3=(M.*cp_HTF.*(Tfo3-T_so)./(m_w*cp_w)+T_in);
Tco_4=(M.*cp_HTF.*(Tfo4-T_so)./(m_w*cp_w)+T_in);
Tco_5=(M.*cp_HTF.*(Tfo5-T_so)./(m_w*cp_w)+T_in);
Tco_6=(M.*cp_HTF.*(Tfo6-T_so)./(m_w*cp_w)+T_in);
Tco_7=(M.*cp_HTF.*(Tfo7-T_so)./(m_w*cp_w)+T_in);
Tco_8=(M.*cp_HTF.*(Tfo8-T_so)./(m_w*cp_w)+T_in);
Tco_8=(M.*cp_HTF.*(Tfo8-T_so)./(m_w*cp_w)+T_in);
Tco_9=(M.*cp_HTF.*(Tfo9-T_so)./(m_w*cp_w)+T_in);
Tco_10=(M.*cp_HTF.*(Tfo10-T_so)./(m_w*cp_w)+T_in);
Tco_11=(M.*cp_HTF.*(Tfo11-T_so)./(m_w*cp_w)+T_in);
Tco_12=(M.*cp_HTF.*(Tfo12-T_so)./(m_w*cp_w)+T_in);
Tco_1=max(0,(M.*cp_HTF.*(Tfo1-T_so)./(m_w*cp_w)+T_in)-273);
Tco_2=max(0,(M.*cp_HTF.*(Tfo2-T_so)./(m_w*cp_w)+T_in)-273);
Tco_3=max(0,(M.*cp_HTF.*(Tfo3-T_so)./(m_w*cp_w)+T_in)-273);
Tco_4=max(0,(M.*cp_HTF.*(Tfo4-T_so)./(m_w*cp_w)+T_in)-273);
Tco_5=max(0,(M.*cp_HTF.*(Tfo5-T_so)./(m_w*cp_w)+T_in)-273);
Tco_6=max(0,(M.*cp_HTF.*(Tfo6-T_so)./(m_w*cp_w)+T_in)-273);
Tco_7=max(0,(M.*cp_HTF.*(Tfo7-T_so)./(m_w*cp_w)+T_in)-273);
Tco_8=max(0,(M.*cp_HTF.*(Tfo8-T_so)./(m_w*cp_w)+T_in)-273);
Tco_9=max(0,(M.*cp_HTF.*(Tfo9-T_so)./(m_w*cp_w)+T_in)-273);
Tco_10=max(0,(M.*cp_HTF.*(Tfo10-T_so)./(m_w*cp_w)+T_in)-273);
Tco_11=max(0,(M.*cp_HTF.*(Tfo11-T_so)./(m_w*cp_w)+T_in)-273);
Tco_12=max(0,(M.*cp_HTF.*(Tfo12-T_so)./(m_w*cp_w)+T_in)-273);
plot(LT,Tfo1-273,'+-r',LT,Tco_1,'+-b',LT,Tfo2-273,'*-g',LT,Tco_2,'o-g',LT,Tfo3-
273,'*-b',LT,Tco_3,'.-',LT,Tfo4-273,'o-m',LT,Tco_4,'o--m',LT,Tfo5-273,'s--
g',LT,Tco_5,'s-y',LT,Tfo6-273,'d--k',LT,Tco_6,'d-k')
legend('Jan 17','Jan 17','Feb 16','Mar 16','Mar 16','Apr 15','Apr 15','May
15','May 15','Jun 11','Jun 11')
plot(LT,Tfo7-273,'+-r',LT,Tco_7,'+-b',LT,Tfo8-273,'*-g',LT,Tco_8,'o-g',LT,Tfo9-
273,'*-b',LT,Tco_9,'.-',LT,Tfo10-273,'o-m',LT,Tco_10,'o--m',LT,Tfo11-273,'s--
g',LT,Tco_11,'s-y',LT,Tfo12-273,'d--k',LT,Tco_12,'d-k')
legend('Jul 17','Jul 17','Aug 16','Aug 16','Sep 15','Sep 15','Oct 15','Oct 15','Nov
14','Nov 14','Dec 10','Dec 10')
grid on
xlabel('Time(hr)')
ylabel('Temperature(oC)')
title('Steam Temp,HTF Temp vs Time')
Tco=488 ;%Required steam temperature(k)
x=M*cp_HTF; %[W/K]capacitance rate of the hot side heat transfer fluid
y=m_w*cp_w; %[W/k]capacitance rate of the cold side water fluid
%%%%%%%%%%%%%Efficiency of the system %%%%%%%%
% % For Black Chrome coating with vacuum, the coefficients are given below.
A=73.6;
B=-0.004206 ;
C=7.44;
D=-0.0958;
Cw=0;
%END LOSSES %%%%%%%%%%%%%%%%%%%%%%%%%%%%%%%%%%%%%%%%
f=1.84;              %[m] focal length
Ls=12.5;             %spacing b/n the row
```

```
EL1=1-f*tan(theta1*pi/180)/Lsca;
EL2=1-f*tan(theta2*pi/180)/Lsca;
EL3=1-f*tan(theta3*pi/180)/Lsca;
EL4=1-f*tan(theta4*pi/180)/Lsca;
EL5=1-f*tan(theta5*pi/180)/Lsca;
EL6=1-f*tan(theta6*pi/180)/Lsca;
EL7=1-f*tan(theta7*pi/180)/Lsca;
EL8=1-f*tan(theta8*pi/180)/Lsca;
EL9=1-f*tan(theta9*pi/180)/Lsca;
EL10=1-f*tan(theta10*pi/180)/Lsca;
EL11=1-f*tan(theta11*pi/180)/Lsca;
EL12=1-f*tan(theta12*pi/180)/Lsca;
%Incident angle modifier
K1=cos(theta1*pi/180)-0.0003512*(theta1)-0.00003137*(theta1).^2;
K2=cos(theta2*pi/180)-0.0003512*(theta2)-0.00003137*(theta2).^2;
K3=cos(theta3*pi/180)-0.0003512*(theta3)-0.00003137*(theta3).^2;
K4=cos(theta4*pi/180)-0.0003512*(theta4)-0.00003137*(theta4).^2;
K5=cos(theta5*pi/180)-0.0003512*(theta5)-0.00003137*(theta5).^2;
K6=cos(theta6*pi/180)-0.0003512*(theta6)-0.00003137*(theta6).^2;
K7=cos(theta7*pi/180)-0.0003512*(theta7)-0.00003137*(theta7).^2;
K8=cos(theta8*pi/180)-0.0003512*(theta8)-0.00003137*(theta8).^2;
K9=cos(theta9*pi/180)-0.0003512*(theta9)-0.00003137*(theta9).^2;
K10=cos(theta10*pi/180)-0.0003512*(theta10)-0.00003137*(theta10).^2;
K11=cos(theta11*pi/180)-0.0003512*(theta11)-0.00003137*(theta11).^2;
K12=cos(theta12*pi/180)-0.0003512*(theta12)-0.00003137*(theta12).^2;
%Row shading
RS1=min(max(0,(Ls/w)*(cos(zenith1*pi/180)./(cos(theta1*pi/180)))),1.0);
RS2=min(max(0,(Ls/w)*(cos(zenith2*pi/180)./(cos(theta2*pi/180)))),1.0);
RS3=min(max(0,(Ls/w)*(cos(zenith3*pi/180)./(cos(theta3*pi/180)))),1.0);
RS4=min(max(0,(Ls/w)*(cos(zenith4*pi/180)./(cos(theta4*pi/180)))),1.0);
RS5=min(max(0,(Ls/w)*(cos(zenith5*pi/180)./(cos(theta5*pi/180)))),1.0);
RS6=min(max(0,(Ls/w)*(cos(zenith6*pi/180)./(cos(theta6*pi/180)))),1.0);
RS7=min(max(0,(Ls/w)*(cos(zenith7*pi/180)./(cos(theta7*pi/180)))),1.0);
RS8=min(max(0,(Ls/w)*(cos(zenith8*pi/180)./(cos(theta8*pi/180)))),1.0);
RS9=min(max(0,(Ls/w)*(cos(zenith9*pi/180)./(cos(theta9*pi/180)))),1.0);
RS10=min(max(0,(Ls/w)*(cos(zenith10*pi/180)./(cos(theta10*pi/180)))),1.0);
RS11=min(max(0,(Ls/w)*(cos(zenith11*pi/180)./(cos(theta11*pi/180)))),1.0);
RS12=min(max(0,(Ls/w)*(cos(zenith12*pi/180)./(cos(theta12*pi/180)))),1.0);
T_amb=19.5 ;              %[oc] assumed ambient temperature
DeltaT_out=T_out-T_amb;  %[oc]difference between output and ambient temperature
DeltaT_in=T_in -T_amb ;  %[oc]difference between input and ambient temperature
%Effective area of parabolic trough%%%%%%%%%%
Tavg_sf = (T_out + T_in)/2;
x=(20*Tavg_sf/225);
y =(2.57*10^6)*Tavg_sf/275; %expansion valve losses
z=Ib.*eta_SF;
% Effective Area of the Solar Field
A_eff= (Q_net +y)./(z-x)
eta_SF1 =max(0,K1.*EL1.*RS1.*((A + B*((DeltaT_in+DeltaT_out)/2)) + (C+ Cw*V)* ...
(((DeltaT_in+DeltaT_out)./(Inb1)))+D*(DeltaT_in*DeltaT_out + ...
((DeltaT_out-DeltaT_in)^2)/3)./(Inb1))/100);%COLLECTOR EFFICIENCY on january 17
 eta_SF2 =max(0, K2.*EL2.*RS2.*((A + B*((DeltaT_in+DeltaT_out)/2)) + (C+ Cw*V)* ...
(((DeltaT_in+DeltaT_out)./(Inb2)))+D*(DeltaT_in*DeltaT_out + ...
((DeltaT_out-DeltaT_in)^2)/3)./(Inb2))/100);
 eta_SF3 = max(0,K3.*EL3.*RS3.*((A + B*((DeltaT_in+DeltaT_out)/2)) + (C+ Cw*V)* ...
(((DeltaT_in+DeltaT_out)./(Inb3)))+D*(DeltaT_in*DeltaT_out + ...
((DeltaT_out-DeltaT_in)^2)/3)./(Inb3))/100);
 eta_SF4 =max(0,K4.*EL4.*RS4.*((A + B*((DeltaT_in+DeltaT_out)/2)) + (C+ Cw*V)* ...
(((DeltaT_in+DeltaT_out)./(Inb4)))+D*(DeltaT_in*DeltaT_out + ...
((DeltaT_out-DeltaT_in)^2)/3)./(Inb4))/100);
 eta_SF5 =   max(0,K5.*EL5.*RS5.*((A  +  B*((DeltaT_in+DeltaT_out)/2))  +  (C+  Cw*V)*
...
(((DeltaT_in+DeltaT_out)./(Inb5)))+D*(DeltaT_in*DeltaT_out + ...
((DeltaT_out-DeltaT_in)^2)/3)./(Inb5))/100);
 eta_SF6  =  max(0,  K6.*EL6.*RS6.*((A  +  B*((DeltaT_in+DeltaT_out)/2))  +  (C+  Cw*V)*
...
(((DeltaT_in+DeltaT_out)./(Inb6)))+D*(DeltaT_in*DeltaT_out + ...
((DeltaT_out-DeltaT_in)^2)/3)./(Inb6))/100);
```

```
eta_SF7 = max(0,K7.*EL7.*RS7.* ((A + B*((DeltaT_in+DeltaT_out)/2)) + (C+ Cw*V)* ...
(((DeltaT_in+DeltaT_out)./(Inb7)))+D*(DeltaT_in*DeltaT_out + ...
((DeltaT_out-DeltaT_in)^2)/3)./(Inb7))/100);
 eta_SF8  =  max(0,K8.*EL8.*RS8.*  ((A  +  B*((DeltaT_in+DeltaT_out)/2))  +  (C+  Cw*V)*
...
(((DeltaT_in+DeltaT_out)./(Inb8)))+D*(DeltaT_in*DeltaT_out + ...
((DeltaT_out-DeltaT_in)^2)/3)./(Inb8))/100);
 eta_SF9  =  max(0,K9.*EL9.*RS9.*  ((A  +  B*((DeltaT_in+DeltaT_out)/2))  +  (C+  Cw*V)*
...
(((DeltaT_in+DeltaT_out)./(Inb9)))+D*(DeltaT_in*DeltaT_out + ...
((DeltaT_out-DeltaT_in)^2)/3)./(Inb9))/100);
 eta_SF10  =max(0,  K10.*EL10.*RS10.*  ((A  +  B*((DeltaT_in+DeltaT_out)/2))  +  (C+
Cw*V)* ...
(((DeltaT_in+DeltaT_out)./(Inb10)))+D*(DeltaT_in*DeltaT_out + ...
((DeltaT_out-DeltaT_in)^2)/3)./(Inb10))/100);
 eta_SF11  =    max(0,K11.*EL11.*RS11.*((A  +  B*((DeltaT_in+DeltaT_out)/2))  +  (C+
Cw*V)* ...
(((DeltaT_in+DeltaT_out)./(Inb11)))+D*(DeltaT_in*DeltaT_out + ...
((DeltaT_out-DeltaT_in)^2)/3)./(Inb11))/100);
 eta_SF12  =max(0,    K12.*EL12.*RS12.*((A  +  B*((DeltaT_in+DeltaT_out)/2))  +  (C+
Cw*V)* ...
(((DeltaT_in+DeltaT_out)./(Inb12)))+D*(DeltaT_in*DeltaT_out + ...
((DeltaT_out-DeltaT_in)^2)/3)./(Inb12))/100);
 plot(LT,eta_SF1,'+-r',LT,eta_SF2,'+-y',LT,eta_SF3,'*-g',LT,eta_SF4,'*-
b',LT,eta_SF5,'d-k',LT,eta_SF6,'o-m')
legend('Jan 17','Feb 16','Mar 16','Apr 15','May 15','Jun 11')
plot(LT,eta_SF7,'+-r',LT,eta_SF8,'+-y',LT,eta_SF9,'*-g',LT,eta_SF10,'*-
b',LT,eta_SF11,'d-k',LT,eta_SF11,'o-m')
legend('Jul 17','Aug 16','Sep 15','Oct 15','Nov 14','Dec 10')
grid on
xlabel('Time(hr)')
ylabel('Efficiency of a system %')
title('Efficiency of a system vs Time(hr)')
```

Appendix C: Simulation result for representative days

Table 1: Clear day direct normal insolation (KW/m^2) of Adama

Time (hr)	6am	7am	8am	9am	10am	11am	12pm	1pm	2pm	3pm	4pm	5pm
Jan-17	0.352	0.607	0.802	0.89	0.933	0.953	0.957	0.946	0.917	0.858	0.734	0.451
Feb-16	0.351	0.619	0.811	0.897	0.938	0.958	0.963	0.954	0.929	0.877	0.771	0.523
Mar-16	0.364	0.698	0.865	0.941	0.98	0.997	1.001	0.991	0.965	0.913	0.807	0.556
Apr-15	0.425	0.728	0.857	0.919	0.951	0.964	0.967	0.955	0.929	0.876	0.77	0.521
May-15	0.504	0.782	0.903	0.963	0.993	1.007	1.007	0.995	0.967	0.911	0.8	0.545
Jun-11	0.476	0.742	0.859	0.918	0.948	0.962	0.963	0.952	0.926	0.875	0.774	0.55
Jul-17	0.453	0.765	0.903	0.97	1.004	1.021	1.024	1.013	0.988	0.937	0.838	0.618
Aug-16	0.428	0.749	0.888	0.955	0.989	1.004	1.007	0.997	0.971	0.92	0.817	0.582
Sep-15	0.496	0.761	0.872	0.927	0.954	0.965	0.963	0.949	0.916	0.852	0.717	0.4
Oct-15	0.464	0.766	0.894	0.955	0.986	0.998	0.996	0.98	0.944	0.871	0.715	0.378
Nov-14	0.431	0.75	0.891	0.956	0.991	1.004	1.002	0.984	0.944	0.862	0.685	0.37
Dec-10	0.379	0.701	0.866	0.944	0.983	0.999	0.999	0.982	0.944	0.867	0.701	0.379

Table 2: Measured global radiation (KW/m^2) in 2014

Time(hr)	6	7	8	9	10	11	12	13	14	15	16	17	18
Jan-17	0.07	0.149	0.529	0.678	0.657	0.524	0.788	0.608	0.476	0.256	0.05	0.006	0.0005
Feb-16	0.205	0.397	0.579	0.709	0.776	0.887	0.820	0.698	0.502	0.291	0.061	0.0006	0.0006
Mar-16	0.0399	0.026	0.052	0.304	0.625	0.973	0.779	0.826	0.212	0.343	0.093	0.0007	0.0006
Apr-15	0.084	0.219	0.766	0.664	0.869	1.014	0.896	0.819	0.584	0.313	0.034	0.0006	0.0006
May-15	0.219	0.493	0.675	0.727	0.671	0.883	0.832	0.611	0.136	0.085	0.047	0.0005	0.0005
Jun-11	0.101	0.271	0.602	0.685	0.774	0.814	0.641	0.348	0.472	0.076	0.033	0.0009	0.0006
Jul-17	0.228	0.420	0.567	0.673	0.522	0.778	0.724	0.574	0.429	0.247	0.057	0.0012	0.0006
Aug-17	0.216	0.541	0.661	0.779	0.862	0.875	0.819	0.705	0.541	0.432	0.132	0.0007	0.0005
Sep-15	0.292	0.525	0.706	0.899	0.692	0.553	0.815	0.801	0.111	0.058	0.028	0.0006	0.0006
Oct-15	0.310	0.536	0.722	0.849	0.901	0.891	0.793	0.640	0.449	0.213	0.013	0.0005	0.0006
Nov-15	0.283	0.499	0.678	0.801	0.856	0.841	0.768	0.627	0.409	0.178	0.007	0.0006	0.0006

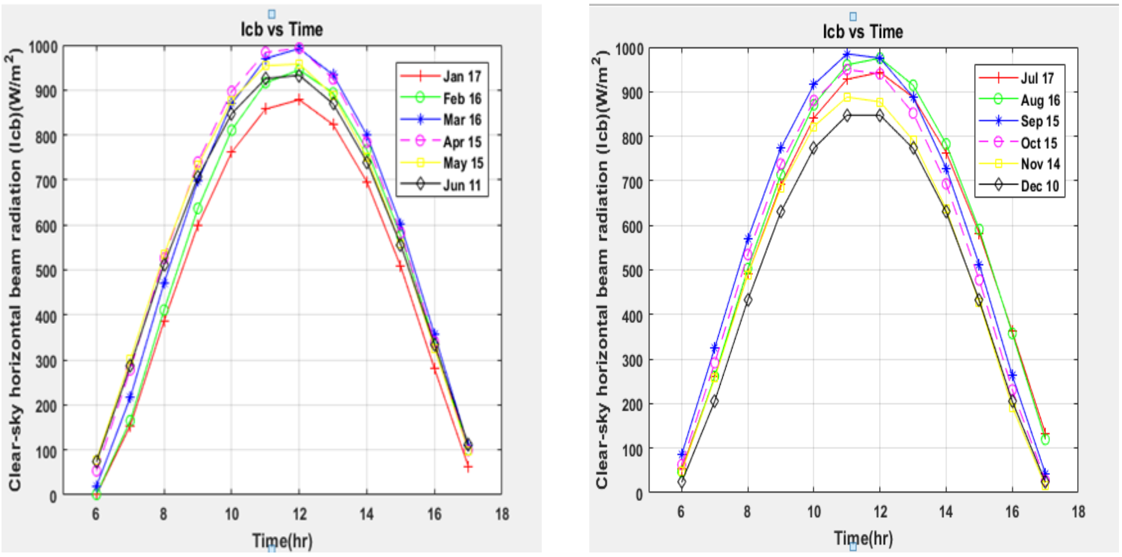

Figure 2: Clear sky horizontal beam radiation

About the author

Abdi Abrahim was born in East Hararge , Chombolcha Wereda in March 1989. He pursued his bachelor at Ambo University in Mechanical Engineering. After he got married with his beloved chaltu, he began master studies at University of Adama Science and Technology under the guidance of Dr. Gezahegn Habtamu.

.